ANALYTICAL SOLUTION TO PRESSURE TRANSIENT ANALYSIS IN NON-NEWTONIAN/NEWTONIAN FLUIDS COMPOSITE RESERVOIRS

A THESIS SUBMITTED TO THE DEPARTMENT OF PETROLEUM ENGINEERING

AFRICAN UNIVERSITY OF SCIENCE AND TECHNOLOGY

IN PARTIAL FULFILLMENT OF THE REQUIREMENTS FOR THE DEGREE OF

MASTER OF PETROLEUM ENGINEERING.

BY

UKWUIGWE, ONYINYECHI CHIZOBAM

ABUJA, NIGERIA

APRIL, 2021

CERTIFICATION

This is to certify that the thesis titled “ANALYTICAL SOLUTION TO PRESSURE TRANSIENT ANALYSIS IN NON-NEWTONIAN/NEWTONIAN FLUIDS COMPOSITE RESERVOIRS” submitted to the school of postgraduate studies, African University of Science and Technology (AUST), Abuja, Nigeria for the award of the Master’s degree is a record of original research carried out by Ukwuigwe Onyinyechi Chizobam in the Department of Petroleum Engineering.

ANALYTICAL SOLUTION TO PRESSURE TRANSIENT ANALYSIS IN NON-NEWTONIAN/NEWTONIAN FLUIDS COMPOSITE RESERVOIRS

By

Ukwuigwe, Onyinyechi Chizobam

A THESIS APPROVED BY THE PETROLEUM ENGINEERING DEPARTMENT.

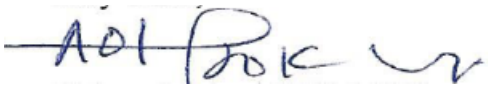 October 23, 2021

RECOMMENDED BY: **……**

Committee Chair**:** **Supervisor, Dr. Alpheus Igbokoyi**

……

Committee Member**:** **Prof. Djebbar Tiab**

……

Committee Member**:** **Prof. David Ogbe**

 October 23, 2021

APPROVED BY: **……**

Head, Department of Petroleum Engineering

……

Chief Academic Officer

……

Date

ABSTRACT

During polymer flooding in the reservoir using shear-thinning non-Newtonian fluids, an interface exists between the in-situ Newtonian crude in the reservoir and the injected polymer solution. This work examines application of well test analysis techniques to develop an analytical solution to investigate the interface boundary conditions for non-Newtonian/Newtonian fluids in composite reservoirs.

Mathematical models were presented and solved analytically using Laplace transform method. The solution was inverted to real domain with the Stehfest algorithm and extended to obtain equations for the three boundary conditions which are: infinite-acting, constant pressure, and no-flow boundaries. New pressure and pressure derivative type curves are developed for homogeneous and naturally fractured reservoirs (NFRs). Cases of non-Newtonian/non-Newtonian and Newtonian/non-Newtonian fluid interface were also considered.

Numerical examples are used to estimate reservoir and power-law flow parameters using type curve matching and Tiab's Direct Synthesis (TDS) technique.

Keywords: Power-law (shear thinning) fluids, Well test (Pressure transient) analysis, Tiab's Direct Synthesis (TDS) technique, Naturally Fractured Reservoirs (NFR). Non-Newtonian/Newtonian fluid interface, Polymer Front.

DEDICATION

I dedicate this work to the Almighty God, He who has plans of good for me; only through His strength could I have succeeded.

ACKNOWLEDGEMENTS

My gratitude goes to my supervisor, Dr Alpheus Igbokoyi, for his commitments to my academic growth. He gave his time freely and was always there at any period of the day I needed clarity. Also his supervision, helpful assistance to problems, and wise guidance throughout the period of this project cannot be underestimated.

I say thanks to all the lecturers who I learnt their courses during my stay. Special thanks go to Prof Djebbar Tiab for my first basic understanding of Well Test Analysis and Dr. David Ogbe for his review of my work.

I cannot fail to praise God for my parents, Mr. W. O. and Mrs. A. O. Ukwuigwe, for their financial and moral support from the beginning of the program. Most especially, their understanding of my 'online classes and home schooling' cannot be disregarded.

I am also grateful to my siblings, Netochukwu, Chidinma, and Chinedum, for their love and support. I know you guys look up to me and with God by my side, I promise not to fail you. And I appreciate my friends, both at AUST and beyond, who always took out time to know how my work was coming along. May the good Lord bless you all in Jesus Christ name.

To all my AUST colleagues, I say 'thank God we made it' and 'let's move on to greater heights'.

TABLE OF CONTENTS

LIST OF FIGURES

LIST OF TABLES

CHAPTER 1

INTRODUCTION

1.1 Background

Enhanced oil recovery (EOR) processes is a means of improving the recovery of hydrocarbons from oil reservoirs after primary production through natural drive and water flooding has declined. This is because a large portion of crude oil remains in the reservoir after the application of primary recovery and secondary recovery processes. Among chemical-based enhanced oil recovery processes, polymer flooding is a highly practiced process in conventional oil reservoirs.

Polymer flooding utilizes the injection of polymer solutions into oil reservoirs. The polymers commonly used in EOR operations are polyacrylamides, xanthan gum, and cellulosic. The presence of a polymer in water increases the viscosity of the injected fluid, which upon injection reduces the water-to-oil mobility ratio and the permeability of the porous media, thereby improving oil recovery. The net result is the increase in oil displacement, reservoir sweep efficiencies, and pressure gradient, especially in heterogeneous oil reservoirs (Ahmad Ali Manzor, 2020).

Polymer flooding can be considered as a waterflooding process in which polymers have been added to the solution to improve mobility control (Manrique et al, 2017). Polymer flooding is able to achieve higher oil recovery than ordinary waterflooding due to improved volumetric sweep efficiency resulting from better mobility control. The objective of polymer flooding is to provide better displacement and volumetric sweep efficiencies during a waterflooding. Many field applications of polymer flooding have been reported as technically and economically successful. However, due to the Non-Newtonian power-law behavior of polymer solutions, various setbacks have been encountered during polymer flooding.

Such setbacks include severe channeling, high polymer production, formation of in-situ emulsions, and productivity, polymer, and operational losses (Manrique et al., 2017). As a result, different studies on have been done to investigate how to maximize the oil recovery and reduce operating costs during polymer flooding, since the recovery technology is promising. For example,

Ahmad Ali Manzoor (2020) studied effect of injection pressure and polymer concentration on flooding performance.

Well test analysis is often carried out before, during, and after polymer flooding to obtain an accurate reservoir description and to evaluate fluid mobility within the project area (Hun and Snow, 1985). Studies have shown however, that pressure transient models used for analysis of these fluids are unlike that observed for Newtonian fluids. For one, the fluids have no simple proportionality relation between shear stress and rate of shear, and another, they show a decrease of apparent viscosity with increasing shear rates (Tariq Fariss Al-Fariss, 1984). Also, the polymer distribution within the reservoir is often not-uniform and not known. Polymer flooding often creates conditions where the reservoir is viewed as made of two regions of different rock and fluid properties.

During polymer flooding, the reservoir is often made up of two or more regions and as such, it is regarded as a composite reservoir. Most times, the two regions, which might be oil and polymer solution/water regions, have different rock and fluid properties. Ikoku and Ramey (1979) in deriving the flow equation for non-Newtonian power law fluid through a porous medium did not consider the presence of Newtonian fluid in the reservoir. Lund and Ikoku (1981) addressed this neglect and also presented the effect of fluid parameters and reservoir boundary conditions on the pressure transient behavior, but they used numerical method. Ertekin et al. (1987) also used numerical method to address the same problem as in Lund and Ikoku's case.

This study considers the analytical solution to the pressure transient derivative behavior experienced in a two-region, composite reservoir. It investigates the behavior for a non-Newtonian/non-Newtonian fluid flow and also that of a non-Newtonian/Newtonian flow.

1.2 Problem Statement

Well test data analysis has enabled many authors to investigate non-Newtonian power-law fluid behaviour in the porous media. This study attempts to successfully provide an analytical solution to the pressure transient analysis for non-Newtonian/Newtonian fluids composite reservoirs. Type-curve matching and the Tiab's Direct Synthesis (TDS) techniques is used for the analysis. The work

considers the pressure behavior of polymer solutions (non-Newtonian fluids) in composite homogeneous and naturally fractured reservoirs. It also considers when the regions comprise of two non-Newtonian fluids and when this is a non-Newtonian inner region and a Newtonian outer region.

1.3 Aim and Objectives of the Research

The aim of this research is to provide an analytical solution to Pressure Transient Analysis in non-Newtonian/Newtonian fluids in composite reservoirs, as illustrated in Figure 1.1.

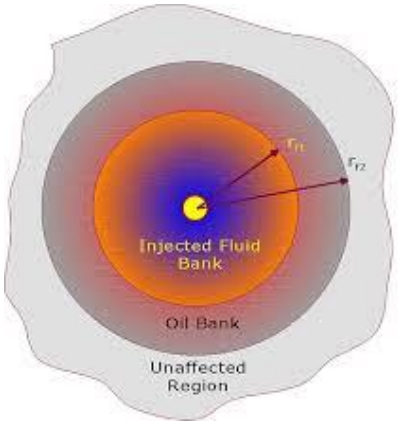

Figure 1.1: An illustration of non-Newtonian fluid injection into a reservoir

The objectives are to:

- Develop mathematical models, based on the published works of Ikoku and Ramey (1979) and Lund and Ikoku (1981), which can be used to analytically solve the pressure transient problems for composite, homogeneous as well as naturally fractured reservoirs.
- Derive equations for the various rock and fluid parameters needed to analyze the reservoir condition.
- Write a Tiab's Direct Synthesis technique to describe relations based on pressure derivative behavior for well tests in either homogeneous or composite reservoirs.
- Analyze a simulated well test exhibiting composite reservoir behavior to validate the analytical solution to Pressure Transient Analysis during polymer flooding.

1.4 Organization of the Thesis

- A review of several published literatures on the flow behavior of non-Newtonian power law fluids.
- The mathematical models for cases of composite reservoir – the homogeneous and NFR
- Transient pressure and pressure derivative type-curves for a two-region radial infinite composite reservoir.
- The TDS procedure for analyzing the simulated well test data used and obtaining the various rock and fluid parameters.
- Conclusions and recommendations for further research.

CHAPTER 2

LITERATURE REVIEW

Numerous works have been done on Newtonian and non-Newtonian fluid flow in a porous media. Greater interest however has been on the non-Newtonian fluids. This is partly due to the application of such fluids in secondary and tertiary oil recovery processes such as polymer flooding, as drilling mud, and also due to the non-Newtonian behavior of most reservoir fluids.

Gogarty (1967) did an analysis on the rheological properties of pseudo-plastic fluids (a type of non-Newtonian fluids) in a porous media. He used unconsolidated and consolidated porous media (cores) to develop effective viscosities that are needed to correlate non-Newtonian fluids to the Darcy equation. He also compared the correlation with experimental and theoretical values with the aim of determining a relationship between the average shear rate and frontal velocity in a core. From the experiment, he concluded that at high frontal velocities, the average shear rate varied proportionally to the frontal velocity at a fractional power.

Van Poollen and Jargon (1969) presented equations for the steady – and unsteady-state linear and radial flow of non-Newtonian fluids through porous media. In their paper, they obtained numerical solutions using finite difference techniques for non-Newtonian fluids located at different distances from the wellbore and injected at different rates. They observed that the buildup well data did not exhibit a straight line curve as expected for Newtonian fluids. The injectivity index was identified to increase with increase in rate for the non-Newtonian fluids used. They also validated their results by a computer model study and isochronal field tests. The results were also consistent with those reported by Gogarty (1967).

Ikoku and Ramey (1979) derived a linearized partial differential equation for describing the radial flow of a slightly compressible non-Newtonian power law fluid through a homogeneous porous medium. Their equations were derived using the modified Blake-Kozeny model and the Ostwald de Waele power-law relationship (Savins, 1969). They obtained approximate analytical solutions to the equation by considering constant rate injection in an infinitely large radial flow system. The solutions provided a new

method of well-test analysis for non-Newtonian fluids injected into reservoirs. These solutions also aided in calculating the effective mobility from the slope of the straight line obtained when pressure drop (Δp) is plotted against time (t^{v}). Ikoku and Ramey (1979) further developed correlations to calculate the radius of investigation and skin.

Odeh and Yang (1979) used the power-law viscosity-shear rate function to derive a partial differential equation for non-Newtonian power law, slightly compressible fluid in porous media. The analytical solution obtained was used to analyze four (field) injection tests. The solution provided new plotting techniques for analyzing injection and falloff test data. Results were used to generate steady state equations of flow, equivalent transient drainage radius, and a method for analyzing isochronal test data.

McDonald (1979) conducted a numerical study using the power-law flow equation of Odeh and Yang. Using three different numerical techniques to solve the non-Newtonian flow equation, he compared the numerical solutions obtained with the analytical results of Odeh and Yang. He found that a finer grid was required to reduce unacceptable truncation error for finite difference simulation of power-law fluids than for black-oil fluids.

Lund and Ikoku (1981) extended the flow of non-Newtonian fluids through a porous media onto composite reservoirs containing non-Newtonian and Newtonian fluids. The paper applied Newtonian/non-Newtonian well test analysis techniques to injectivity and falloff tests in selected wells. It analyzed the effect of fluid parameters and reservoir boundary conditions on the pressure transient behavior. An equation was also presented for calculating reservoir shear rates and non-Newtonian apparent viscosities at reservoir conditions during constant rate of injection.

Murtha and Ertekin (1983) used a numerical finite-difference model to study the flow of a slightly compressible power-law fluid in a vertically fractured reservoir. The study generalized the analytical solutions for non-Newtonian fluids in radial systems and Newtonian fluids in fractured systems using a polar grid approach.

Gencer and Ikoku (1984) analyzed injectivity and falloff test data during two-phase flow of non-Newtonian (power-law) and Newtonian fluids to determine the saturation gradients that can develop.

They considered simultaneous (multiphase) flow of oil and water, and used a two-phase flow model to analyze the transient pressure response of composite reservoir systems. The effects of relative permeability characteristics of the porous media, finite radius of the skin region, skin factor, injectivity time, viscosity of the Newtonian fluid, and rock compressibility on the pressure response were also considered.

Huh and Snow (1985) presented a well testing method which used finite difference numerical approach to solve the non-linear pressure equations instead of linearizing them. The study took into account the polymer concentration distribution in the reservoir and non-Newtonian fluid rheology. It also assumed radial distribution of polymer fluid within the reservoir. The fluid rheology was represented with an adaptation of the Carreau model (Vogel and Pusch, 1981) for apparent viscosity which presented better results compared to the often used power law model.

Ertekin et al (1987) studied the pressure transient behavior of non-Newtonian/Newtonian composite fluid flow in a porous media. Their work however was primarily focused on a porous media with a finite-conductivity vertical fracture. In their paper, they addressed how to determine the location of the flood front using elliptical model, but there was no practical method to demonstrate the usage of their model.

Vongvuthipornchai and Raghavan (1987) used the pressure-derivative method to examine pressure falloff behavior in a reservoir dominated by wellbore storage and skin during non-Newtonian power law fluid injection. They also showed that for certain combinations of skin factor and power-law index, that the effective wellbore radius vanishes.

Olarewaju and Lee (1987) presented a model of a complete characteristic transient response from a composite reservoir. They included the effects of skin, wellbore storage, and phase distribution at the wellbore. The model is analyzed using a history matching approach and the writers demonstrated the effectiveness of their work and pointed out misinterpretations that may arise. Olarewaju and Lee (1989) also presented analytical solutions that interpret pressure transient tests for wells producing from a finite composite reservoir system. These composite reservoirs were described as modelling an injection well in

the early stages of a secondary or tertiary recovery project among which polymer flooding is comprised. Rate solutions and methods for analyzing long-term production data and forecasting production of oil or gas in a finite composite reservoir are also included.

Katime-Meindl and Tiab (2001) applied Tiab's Direct Synthesis (TDS) technique to the case of flow of non-Newtonian fluid through porous media. Pressure and pressure derivative data of a well test data in a homogeneous reservoir are interpreted without the use of type curve matching or regression analysis. The TDS technique is used to interpret pressure behavior for a well in an infinite reservoir and also for well located near a linear boundary. The analysis considered the effect of skin factor and wellbore storage, and equations for calculating mobility and radius from wellbore to the nearest boundary were obtained.

Igbokoyi and Tiab (2007) developed type curves for well test analysis for non-Newtonian fluids in petroleum reservoirs using the analytical solution presented by Ikoku and Ramey (1978). The type curve considered pressure transient data dominated by wellbore storage and skin factor. In addition to the type curve generated, the authors evaluated the same well test data using Tiab Direct Synthesis (TDS) based on the long time solution. The satisfactory answers validated the TDS technique and the type curves developed.

Escobar, Martinez and Montealegre-Madero (2010) utilized the pressure derivative curve in interpreting well test data in reservoirs with non-Newtonian power law fluids. They obtained equations to estimate the permeability, skin factor and non-Newtonian bank radius. The characteristics features found on the pressure and pressure derivative curves enabled the application of Tiab's Direct Synthesis (TDS) technique to their work. The paper considered a finite outer radius and did not account for wellbore storage effects as well as variable rate injection tests.

Jia, Li, and Lu (2015) proposed a well test model for polymer-surfactant flooding and developed a pressure transient response study. Their model considered the physio-chemical properties such as permeability reduction, adsorption, capillary desaturation, polymer in-situ viscosity, relative permeability, and other vital properties. They concluded that the polymer concentration affects the pressure transient

response and that increase in polymer concentration will increase the peak value of the pressure derivative curve and cause a longer wellbore storage and transition regime.

Jia et al. (2015) presented a numerical well test analysis that considers the non-Newtonian effect of polymer solution. They performed studies to quantify effect of shear thinning and polymer concentration on the pressure transient response. Their analysis was done using a two-phase four component fully implicit numerical model based on PEBI (Perpendicular Bisection) grid.

Omotayo and Igbokoyi (2015) presented an analytical technique to interpret pressure falloff tests of these non-Newtonian power law fluids in wells near boundaries in dual-porosity reservoirs. They validated and demonstrated the application of their technique by using it to solve two examples and compared with conventional type-curve matching method.

Alzaabi et al. (2020) designed optimized polymer injectivity tests that explain better about the rheological behavior of polymer solutions and enhance the designs of polymer flood projects. Their work was carried out by varying the bottom-hole pressure (BHP) with rate and time, and results showed the possibility of distinguishing between water and polymer floods based on BHP pressure build-up time.

From the review above, it can be seen that though several models have been developed to interpret pressure tests during polymer flooding and to determine stability of non-Newtonian fluids at reservoir conditions, that analytical solutions to interface boundary conditions have not been investigated thoroughly.

2.1. Rheology of Non-Newtonian Fluids (Polymeric Solutions)

Fluids are classified based on their response to applied stress. While Newtonian fluids such as water, air, and light crude oil have a constant viscosity and obey the Newtonian law of viscous resistance, non-Newtonian fluids have varied viscosity and do not obey the law. These non-Newtonian fluids include emulsions (macro and micro) and polymer solutions.

A polymer is a chemical that is composed of a number of individual molecules that are attached in some manner. Polymer flooding operations use high-molecular-weight organic chemicals to alter the flow of water in the formation. This polymer solutions used are non-Newtonian fluids which are described by Poollen and Jargon (1969) as fluids that the viscosity depends not only on temperature and pressure, but also on the rate of shear applied to them. As such these fluids need to be studied differently from the crude oil which are classified under Newtonian fluids.

According to Ikoku and Ramey (1979), the rheological behavior of the flow of these non-Newtonian fluids through porous media can be divided into regions. At the low shear rates, the apparent viscosity approaches a maximum limiting value. For a large range of shear rates, the fluid is pseudoplastic (shear-thinning fluids without yield stress) and the apparent viscosity decreases with increasing application of shear rate. At high shear rates, there is a minimum limiting apparent viscosity. Most polymer solutions are shear thinning fluids.

Some of the rheological models that represent non-Newtonian fluids include the Bingham model, Robertson and Stiff model, and the Ostwald de Waele power law model. The Ostwald de Waele power law is a relationship that expresses steady state shear stress as a function of velocity gradient (Rajput, 2011). It is given as:

$$\tau = A\gamma^{n} \tag{2.1}$$

The equation is also written logarithmically as:

$$log\,(\tau) = \log A + n\log\,(\dot{\gamma}) \tag{2.2}$$

The apparent viscosity is expressed as

$$\eta = \frac{\tau}{\gamma} \tag{2.3}$$

Combining this with the Oswald de Waele equation, we obtain a generally power law equation for the apparent viscosity:

$$\mu_{app} = A\dot{\gamma}^{n-1} \tag{2.4}$$

Where τ = shear stress

μ = dynamic viscosity, and

γ = shear rate

A= power-law index

n = power law co-efficient

A rheological flow curve illustrates the variation in the plot of shear stress versus shear rate.

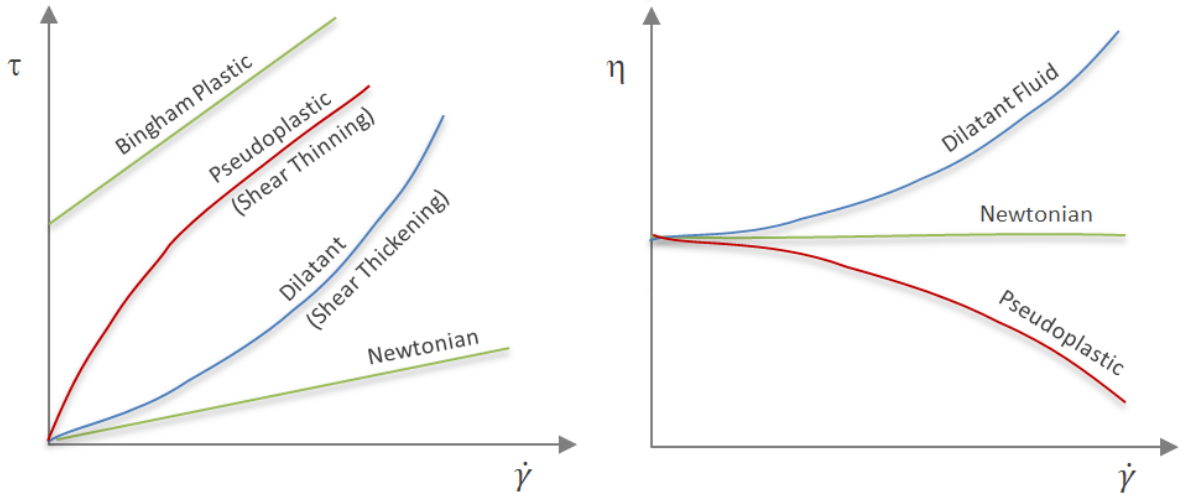

Figure 2.1: An illustration of the rheological flow curve showing the variation in the plot of shear stress versus shear rate for different fluid types.

When n which is the flow index is less than 1 ($0 < n < 1$), the fluid is known as pseudo-plastics and when n is greater than 1 ($n > 1$), the fluid is dilatant. For a Newtonian fluid, the shear viscosity becomes A, n becomes 1, the slope of the curve is constant, and the relationship is expressed as $\tau = \mu\gamma$

The logarithmic lot of τ against γ for pseudo plastics is often linear over a wide range of shear rates. The n is seen to be the slope of the log plot and A (the consistency index) is the intercept on the τ axis at unit shear rate.

Tariq Fariss (1984) gave a porous medium as an innumerable flow constrictions and expansions with interconnecting curved pore channels often characterized by its average properties such as porosity,

permeability, etc. A porous media can be consolidated such as in naturally occurring rocks, or unconsolidated. For flow of Newtonian fluids through a porous media, the law used primarily to describe it is the Darcy's law which is given as (Savins, 1969)

$$v(x,t) = -\frac{k}{\mu_{app}}\frac{\partial p(x,t)}{\partial x}, \text{ and} \tag{2.5}$$

$$\frac{k}{\mu_{app}} = \lambda_{app} \tag{2.6}$$

The review of these petroleum literature shows that although significant interest has been on Non-Newtonian fluids and Non-Newtonian/Newtonian fluid flow through porous media, not much work has been done in developing an analytical solution for its pressure transient analysis. This study attempts to successfully provide an analytical solution to the pressure transient analysis for non-Newtonian/Newtonian fluids composite reservoirs.

CHAPTER 3

POWER-LAW RADIAL FLOW MODEL FOR HOMOGENEOUS AND NATURALLY FRACTURED RESERVOIR SYSTEMS

This chapter shows the step-by-step analysis utilized for developing the mathematical model for pressure transient behavior of power law fluids in single region homogeneous and naturally fractured reservoirs.

3.1 Homogeneous System for a Linearized non – Newtonian Fluid Flow Model

3.1.1 Model Assumptions

1. Fluid flow into the wellbore is radial

2. Laminar and Darcy's flow is valid

3. Isothermal, single phase and slightly compressible fluid with constant properties

4. Homogenous and isotropic system

5. Pseudoplastic (shear-thinning) fluid obeys Ostwald de Waele power-law relationship

6. Steady state effective viscosity

7. Infinite-acting behavior is experienced

3.1.2 Dimensionless Mathematical Model Development

The linearized dimensionless partial differential equation for radial flow of non – Newtonian fluids through a porous media was presented by Ikoku and Ramey (1978) as

$$\frac{\partial^2 P_D}{\partial r_D^2} + \frac{n}{r_D}\frac{\partial P_D}{\partial r_D} = r_D^{1-n}\frac{\partial P_D}{\partial t_D}, t_D > 0 \quad (3.1)$$

Where,

$$P_D = \frac{P - P_i}{\left(\frac{q}{2\pi h}\right)^n \left(\frac{\mu_{eff} r_w^{1-n}}{k_r}\right)} \quad (3.2)$$

$$t_D = \frac{t}{Gr_w^{3-n}} \tag{3.3}$$

$$G = \frac{n\varphi c_t \mu_{eff}}{k_r}\left(\frac{2\pi h}{q}\right)^{1-n} \tag{3.4}$$

$$C_D = \frac{C}{2\pi h n \varphi c_t r_w^2} \tag{3.5}$$

The dimensionless initial and boundary conditions are:

1. Initial condition:

$$P_D(r_D, 0) = 0 \tag{3.6}$$

2. Inner boundary condition:

$$C_D \frac{\partial P_{wD}}{\partial t_D} - \left(r_D \frac{\partial P_D}{\partial r_D}\right)_{r_D=1} = 1 \ (Wellbore\ storage) \tag{3.7}$$

$$P_{wD} = P_D - \left(sr_D \frac{\partial P_D}{\partial r_D}\right)_{r_D=1}, t_D > 0 \ (Skin\ effect) \tag{3.8}$$

3. Outer boundary condition

$$P_D(r_D, t_D)_{r_D \to \infty} = 0 \ (Infinite\ system) \tag{3.9}$$

In Laplace space, the equation (3.1) becomes

$$\frac{\partial^2 \bar{P}}{\partial r_D^2} + \frac{n}{r_D}\frac{\partial \bar{P}}{\partial r_D} = r_D^{1-n} z\bar{P}, t_D > 0 \tag{3.10}$$

The solution of the above equation in Laplace space as given by Ikoku and Ramey (1978) is achieved for the constant injection rate in an infinite reservoir as:

$$\bar{P}(r_D, z) = \frac{r_D^{\frac{v}{\beta}} K_V\left(\beta\sqrt{z}\, r_D^{\frac{1}{\beta}}\right)}{z\{\sqrt{z}K_\beta(\beta\sqrt{z})\}} \tag{3.11}$$

At the wellbore and considering skin factor, the solution is:

$$\bar{P}(r_D = 1, z) = \frac{K_V(\beta\sqrt{z}) + s\sqrt{z}K_\beta(\beta\sqrt{z})}{z\{\sqrt{z}K_\beta(\beta\sqrt{z}) + s\sqrt{z}K_\beta(\beta\sqrt{z})]\}} \tag{3.12}$$

Incorporating wellbore storage and skin, it becomes

$$\bar{P}(r_D = 1, z) = \frac{K_V(\beta\sqrt{z}) + s\sqrt{z}K_\beta(\beta\sqrt{z})}{z\{\sqrt{z}K_\beta(\beta\sqrt{z}) + zC_D[K_V(\beta\sqrt{z}) + s\sqrt{z}K_\beta(\beta\sqrt{z})]\}} \tag{3.13}$$

Where, $v = \frac{1-n}{3-n}$ (3.14)

$$\beta = \frac{2}{3-n} \tag{3.15}$$

For Newtonian fluid (n=1), when v=0, β=1 and s=0 and C_D=0 the equation for an infinite reservoir system becomes

$$\overline{P_{wD}}(r_D = 1, z) = \frac{I_0(\sqrt{z})K_1(\sqrt{z}r_{eD}) + K_0(\sqrt{z})I_1(\sqrt{z}r_{eD})}{z\{\sqrt{z}[K_1(\sqrt{z})I_1(\sqrt{z}r_{eD}) - I_1(\sqrt{z})K_1(\sqrt{z}r_{eD})]\}} \tag{3.16}$$

Igbokoyi and Tiab (2007) presented the following analytical Laplace space inversion solution for skin and wellbore storage dominated flow in infinite system.

$$P_{wD}(1, t_D) = \frac{(3-n)^{\frac{2(1-n)}{3-n}}}{(1-n)\Gamma(\frac{2}{3-n})} t_D^{\frac{1-n}{3-n}} - \frac{1}{1-n} + S \tag{3.17}$$

The pressure derivative of the long time solution for a non-Newtonian fluid is given as:

$$t_D * P'_{wD} = \frac{(3-n)^{\left(\frac{1-n}{3-n}\right)}}{\Gamma\left(\frac{2}{3-n}\right)} t_D^{\left(\frac{1-n}{3-n}\right)} \tag{3.18}$$

3.1.3 Development of Type Curves

This section presents procedures used to develop the type curves. The equation (3.17) developed above were inverted using the Stehfest algorithm (1970). Dimensionless pressures were computed on MATLAB simulation platform for different values of flow behavior index, skin factor, and dimensionless wellbore storage. Then the pressure and pressure derivative type curves were developed. The dimensionless pressure for the case of S = 0 and C_D = 0 for some values of flow behavior index is computed and compared with the results of Ikoku and Ramey (1978). Once a perfect match is obtained, the dimensionless pressure and pressure derivative type curves were then generated for the case S ≠ 0 and $C_D \neq 0$.

3.1.4 Type curves

A summary of the developed type curves is given below. Figure 3.1 shows the pressure and pressure derivative for different values of flow behavior index at S = C_D = 0. From the graph, it is

observed that during radial flow regime, Non-Newtonian fluids exhibit a pressure derivative curve that is inclined. This is opposed to that of a Newtonian flow which is horizontal. Also, the smaller the value of the flow behavior index, the more steep the inclination of the derivative curve.

Figures 3.2-3.5 are the curves for various values of flow behavior index each showing the pressure and pressure derivatives for skin factor S = 0-10 and wellbore storage, C_D = 0-10. The plots (Figures 3.2-3.5) validate the solution given in this work since they match the results of Ikoku and Ramey (1969).

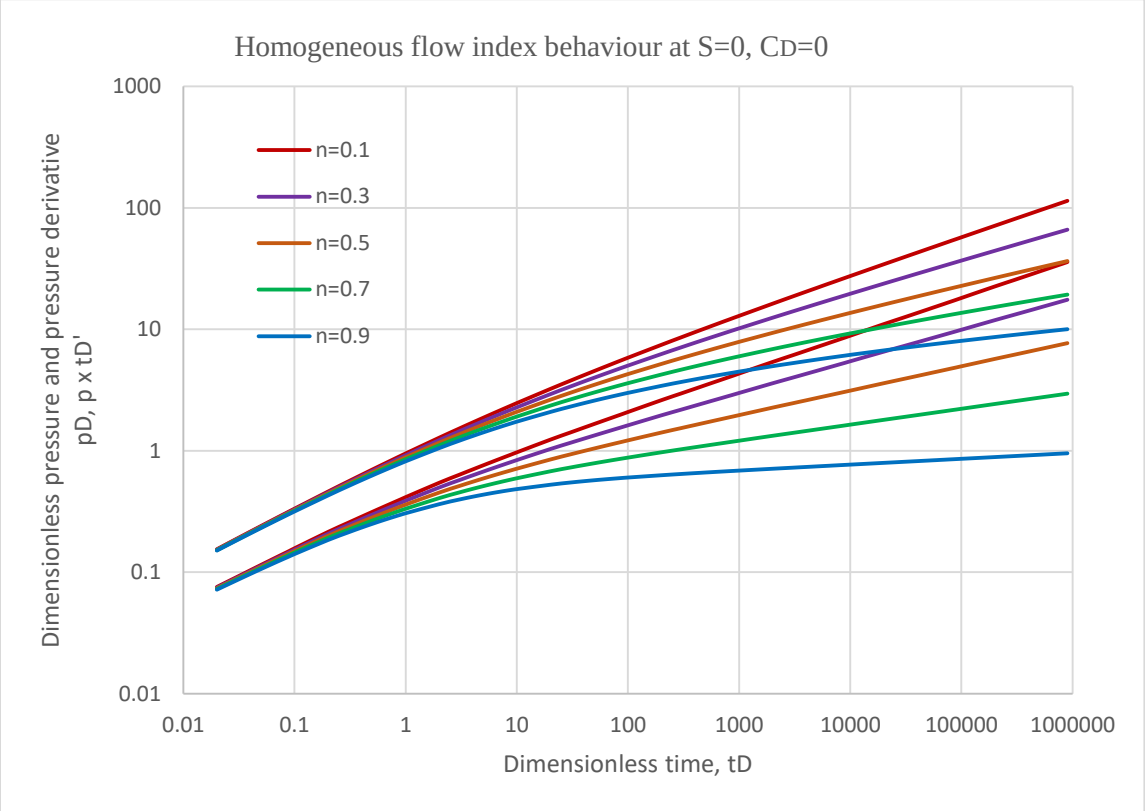

Figure 3.1: Dimensionless pressure and pressure derivative plot of radial flow behavior of power law fluid in homogeneous system for skin = 0 and C_D = 0

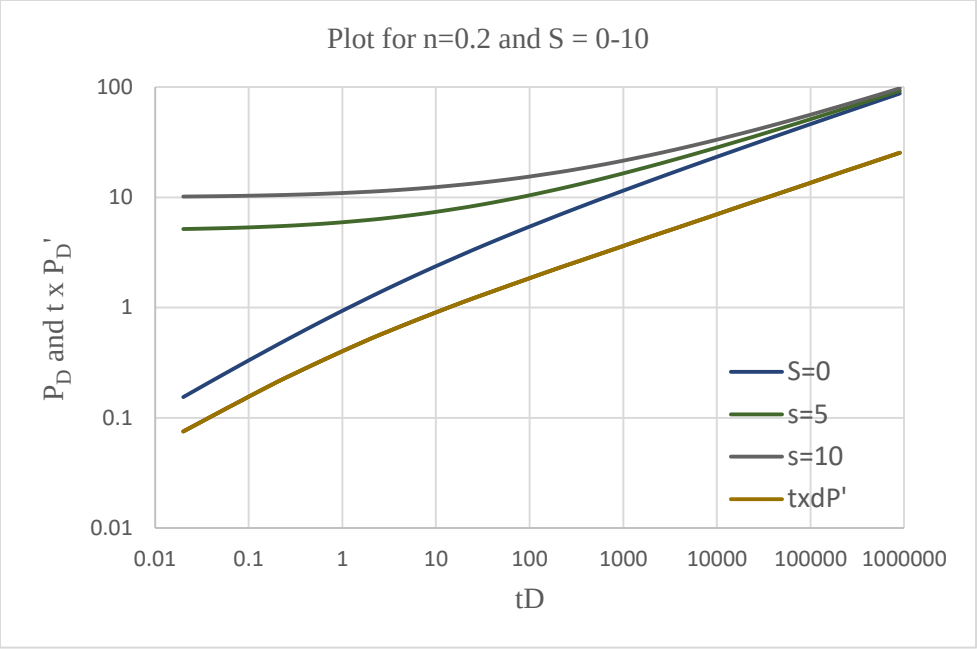

Figure 3.2: Dimensionless pressure and pressure derivative plot of radial flow behavior of power law fluid in homogeneous system for n = 0.2 and S = 0-10

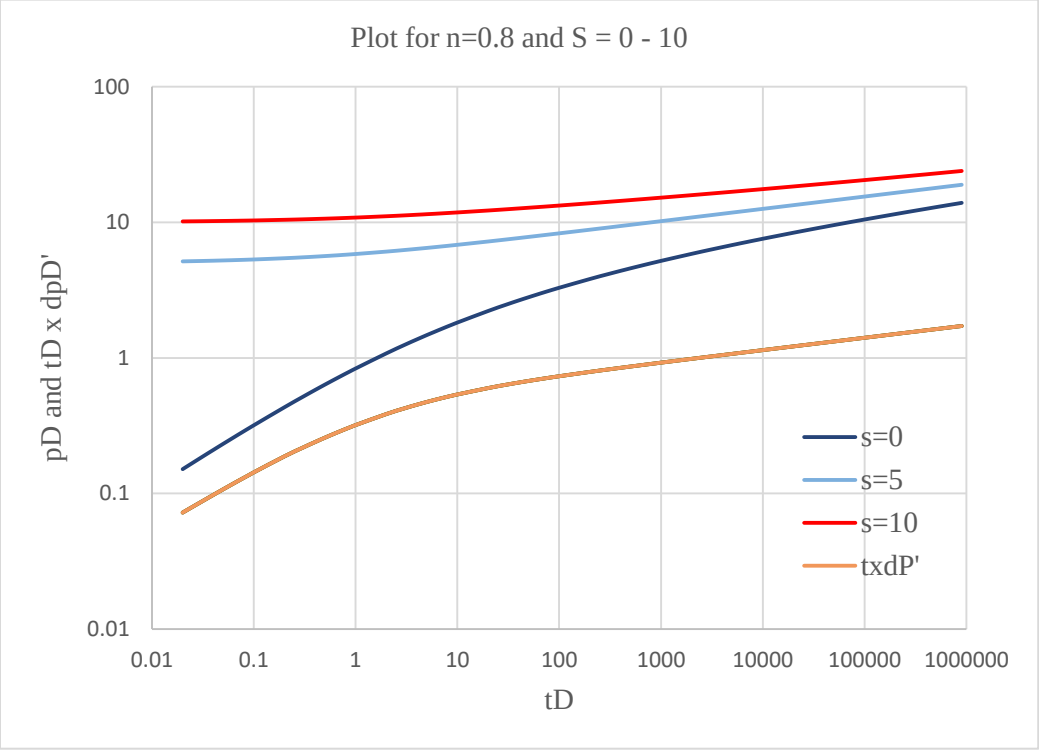

Figure 3.3: Dimensionless pressure and pressure derivative plot of radial flow behavior of power law fluid in homogeneous system for n = 0.8 and S = 0-10

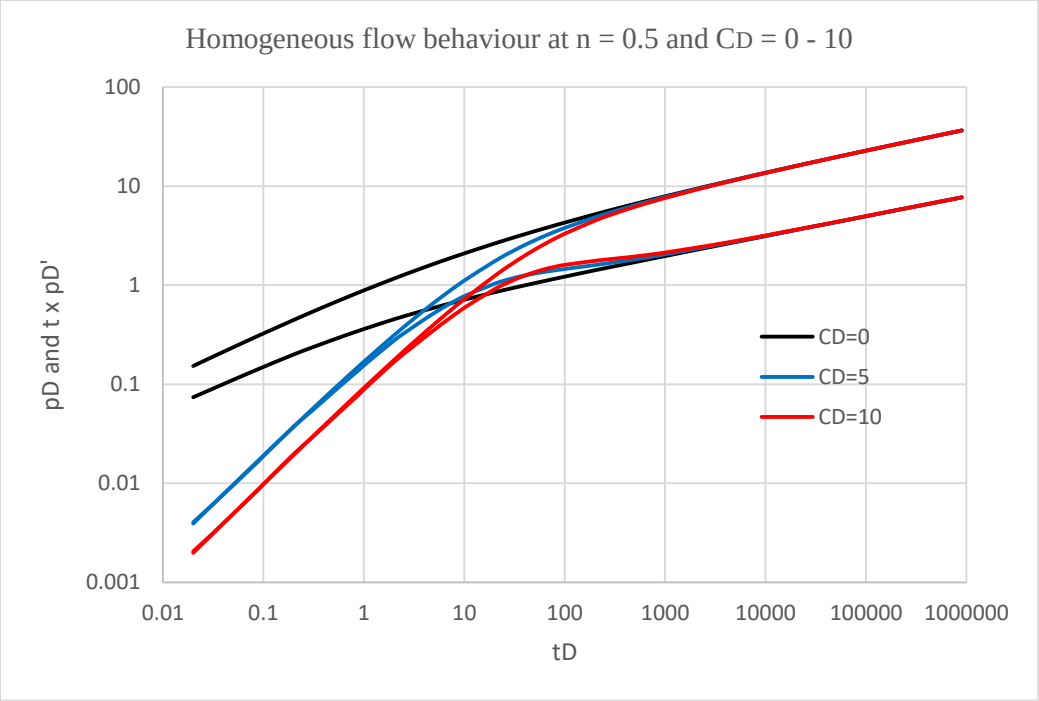

Figure 3.4: Dimensionless pressure and pressure derivative plot of radial flow behavior of power law fluid in homogeneous system for n = 0.5 and C_D = 0-10

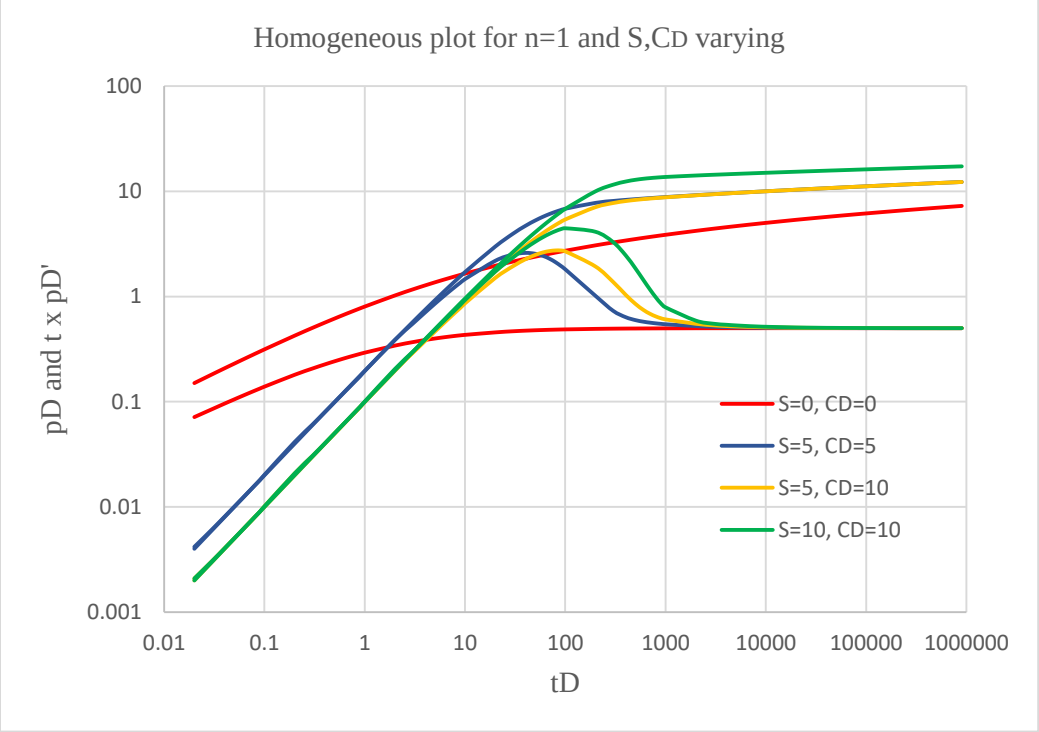

Fig 3.5: Dimensionless pressure and pressure derivative plot of radial flow behavior of power law fluid in homogeneous system for n = 1.0, C_D = 0 - 10 and S = 0-10

3.2 Naturally Fractured Reservoir

A naturally fractured reservoir is a heterogeneous system comprising of vugs, fractures, and matrix in a random distribution. Warren and Root (1963) analyzed such a system by using two major dimensionless parameters which are the inter-porosity flow parameter, λ, and the dimensionless storage capacity ratio, ω.

This section outlines stepwise method of developing mathematical model for pressure transient behavior of power-law fluids in Naturally Fractured Reservoir including the mathematical model assumptions.

3.2.1 Model Assumptions

- Steady state effective viscosity
- Homogenous Isotropic formation (matrix and fracture each has uniform properties)
- Slightly compressible isothermal fluid with single phase flow in both the matrix and fracture
- Reservoir is at the same initial reservoir pressure at time t = 0
- Radial fluid flow into the wellbore
- Fracture provides the essential permeability of fluid flow into the wellbore
- Darcy's law is valid for fluid flow near the wellbore
- Pseudo-steady state inter-porosity fluid (Warren and Root model).

3.2.2 Model Development

The continuity partial differential equations for power law fluid flow through the fracture and matrix in NFR are given as

$$\frac{\partial^2 P_{fD}}{\partial r_D^2} + \frac{1}{r_D}\frac{\partial P_{fD}}{\partial r_D} = (1-\omega)\frac{\partial P_{fD}}{\partial t_D} + \omega\frac{\partial P_{fD}}{\partial t_D} \tag{3.19}$$

$$(1-\omega)\frac{\partial P_{mD}}{\partial t_D} = \lambda(P_{fD} - P_{mD}) \tag{3.20}$$

Where ω and λ are the storativity ratio and inter-porosity flow parameter respectively and are given as:

$$\omega = \frac{(\varphi c_t)_f}{(\varphi c_t)_f + (\varphi c_t)_m} \tag{3.21}$$

$$\lambda = \alpha \frac{k_m}{k_f} \frac{r_w^2}{x_m^2} \tag{3.22}$$

$\varphi_f = fracture\ porosity, \varphi_m = matrix\ porosity, c_m = matrix\ compressibility$

$c_f = fracture\ compressibility$

The linearized dimensionless PDE for radial flow of non-Newtonian fluids for the infinite-acting NFR systems is presented by Omosebi and Igbokoyi (2015) in Laplace form as:

$$\frac{\partial^2 \bar{P}_D}{\partial r_D^2} + \frac{n}{r_D} \frac{\partial \bar{P}_D}{\partial r_D} - r_D^{1-n} z f(z) \overline{P_D} = 0 \tag{3.23}$$

Initial condition:

$$P_{fD}(r_D, 0) = P_{mD}(r_D, 0) = 0 \tag{3.24}$$

Outer boundary condition (infinite reservoir):

$$P_{fD}(r_D \to \infty, t_D) = 0 \tag{3.25}$$

The wellbore storage condition is:

$$c_D \frac{\partial P_{fwD}}{\partial t_D} - \left(\frac{\partial P_{fD}}{\partial r_D}\right)_{r_D} = 1 \tag{3.26}$$

Where

$$c_D = \frac{c}{2\pi h(\varphi_f c_f + \varphi_m c_m) r_w^2} \tag{3.27}$$

The skin effect condition is:

$$P_{fwD} = P_{fD} - S\left(\frac{\partial P_{fD}}{\partial r_D}\right) \tag{3.28}$$

And the Laplace space wellbore pressure solution of radial flow behavior of power law fluid in NFR incorporating skin and wellbore storage effect is written as:

$$\bar{P}_{fwD}(1, z) = \frac{K_V\left(\beta\sqrt{zf(z)}\right) + s\left(\sqrt{zf(z)}\right) K_\beta\left(\sqrt{\beta z f(z)}\right)}{z\left[\sqrt{zf(z)} K_\beta\left(\beta\sqrt{zf(z)}\right) + z c_D \left(K_V\left(\beta\sqrt{zf(z)}\right) + S\sqrt{zf(z)} K_\beta\left(\beta\sqrt{zf(z)}\right)\right)\right]} \tag{3.29}$$

Where:

$$f(z) = \frac{\omega(1-\omega)z+\lambda}{(1-\omega)z+\lambda} \tag{3.30}$$

And z= Laplace space variable

Inverting the solution and at r_D=1, we have the real solution (Omosebi & Igbokoyi, 2015) as:

$$P_{wD}(1,t_D) \approx \left(\frac{\beta}{2}\right)^{\beta-v} \frac{1}{\Gamma(\beta)}\left[\frac{t_D^v}{v} + f_{\omega,\lambda}t_D^{-\beta}\right] - (\beta - v)f_{\omega,\lambda}\left(\frac{\beta}{2}\right)^{\beta-v}\frac{1}{\Gamma(\beta)}\left[t_D^{-\beta} + \frac{f_{\omega,\lambda}\Gamma(v)t_D^{-(\beta+1)}}{\Gamma(\beta)}\right] - \frac{1}{v}\left(\frac{\beta}{2}\right)^{\beta-v} \tag{3.31}$$

And the derivative form as

$$t_D * P'_{wD} = \left(\frac{\beta}{2}\right)^{\beta-v}\frac{1}{\Gamma(\beta)}\left[t_D^v + \beta f_{\omega,\lambda}t_D^{-\beta}\right] + (\beta - v)f_{\omega,\lambda}\left(\frac{\beta}{2}\right)^{\beta-v}\frac{1}{\Gamma(\beta)}\left[\beta t_D^{-\beta} + (\beta+1)\frac{f_{\omega,\lambda}\Gamma(v)t_D^{-(\beta+1)}}{\Gamma(\beta)}\right] \tag{3.32}$$

Where,

$$f_{\omega,\lambda} = \frac{(1-\omega)^2}{2\lambda} \tag{3.33}$$

Interporosity flow parameter is obtained by substituting the co-ordinates of the minimum point of the trough on a type curve, t_{min} and $(t \times \Delta P')_{min}$ according to Tiab et al (2006). At that point,

$$\lambda = \frac{42.5\mu r_w^2 h(\varphi c_t)_{m+f}}{qB}\frac{(t \times \Delta P_w)_{min}}{(t)_{min}} \tag{3.34}$$

For storage capacity ratio, the method of calculation is obtained using the pressure derivative co-ordinate of the minimum point and the radial flow regime line, according to Tiab et al (2006). It is given as:

$$\omega = 10^{-0.8684\left(1-\left(\frac{(t \times \Delta P_w)_{min}}{(t \times \Delta P_w)_{IARF}}\right)\right)} \tag{3.35}$$

Where λ = interporosity flow parameter

ω= storage capacity ratio

μ= viscosity

φ= porosity

r_w = radius of wellbore

q = flow rate of fluid flow

B = formation factor

t_{min} = minimum point of the trough on a type curve

$(t \times \Delta P')_{min}$ = pressure derivative at minimum point of the trough

The equation assumes that wellbore storage and boundary effects do not affect the trough, and also that the infinite radial flow regime is well defined.

3.2.3 Type Curve Development

The Stefest algorithm (1970) is used to invert the Laplace space solution of radial flow behaviour of power law fluid in NFR. The pressure and pressure derivative type curves are plotted for different flow behaviour index, inter-porosity flow parameters and various dimensionless storage coefficient values at a constant skin and wellbore storage factor.

Figure 3.6 shows the dimensionless pressure and pressure derivative plot for various flow behaviour index (n = 0-1.0) at a constant value of inter-porosity flow parameter (λ = 0.01), dimensionless storage coefficient (ω = 0. 1) and skin factor (S = 0).

The log-log plot of pressure versus time, shows straight line corresponding to the early time and late time. The pressure derivative plot versus time plot, shows a unique finger print of two parallel straight lines common to natural fractures. The first straight line corresponds to the effect of inter-porosity parameter, while the second straight corresponds to the effect of the storage capacity ratio, with a short transition zone in-between.

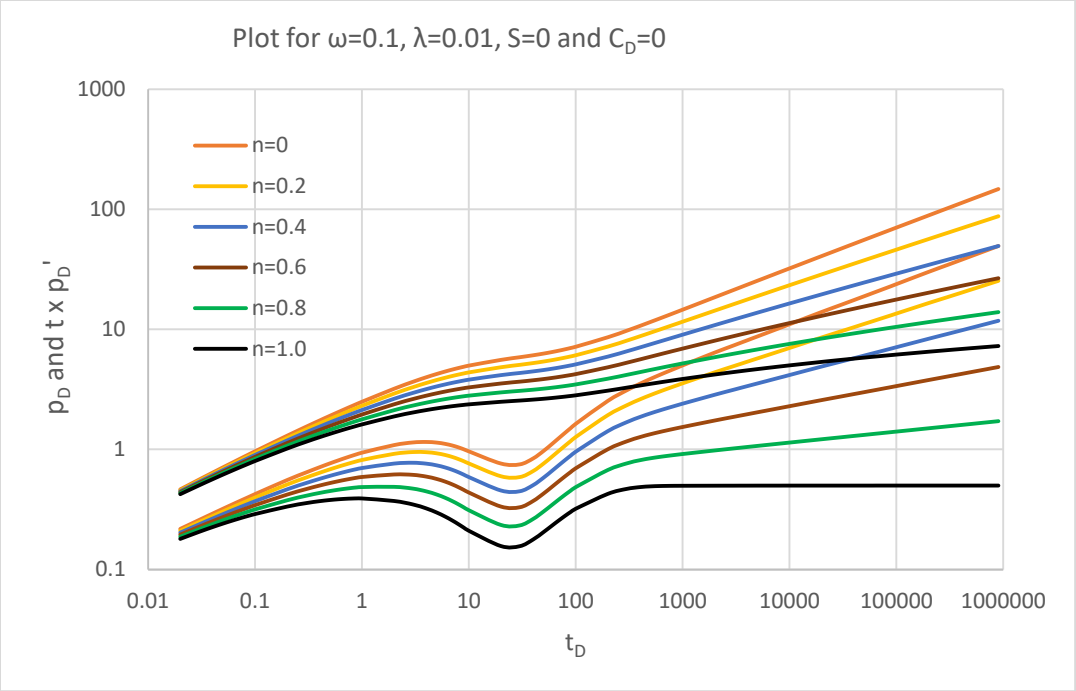

Figure 3.6: Pressure and Pressure derivative plot for radial flow behavior of non-Newtonian fluids in NFR. (Skin=0, lambda=0.01, omega=0.1)

Figures 3.7-3.8 show the pressure and pressure derivative plots for different values of inter-porosity flow parameter (λ = 0.000001-10.0) at varying skin, while other parameters are kept constant. From the plots, as the value of λ decreases, the curves of pressure derivatives shifted to the right. The low λ value suggests that fracture depletion takes a while before transition sets in.

Figures 3.9 – 3.10 follow the same trend for various values of storage co-efficient (ω =0.001-1) at a flow behaviour index of 0.4 and an inter-porosity flow parameter of 0.0001. The depth of the trough for the pressure dervivative curve is seen to increase with decrease in storativity ratio and the transition zone also widened. This is because for a high storativity ratio, the storage capacity of the fracture is high and so, the depletion takes longer before a transition starts. For ω = 1, the trough is not evident as the storativity ratio approaches one at that point. This makes the dual porosity in the NFR to be replaced by single porosity and so becomes a homogeneous formation.

Figures 3.11 and 3.12 show the values for varying skin and wellbore storage effect respectively while other parameters remain constant. The wellbore storage is considerably known for hiding the early radial flow regime. The pressure derivative curve for Figure 3.11 for the varying skin values is seen to be same while the pressure curves increased with increase in skin factor.

These figures all agree with literature on naturally fractured reservoirs (Tiab et al., 2006,and Tiab & Igbokoyi, 2007).

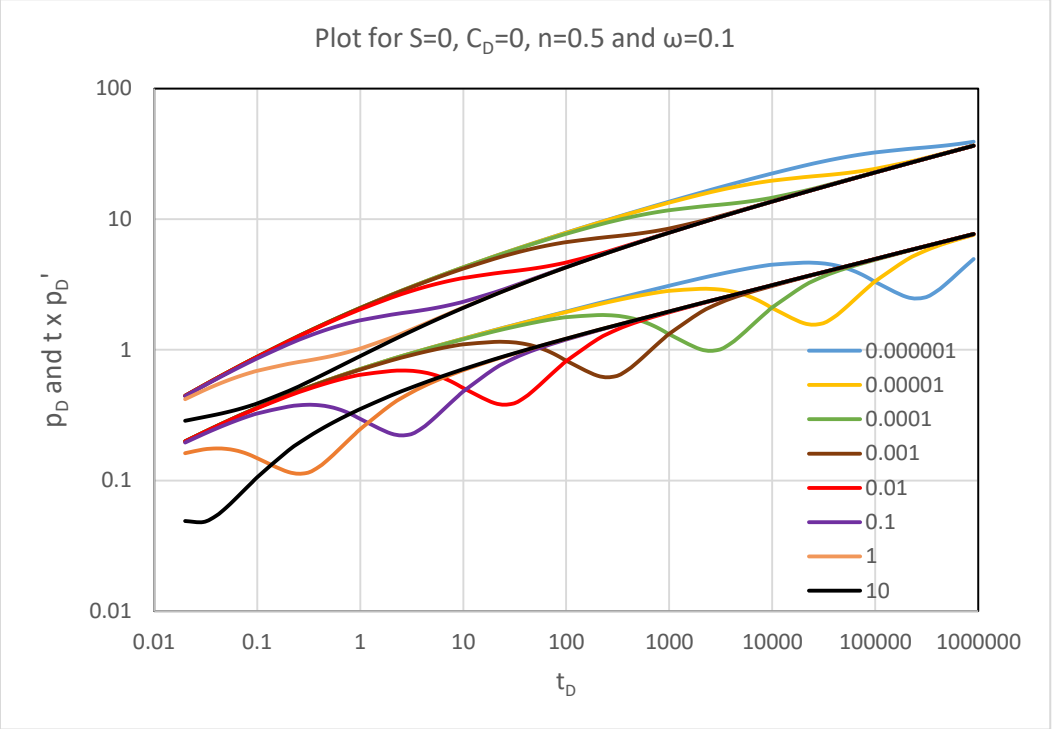

Figure 3.7: Pressure and Pressure derivative plot for radial flow behavior of non-Newtonian fluids in NFR. (Skin = 0, λ = varying, flow index, n = 0.5, ω = 0.1)

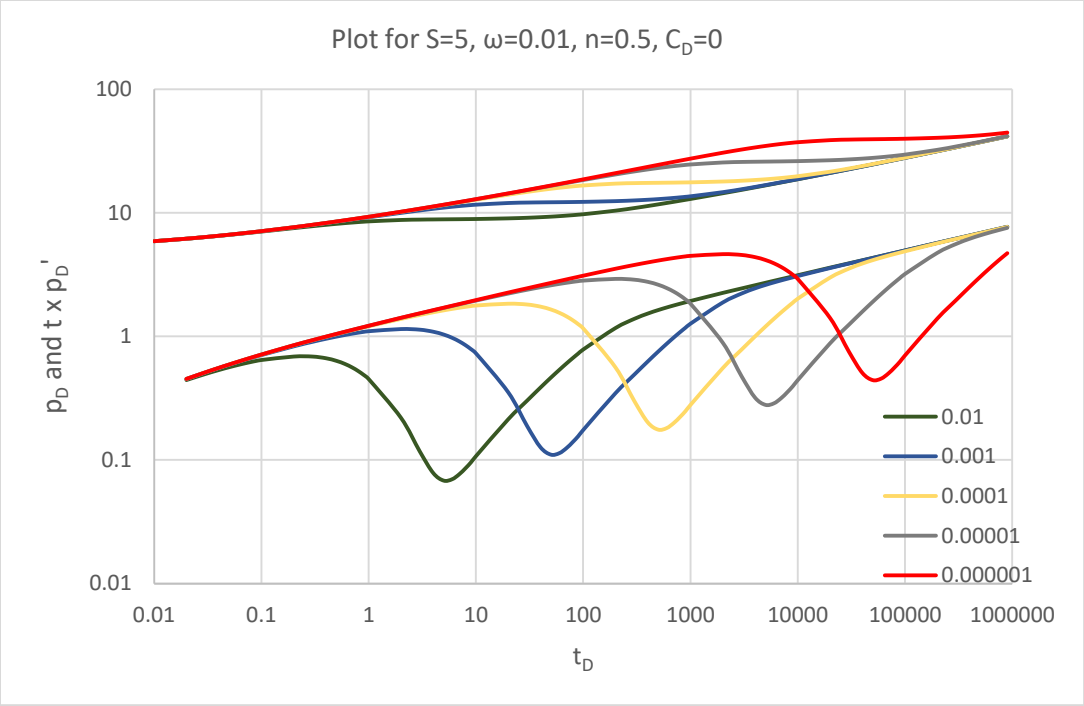

Figure 3.8: Pressure and Pressure derivative plot for radial flow behavior of non-Newtonian fluids in NFR. (Skin = 5, C_D = 0, λ = varying, flow index, n = 0.5, ω = 0.01)

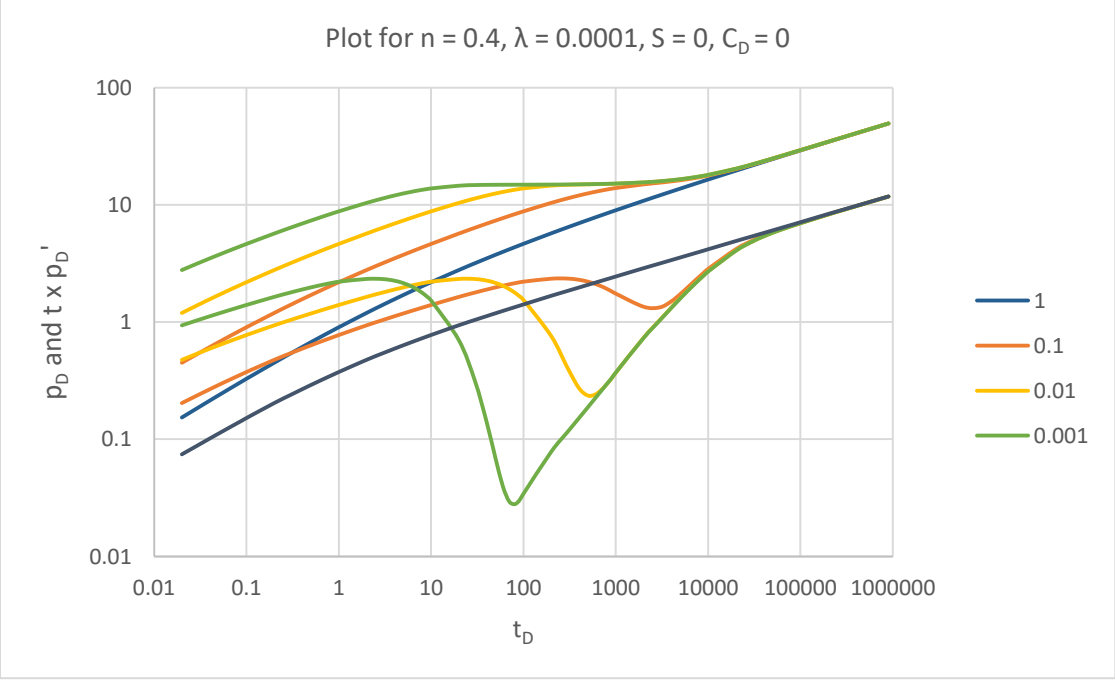

Figure 3.9: Pressure and Pressure derivative plot for radial flow behavior of non-Newtonian fluids in NFR. (Skin=0, C_D=0, lambda=0.0001, omega=varying, n=0.4)

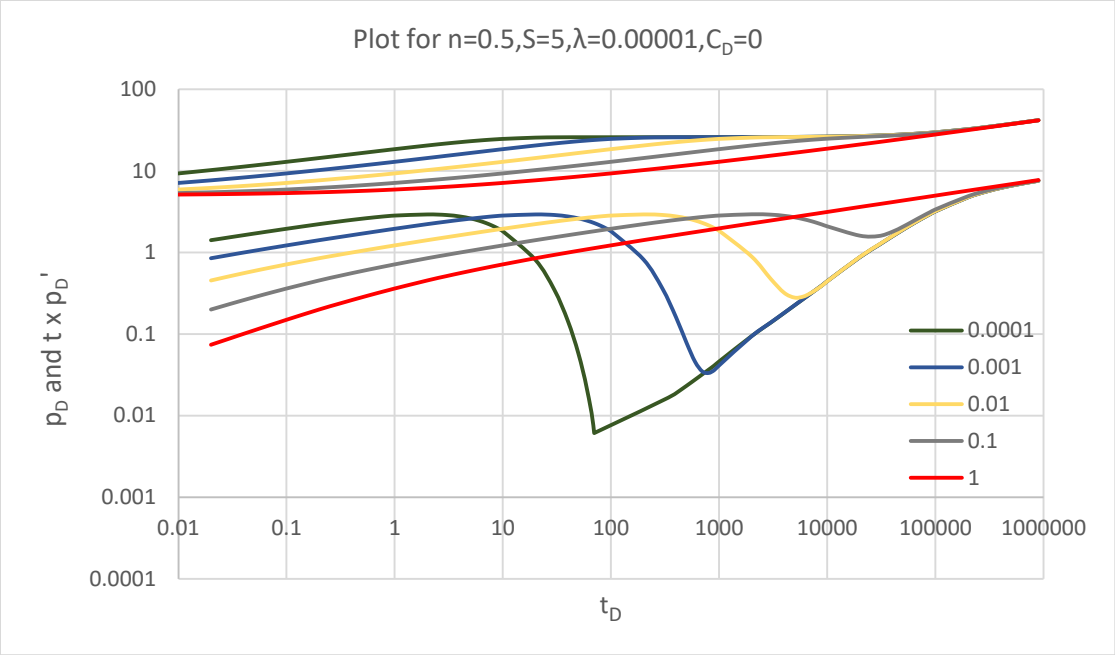

Figure 3.10: Pressure and Pressure derivative plot for radial flow behavior of non-Newtonian fluids in NFR. (Skin=5, C_D=0, lambda=0.00001, omega=varying, n=0.5)

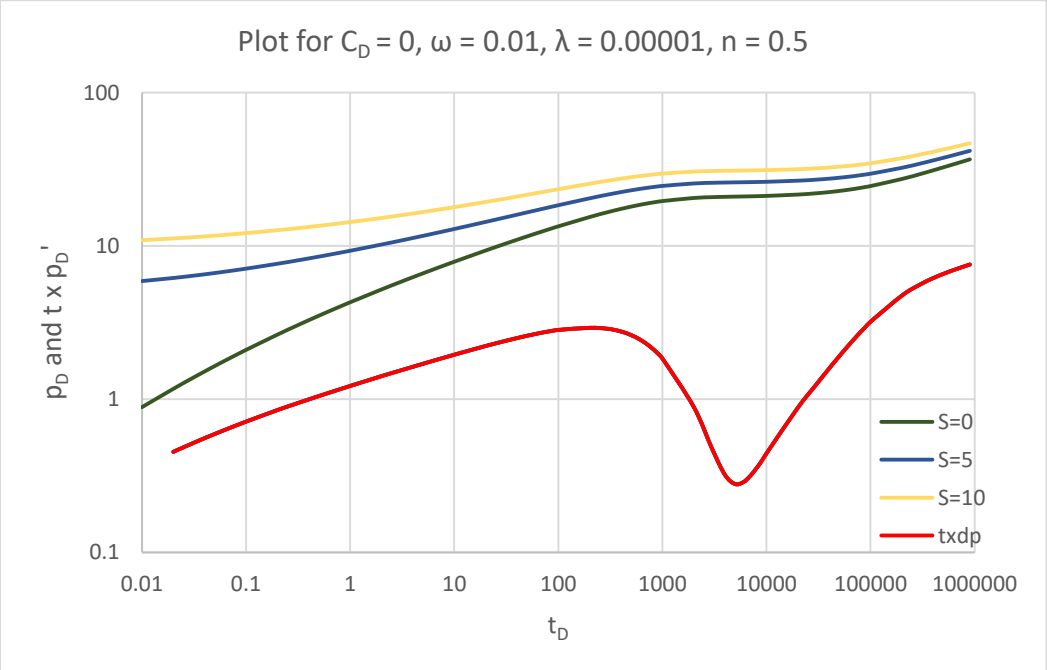

Figure 3.11: Pressure and Pressure derivative plot for radial flow behavior of non-Newtonian fluids in NFR. (Skin varying, C_D=0, lambda=0.00001, omega=0.01, n=0.5)

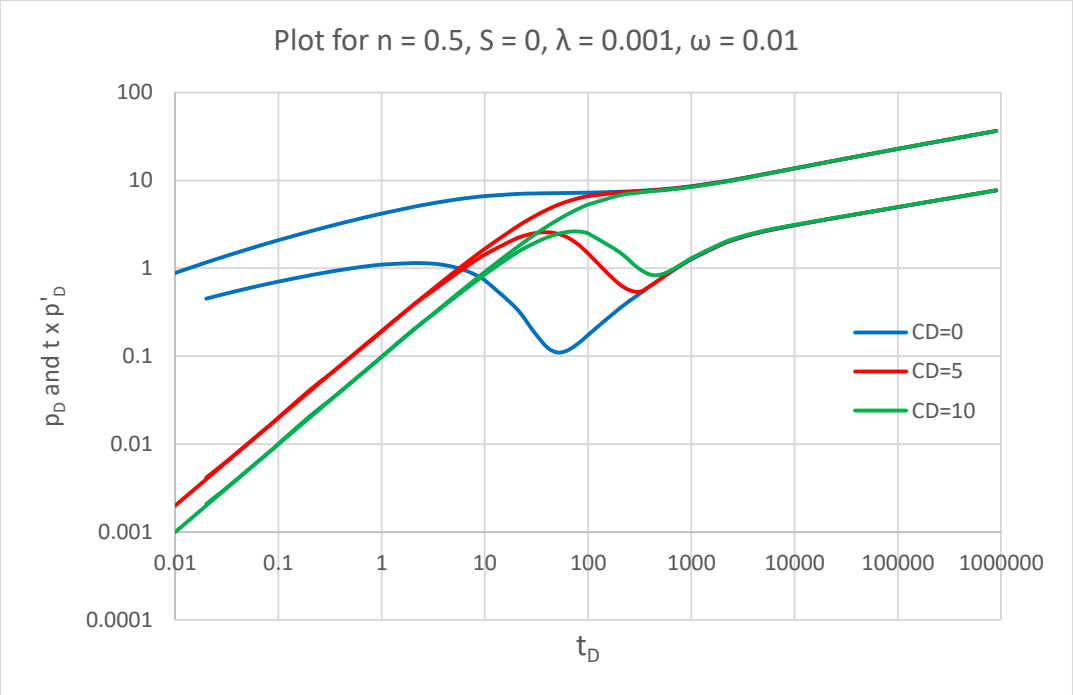

Figure 3.12: Pressure and Pressure derivative plot for radial flow behavior of non-Newtonian fluids in NFR. (Skin = 0, C_D = 0 - 10, λ = 0.001, ω = 0.01, n = 0.5)

CHAPTER 4

NON-NEWTONIAN/NON-NEWTONIAN COMPOSITE RADIAL FLUID FLOW IN A TWO-REGION, HOMOGENEOUS, AND NATURALLY FRACTURED RESERVOIR

This chapter shows the step-by-step analysis utilized for developing the mathematical model for pressure transient behavior of power law fluids in homogeneous and naturally fractured reservoirs.

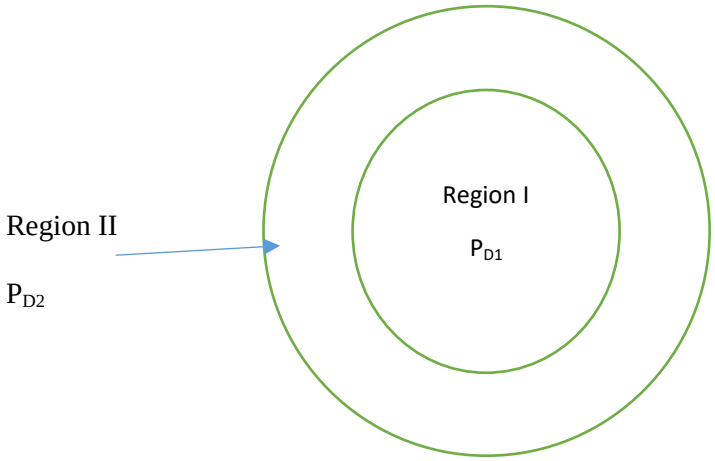

Figure 4.1: A schematic diagram of a two-region radial composite reservoir.

4.1 Homogeneous System for a Linearized non – Newtonian/non-Newtonian Fluid Flow Model

In this section, a mathematical model for a two-region, radial composite reservoir with wellbore storage and skin at the active (injection) well is presented.

4.2 Model Assumptions

1. Fluid flow in the wellbore is radial
2. Laminar and Darcy's flow is valid
3. Isothermal, single phase and slightly compressible fluid with constant properties in each region
4. Homogenous and isotropic system
5. Pseudoplastic (shear-thinning) fluid obeys Ostwald de Waele power-law relationship

6. Steady state effective viscosity

7. Infinite-acting behavior is experienced in outer boundary

4.3 Mathematical Development for Non-Newtonian/Non-Newtonian Fluid Flow

The linearized partial differential equation and dimensionless form for radial flow of non-Newtonian power law fluids in a porous medium for Region I are:

$$\frac{\partial^2 P}{\partial r^2} + \frac{n}{r}\frac{\partial P}{\partial r} = Gr^{1-n}\frac{\partial P}{\partial t} \tag{4.1}$$

$$\frac{\partial^2 P_{D1}}{\partial r_D^2} + \frac{n}{r_D}\frac{\partial P_{D1}}{\partial r_D} = r_D^{1-n}\frac{\partial P_{D1}}{\partial t_D}, for\ P_{D1}(1 \le r_D \le R_D) \tag{4.2}$$

For region II, we have:

$$\frac{\partial^2 P_2}{\partial r^2} + \frac{n}{r}\frac{\partial P_2}{\partial r} = G_2 r^{1-n}\frac{\partial P_2}{\partial t}, t > 0 \tag{4.3}$$

$$\frac{\partial^2 P_{D2}}{\partial r_D^2} + \frac{n}{r_D}\frac{\partial P_{D2}}{\partial r_D} = r_w^2 G_2 r_D^{1-n} r_w^{1-n}\frac{\partial P_D}{\partial t} \tag{4.4}$$

Where,

$$P_D = \frac{P - P_i}{\left(\frac{q}{2\pi h}\right)^n \left(\frac{\mu_{eff} r_w^{1-n}}{k_r}\right)} \tag{4.5}$$

$$C_D = \frac{C}{2\pi h n \varphi c_t r_w^2} \tag{4.6}$$

$$t_D = \frac{t}{G_1 r_w^{3-n}} \tag{4.7}$$

$$\partial t_D = \frac{\partial t}{G_1 r_w^{3-n}} \tag{4.8}$$

$$\partial t = G_1 r_w^{3-n}\partial t_D \tag{4.9}$$

$$G_1 = n\left(\frac{\varphi c_t \mu_{eff}}{k}\right)_1 \left(\frac{2\pi h}{q}\right)^{1-n} \tag{4.10}$$

Substituting (4.9) and (4.10) into (4.4), we have:

$$\frac{\partial^2 P_{D2}}{\partial r_D^2} + \frac{n}{r_D}\frac{\partial P_{D2}}{\partial r_D} = \frac{G_2 r_D^{1-n} r_w^{3-n}}{G_1 r_w^{3-n}}\frac{\partial P_{D2}}{\partial t_D} \tag{4.14}$$

$$\frac{\partial^2 P_{D2}}{\partial r_D^2} + \frac{n}{r_D}\frac{\partial P_{D2}}{\partial r_D} = r_D^{1-n}\frac{G_2}{G_1}\frac{\partial P_{D2}}{\partial t_D} \tag{4.15}$$

But,

$$\frac{G_2}{G_1} = \frac{n\left(\frac{\varphi c_t \mu_{eff}}{k}\right)_2 \left(\frac{2\pi h}{q}\right)^{1-n}}{n\left(\frac{\varphi c_t \mu_{eff}}{k}\right)_1 \left(\frac{2\pi h}{q}\right)^{1-n}} = \alpha \tag{4.16}$$

Therefore for region II, the dimensionless diffusivity equation is given as:

$$\frac{\partial^2 P_{D2}}{\partial r_D^2} + \frac{n}{r_D}\frac{\partial P_{D2}}{\partial r_D} = \alpha r_D^{1-n}\frac{\partial P_{D2}}{\partial t_D}, for\ P_{D2}(R_D \leq r_D \leq \infty) \tag{4.17}$$

The boundary conditions in dimensionless form for a radial two-region composite reservoir with non-Newtonian/non-Newtonian fluid are:

Inner boundary conditions:

$$C_D \frac{\partial P_{wD}}{\partial t_D} - \left(r_D \frac{\partial P_D}{\partial r_D}\right)_{r_D=1} = 1\ (Wellbore\ storage) \tag{4.20}$$

$$P_{wD} = P_D - \left(s r_D \frac{\partial P_D}{\partial r_D}\right)_{r_D=1}, t_D > 0\ (Skin\ effect) \tag{4.21}$$

Initial conditions:

$$P_{D1}(r_D, 0) = 0 \tag{4.22}$$

$$P_{D2}(r_D, 0) = 0 \tag{4.23}$$

At wellbore, inner boundary condition:

$$\frac{\partial P_{D1}}{\partial r_D}(1, s) = -\frac{1}{s} \tag{4.24}$$

Outer boundary condition:

$$P_D(r_D, t_D)_{r_D \to \infty} = 0\ (Infinite\ system) \tag{4.25}$$

Solution:

Flow equations for non-Newtonian fluid is given as:

$$q_1 = -2\pi r h \left(\frac{k_1}{\mu_{eff1}}\frac{\partial P_1}{\partial r}\right)^{\frac{1}{n}} \tag{4.26}$$

Taking the derivative of (4.5) with respect to radius r, we have:

$$\frac{\partial P_D}{\partial r} = -\frac{\partial P}{\partial r}\frac{k_1}{\left(\frac{q}{2\pi h}\right)^n \mu_{eff} r_w^{1-n}} \tag{4.27}$$

Re-arranging,

$$\frac{\partial P}{\partial r} = -\left(\frac{q}{2\pi h}\right)^n \frac{\mu_{eff} r_w^{1-n}}{k_1}\frac{\partial P_D}{\partial r} \tag{4.28}$$

Substituting (4.28) into (4.26),

$$q_1 = 2\pi rh\frac{k_1}{\mu_{eff1}B_1}\left[\left(\frac{qB_1}{2\pi h}\right)^n \frac{\mu_{eff}r_w^{1-n}}{k_1}\frac{\partial P_{D1}}{\partial r}\right]^{\frac{1}{n}} \quad (4.29)$$

$$q_1 = 2\pi rh\frac{k_1}{\mu_{eff1}B_1}\frac{qB_1}{2\pi h}\left[\frac{\mu_{eff}r_w^{1-n}}{k_1}\frac{\partial P_{D1}}{\partial r}\right]^{\frac{1}{n}} \quad (4.30)$$

$$q_{D1} = \frac{rk_1}{\mu_{eff1}}\left[\frac{\mu_{eff}}{k_1}\frac{r_w^{1-n}}{r_w}\frac{\partial P_{D1}}{\partial r_D}\right]^{\frac{1}{n}} \quad (4.31)$$

$$q_{D1} = \frac{r_D r_w k_1}{\mu_{eff1}}\left[\frac{\mu_{eff}}{k_1}\frac{r_w^{1-n}}{r_w}\frac{\partial P_{D1}}{\partial r_D}\right]^{\frac{1}{n}} \quad (4.32)$$

$$q_{D1} = \frac{r_D k_1}{\mu_{eff1}}\left[\frac{\mu_{eff}}{k_1}\frac{\partial P_{D1}}{\partial r_D}\right]^{\frac{1}{n}} \quad (4.33)$$

And Region 2:

$$q_2 = 2\pi rh\frac{k_2}{\mu_{eff2}B_2}\left[\left(\frac{qB_1}{2\pi h}\right)^n \frac{\mu_{eff}r_w^{1-n}}{k_1}\frac{\partial P_{D2}}{\partial r}\right]^{\frac{1}{n}} \quad (4.34)$$

$$q_{D2} = \frac{rk_2B_1}{\mu_{eff2}B_2}\left[\frac{\mu_{eff}}{k_1}\frac{r_w^{1-n}}{r_w}\frac{\partial P_{D2}}{\partial r_D}\right]^{\frac{1}{n}} \quad (4.35)$$

$$q_{D2} = \frac{r_D k_2B_1}{\mu_{eff2}B_2}\left[\frac{\mu_{eff}}{k_1}\frac{\partial P_{D2}}{\partial r_D}\right]^{\frac{1}{n}} \quad (4.36)$$

At interface R_D, $q_{D1} = q_{D2}$ and so:

$$\frac{k_1}{\mu_{eff1}}\left[\frac{\mu_{eff}}{k_1}\frac{\partial P_{D1}}{\partial r_D}\right]^{\frac{1}{n}} = \frac{k_2B_1}{\mu_{eff2}B_2}\left[\frac{\mu_{eff}}{k_1}\frac{\partial P_{D2}}{\partial r_D}\right]^{\frac{1}{n}} \quad (4.37)$$

$$\frac{k_1}{\mu_{eff1}B_1}\frac{\mu_{eff2}B_2}{k_2}\left[\frac{\mu_{eff}}{k_1}\frac{\partial P_{D1}}{\partial r_D}\right]^{\frac{1}{n}} = \left[\frac{\mu_{eff}}{k_1}\frac{\partial P_{D2}}{\partial r_D}\right]^{\frac{1}{n}} \quad (4.38)$$

Let $\lambda = \frac{k}{\mu_{eff}B}$

$$\frac{\lambda_1}{\lambda_2}\left[\frac{\mu_{eff}}{k_1}\frac{\partial P_{D1}}{\partial r_D}\right]^{\frac{1}{n}} = \left[\frac{\mu_{eff}}{k_1}\frac{\partial P_{D2}}{\partial r_D}\right]^{\frac{1}{n}} \quad (4.39)$$

$$\left(\frac{\lambda_1}{\lambda_2}\right)^n \frac{\partial P_{D1}}{\partial r_D} = \frac{\partial P_{D2}}{\partial r_D} \quad (4.40)$$

A general Laplace solution for the dimensionless pressure drops in infinite flow for regions I and II is:

Region 1:

$$\bar{P}_{D1}(1 \le r_D \le R_D) = r_D^{\frac{V}{\beta}}\left(C_1 I_V\left(\beta r_D^{\frac{1}{\beta}}\sqrt{sfs}\right) + C_2 K_V\left(\beta r_D^{\frac{1}{\beta}}\sqrt{sfs}\right)\right) \quad (4.41)$$

Region 2:

$$\bar{P}_{D2}(R_D \le r_D \le \infty) = r_D^{\frac{V}{\beta}} C_3 K_V\left(\beta r_D^{\frac{1}{\beta}}\sqrt{\alpha s f s}\right) \tag{4.42}$$

Where C_1, C_2 and C_3 are constants to be defined by boundary conditions.

Differentiating equations 4.41 and 4.42:

$$\frac{\partial \bar{P}_{D1}}{\partial r_D} = r_D^{\frac{V}{\beta}+\frac{1}{\beta}-1}\sqrt{z}\left(C_1 I_\beta\left(\beta\sqrt{z} r_D^{\frac{1}{\beta}}\right) - C_2 K_\beta\left(\beta\sqrt{z} r_D^{\frac{1}{\beta}}\right)\right) \tag{4.43}$$

$$\frac{\partial \bar{P}_{D2}}{\partial r_D} = -r_D^{\frac{V}{\beta}+\frac{1}{\beta}-1}\sqrt{z} C_3 K_\beta\left(\beta\sqrt{z} r_D^{\frac{1}{\beta}}\right) \tag{4.44}$$

Therefore equation (4.37) becomes:

$$\left[\frac{\lambda_1}{\lambda_2}\right]^n R_D^{\frac{V}{\beta}+\frac{1}{\beta}-1}\sqrt{sfs}\left(C_1 I_\beta\left(\beta\sqrt{sfs} R_D^{\frac{1}{\beta}}\right) - C_2 K_\beta\left(\beta\sqrt{sfs} R_D^{\frac{1}{\beta}}\right)\right) =$$

$$-\sqrt{\alpha s f s}\, R_D^{\frac{V}{\beta}+\frac{1}{\beta}-1} C_3 K_\beta\left(\beta\sqrt{\alpha s f s} R_D^{\frac{1}{\beta}}\right) \tag{4.45}$$

And:

$$C_3 = \frac{\theta^n R_D^{\frac{V}{\beta}+\frac{1}{\beta}-1}\left(C_1 I_\beta\left(\beta R_D^{\frac{1}{\beta}}\sqrt{sfs}\right) - C_2 K_\beta\left(\beta R_D^{\frac{1}{\beta}}\sqrt{sfs}\right)\right)}{-\sqrt{\alpha} K_\beta\left(R_D\sqrt{\alpha s f s}\right)} \tag{4.46}$$

Where

$$\theta = \left[\frac{\lambda_1}{\lambda_2}\right] = mobility\ ratio$$

Also, at interface condition $r_D = R_D$, and $\bar{P}_{D1} = \bar{P}_{D2}$

$$\left(C_1 I_V\left(\beta\sqrt{sfs} R_D^{\frac{1}{\beta}}\right) + C_2 K_V\left(\beta\sqrt{sfs} R_D^{\frac{1}{\beta}}\right)\right) = C_3 K_V\left(\beta\sqrt{\alpha s f s} R_D^{\frac{1}{\beta}}\right) \tag{4.47}$$

Substituting the value of C_3 into (4.44) and re-arranging, we have:

$$C_1 A = C_2 B \tag{4.48}$$

Where:

$$A = \frac{I_V\left(\beta R_D^{\frac{1}{\beta}}\sqrt{sfs}\right)\sqrt{\alpha} K_\beta\left(\beta R_D^{\frac{1}{\beta}}\sqrt{\alpha s f s}\right) + \left[\frac{\lambda_1}{\lambda_2}\right]^n I_\beta\left(\beta R_D^{\frac{1}{\beta}}\sqrt{sfs}\right) K_V\left(\beta R_D^{\frac{1}{\beta}}\sqrt{\alpha s f s}\right)}{K_V\left(\beta R_D^{\frac{1}{\beta}}\sqrt{\alpha s f s}\right)\sqrt{\alpha} K_\beta\left(\beta R_D^{\frac{1}{\beta}}\sqrt{\alpha s f s}\right)} \tag{4.49}$$

$$B = \frac{K_V\left(\beta R_D^{\frac{1}{\beta}}\sqrt{sfs}\right)\sqrt{\alpha}K_\beta\left(\beta R_D^{\frac{1}{\beta}}\sqrt{\alpha sfs}\right)+\left[\frac{\lambda_1}{\lambda_2}\right]^n K_\beta(\beta R_D^{\frac{1}{\beta}}\sqrt{sfs})K_V\left(\beta R_D^{\frac{1}{\beta}}\sqrt{\alpha sfs}\right)}{K_V\left(\beta R_D^{\frac{1}{\beta}}\sqrt{\alpha sfs}\right)\sqrt{\alpha}K_\beta\left(\beta R_D^{\frac{1}{\beta}}\sqrt{\alpha sfs}\right)} \quad (4.50)$$

Therefore:

$$C_2 = C_1\frac{A}{B}$$

$$C_2 = C_1\frac{I_V\left(\beta R_D^{\frac{1}{\beta}}\sqrt{sfs}\right)\sqrt{\alpha}K_\beta\left(\beta R_D^{\frac{1}{\beta}}\sqrt{\alpha sfs}\right)+\left[\frac{\lambda_1}{\lambda_2}\right]^n I_\beta(\beta R_D^{\frac{1}{\beta}}\sqrt{sfs})K_V\left(\beta R_D^{\frac{1}{\beta}}\sqrt{\alpha sfs}\right)}{K_V\left(\beta R_D^{\frac{1}{\beta}}\sqrt{sfs}\right)\sqrt{\alpha}K_\beta\left(\beta R_D^{\frac{1}{\beta}}\sqrt{\alpha sfs}\right)+\left[\frac{\lambda_1}{\lambda_2}\right]^n K_\beta(\beta R_D^{\frac{1}{\beta}}\sqrt{sfs})K_V\left(\beta R_D^{\frac{1}{\beta}}\sqrt{\alpha sfs}\right)} \quad (4.51)$$

At the wellbore, $r_D = 1$ and dimensionless pressure gradient at the wellbore is given as:

$$\bar{P}'_{D1}(r_D = 1) = \sqrt{sfs}\left(C_1 I_\beta\left(\beta\sqrt{sfs}\right) - C_2 K_\beta\left(\beta\sqrt{sfs}\right)\right) = -\frac{1}{s} \quad (4.52)$$

$$sC_2\sqrt{sfs}K_\beta\left(\beta\sqrt{sfs}\right) = sC_1\sqrt{sfs}I_\beta\left(\beta\sqrt{sfs}\right) + 1 \quad (4.53)$$

$$C_2 = \frac{sC_1\sqrt{sfs}I_\beta\left(\beta\sqrt{sfs}\right)+1}{s\sqrt{sfs}K_\beta\left(\beta\sqrt{sfs}\right)} \quad (4.54)$$

Let, $C_1 = \frac{C_2}{A}$

$$AC_1 = \frac{sC_1\sqrt{sfs}I_\beta\left(\beta\sqrt{sfs}\right)+1}{s\sqrt{sfs}K_\beta\left(\beta\sqrt{sfs}\right)} \quad (4.55)$$

$$sAC_1\sqrt{sfs}K_\beta\left(\beta\sqrt{sfs}\right) - sC_1\sqrt{sfs}I_\beta\left(\beta\sqrt{sfs}\right) = 1 \quad (4.56)$$

$$C_1 = \frac{1}{sA\sqrt{sfs}K_\beta\left(\beta\sqrt{sfs}\right)-s\sqrt{sfs}I_\beta\left(\beta\sqrt{sfs}\right)} \quad (4.57)$$

$$C_2 = \frac{-1}{\frac{1}{A}I_\beta\left(\beta\sqrt{sfs}\right)-s\sqrt{sfs}K_\beta\left(\beta\sqrt{sfs}\right)} \quad (4.58)$$

And so at $r_D = 1$, the Laplace space solution of region I becomes:

$$\bar{P}_{wD1} = C_2\left(\frac{1}{A}I_V\left(\beta\sqrt{sfs}\right) + K_V\left(\beta\sqrt{sfs}\right)\right) \quad (4.59)$$

4.4 Development of Type Curves

This section presents procedures used to develop the type curves. The equations developed above were inverted using the Stehfest algorithm (1970). Dimensionless pressures were computed for infinite conditions on MATLAB simulation platform for different values of flow behavior index,

alpha, γ, skin factor, and dimensionless wellbore storage. Then the pressure and pressure derivative type curves were developed.

4.4.1 Type curves for Homogeneous System

A summary of the type curves developed for a homogeneous composite system is given below. Fig 4.2 shows the pressure and pressure derivative for flow behavior index, n=0.6 and 1 while other parameters are set as constant values. The curves are shown to be horizontal for n=1 with a dip in between showing the transition from one fluid to the other.

Figs 4.3-4.5 are the curves for values of flow behavior index showing the pressure and pressure derivatives for different values of theta, alpha, skin and wellbore storage, C_D = 0-10. For Figure 4.3, the curves start showing differences at t=2000 on the derivative plot, with alpha=0.01 showing the greatest deviation from a straight line. The same type of deviation is seen at Fig 4.4 with fluid mobility at 100. The wellbore storage and skin masked the early time radial regime in Fig 4.5.

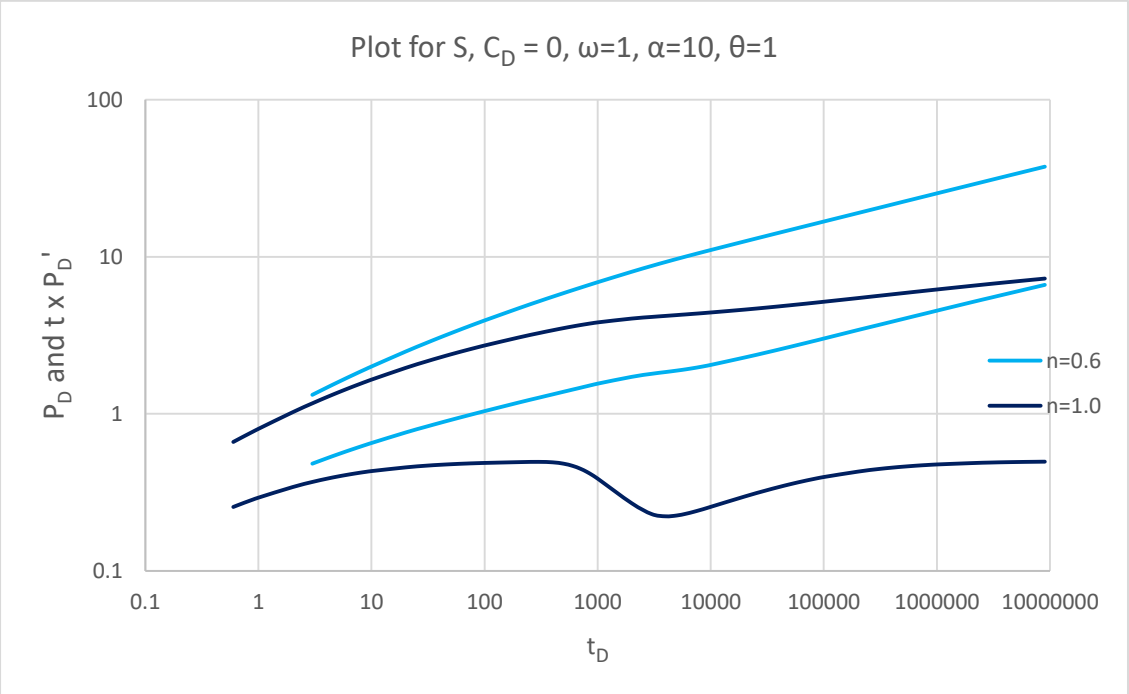

Figure 4.2: Dimensionless pressure and pressure derivative plot of radial flow behavior of power law fluid in composite system for varying alpha with S = C_D = 0, ω=1, α=10, θ =1, and n=0.6, 1.

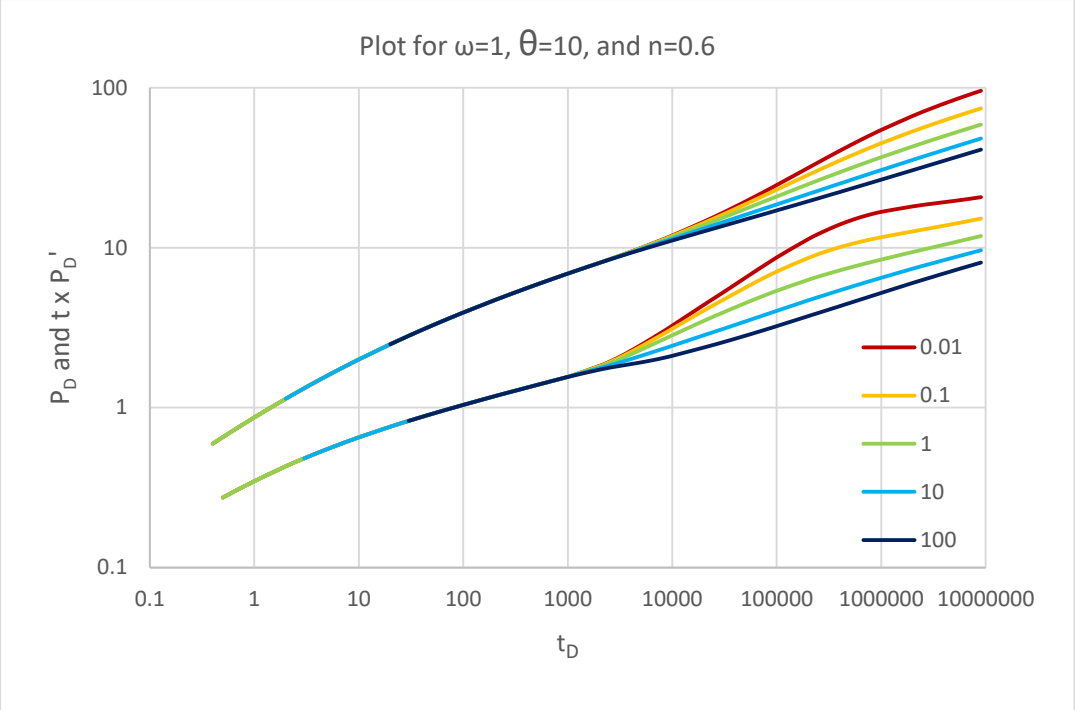

Figure 4.3: Dimensionless pressure and pressure derivative plot of radial flow behavior of power law fluid in composite system for varying alpha (0.01-100) with S = C_D = 0, ω=1, θ = 10, and n=0.6.

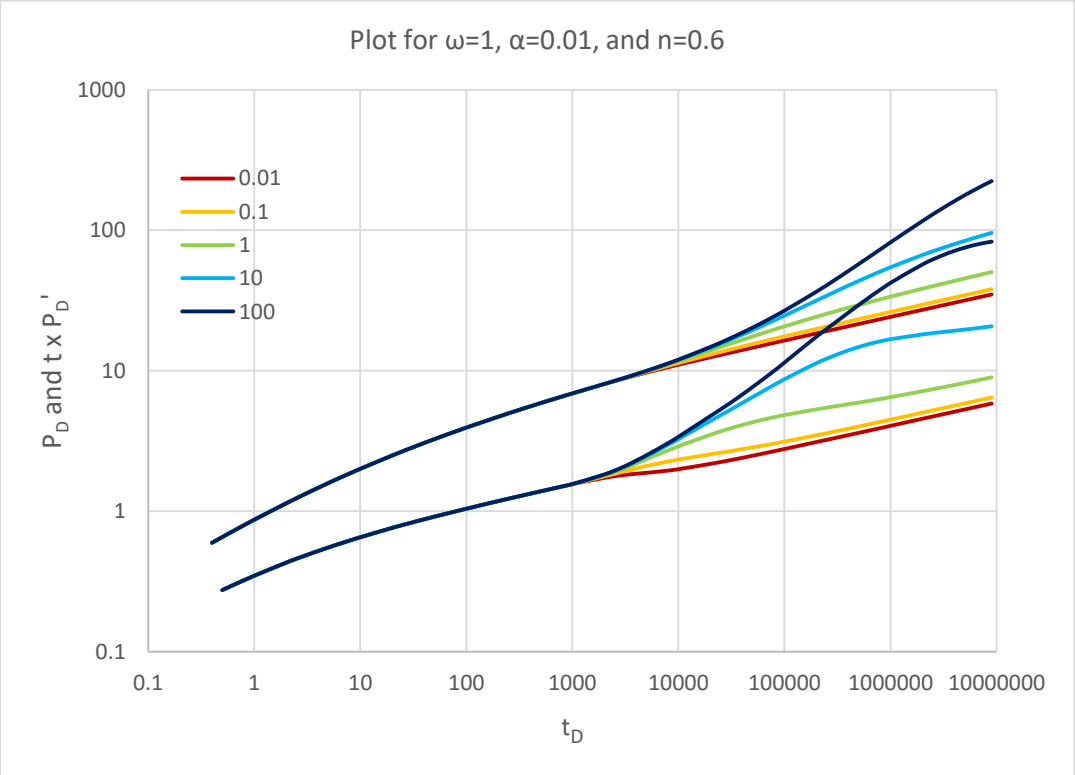

Figure 4.4: Dimensionless pressure and pressure derivative plot of radial flow behavior of power law fluid in composite system for n = 0.6, ω=1, α=0.01 and θ = 0.01-100

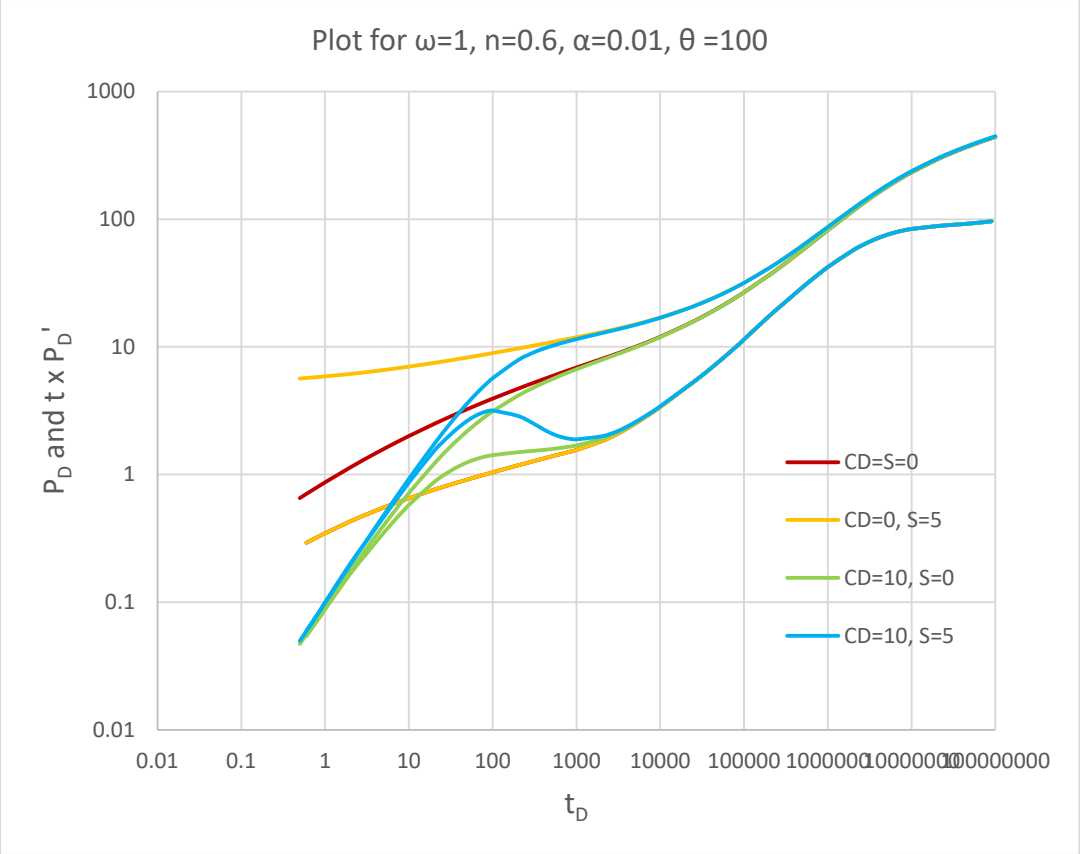

Figure 4.5: Dimensionless pressure and pressure derivative plot of radial flow behavior of power law fluid in composite system for ω=1, n=0.6, α=0.01, θ =100 and varying skin and C_D.

4.4.2 Type Curves for Naturally Fractured Reservoir

A summary of the developed type curves for a composite NFR system is given below. Figure 4.6 shows the pressure and pressure derivative for flow behavior index, n=0.6 and 1 while other parameters are at different constant values, and Figures 4.7-4.13 are the curves for values of flow behavior index showing the pressure and pressure derivatives for different values of mobility ratio (θ), alpha, interporosity parameter(λ), dimensionless wellbore co-efficient, skin and wellbore storage. In Fi 4.8-4.11, the trough between the two non-Newtonian fluids is shown to be deeper for storativity ratio of 0.001. This shows that the more naturally fractured the reservoir is, the more time it takes for the transitioning from one fluid to the other.

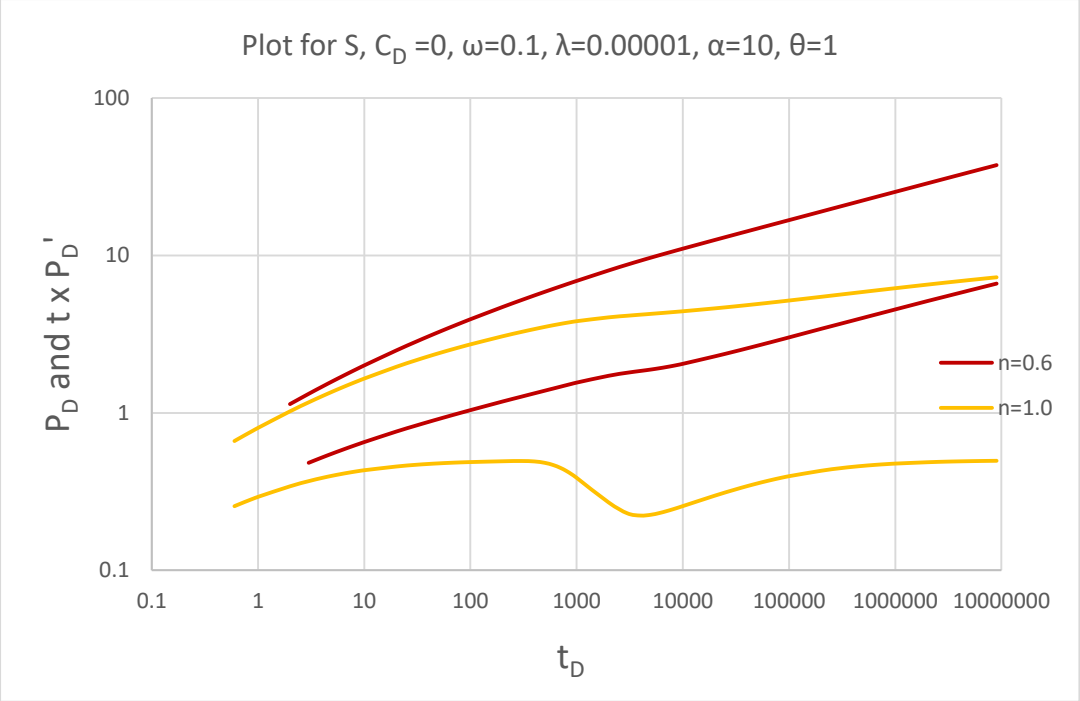

Figure 4.6: Pressure and Pressure derivative plot for radial flow behavior of non-Newtonian fluids in composite NFR. (Skin = 0, λ = 0.00001, flow index, n = 0.6, 1, ω = 0.1, α=10, θ = 1)

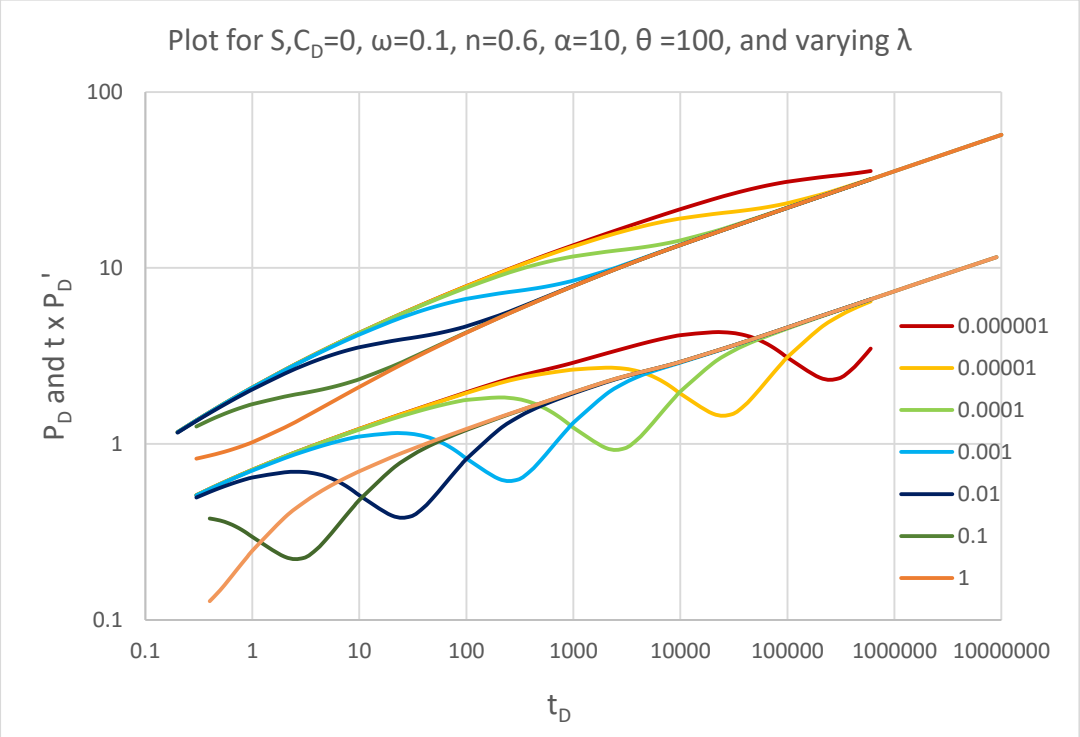

Figure 4.7: Dimensionless pressure and pressure derivative plot of radial flow behavior of power law fluid in composite system for S, C_D=0, ω=0.1, n=0.6, α=10, θ =100, and varying λ

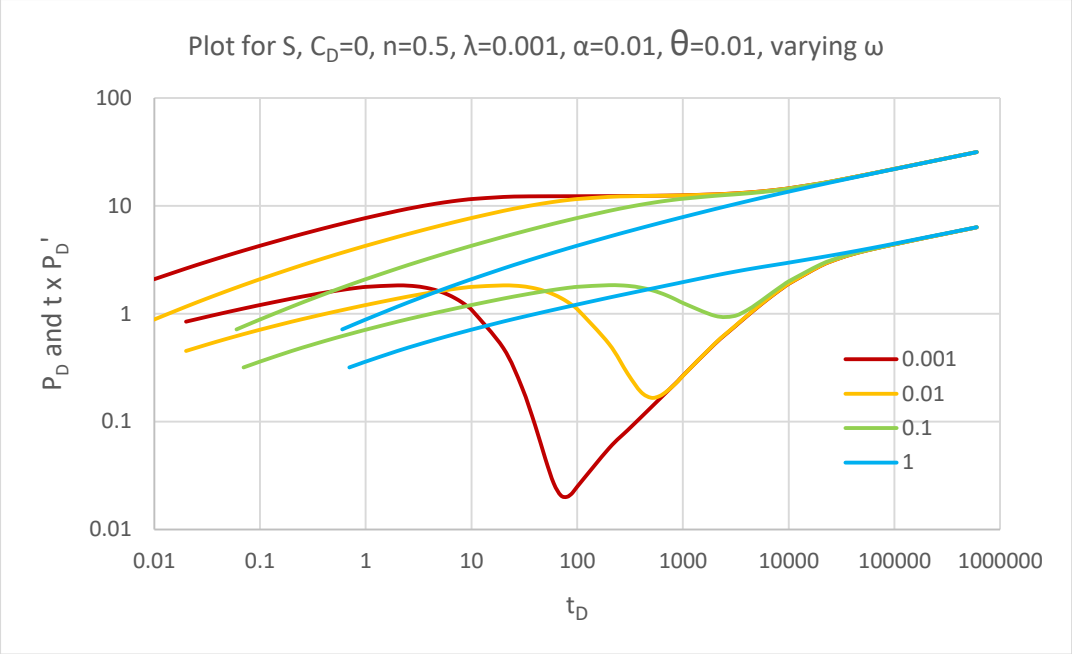

Figure 4.8: Dimensionless pressure and pressure derivative plot of radial flow behavior of power law fluid in composite system for S, C_D=0, n=0.5, λ=0.001, α=0.01, θ =0.01, varying ω

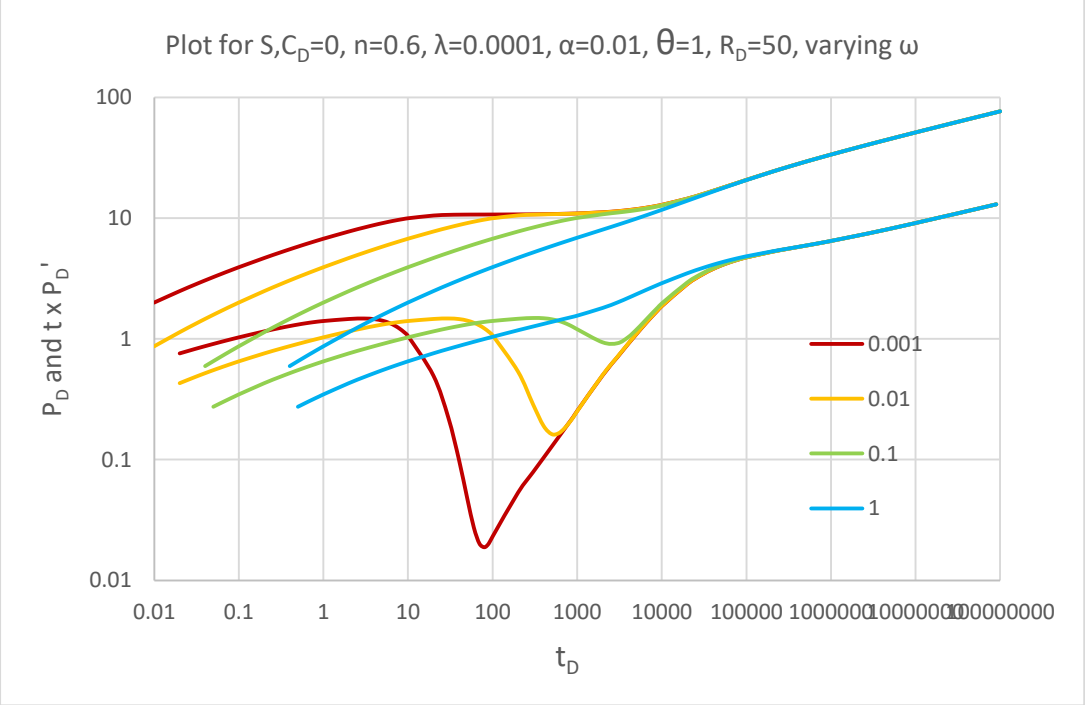

Figure 4.9: Dimensionless pressure and pressure derivative plot of radial flow behavior of power law fluid in composite system for S, C_D=0, n=0.5, λ=0.0001, α=0.01, θ =0.01, R_D=50, varying ω

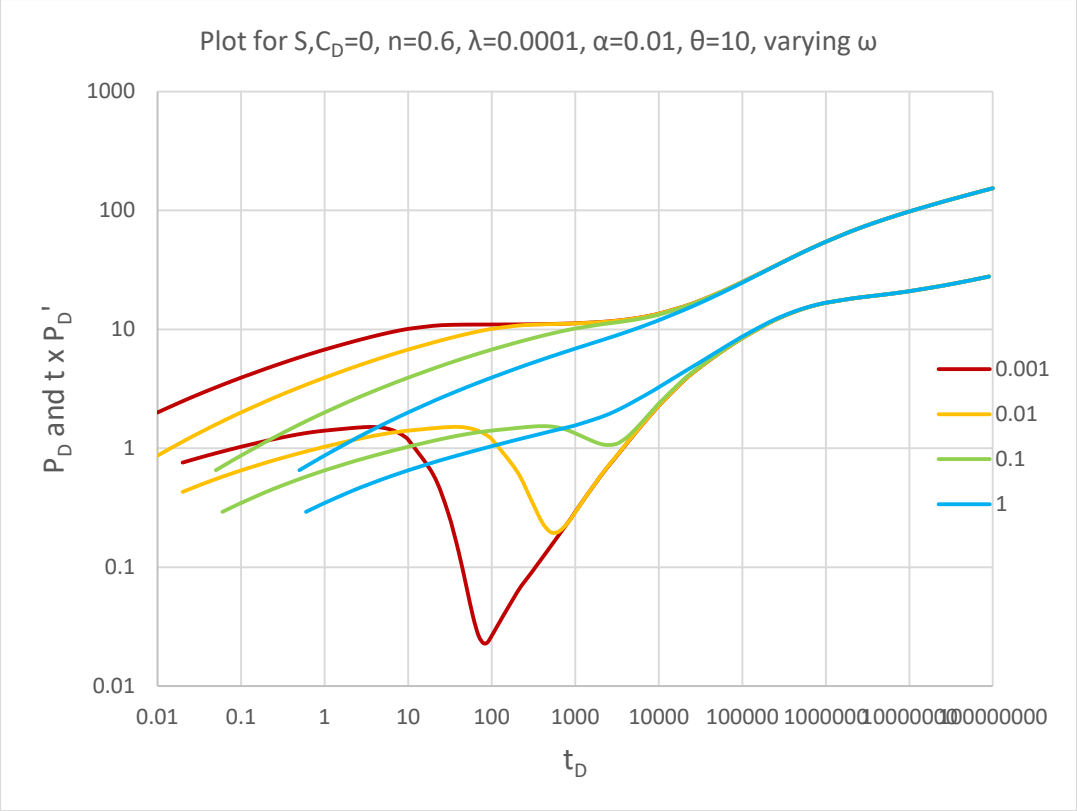

Figure 4.10: Dimensionless pressure and pressure derivative plot of radial flow behavior of power law fluid in composite system for S, C_D=0, n=0.6, λ=0.0001, α=0.01, θ =10, varying ω (0.001-1)

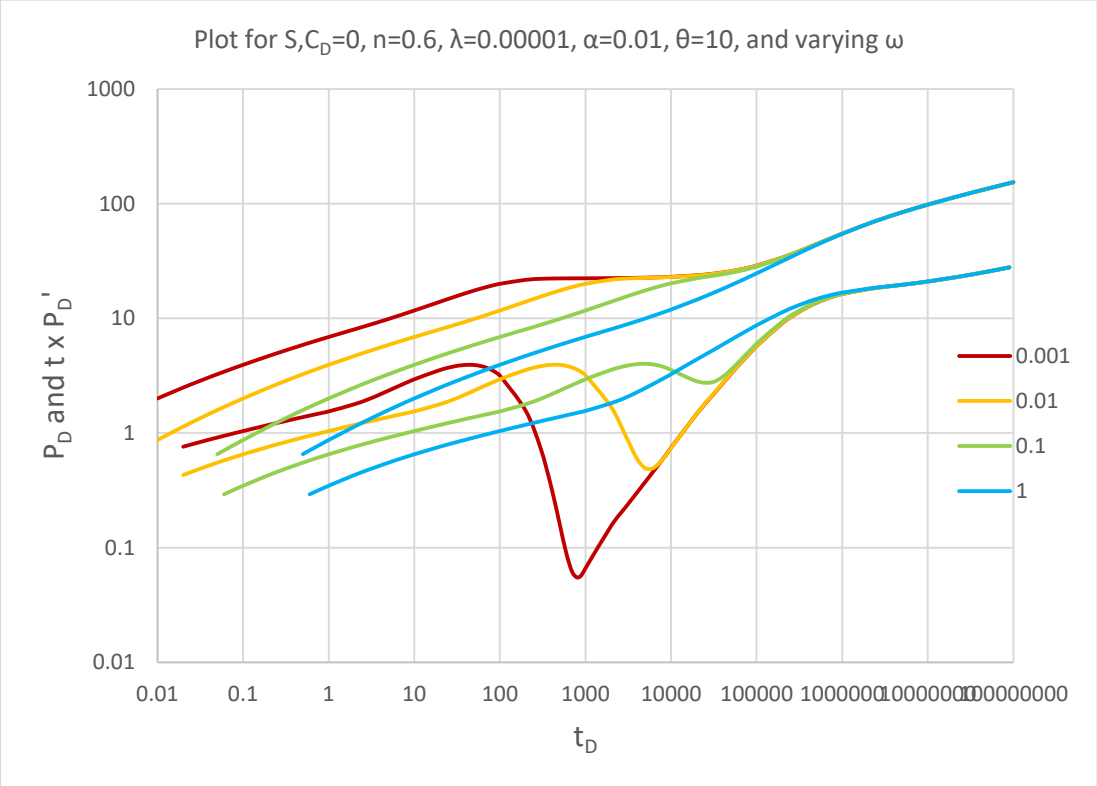

Figure 4.11: Dimensionless pressure and pressure derivative plot of radial flow behavior of power law fluid in composite system for S, C_D=0, n=0.6, λ=0.00001, α=0.01, θ =10, and varying ω

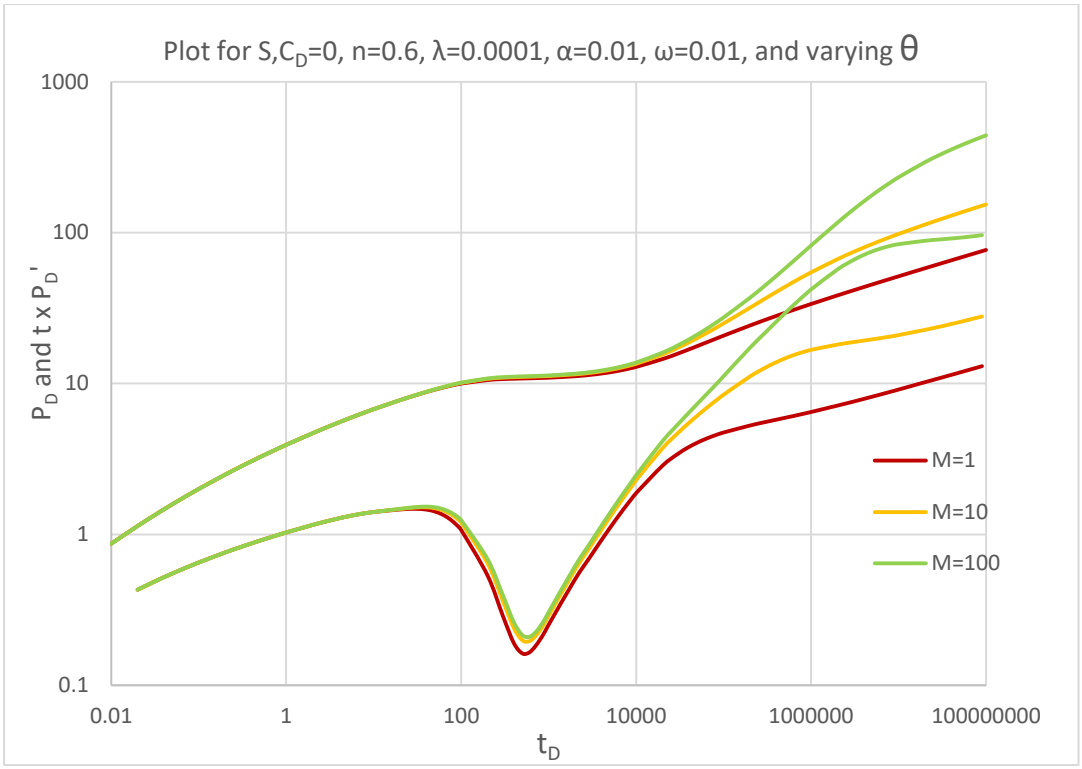

Figure 4.12: Dimensionless pressure and pressure derivative plot of radial flow behavior of power law fluid in composite system for S, CD=0, n=0.6, λ=0.0001, α=0.01, ω=0.01, and varying θ.

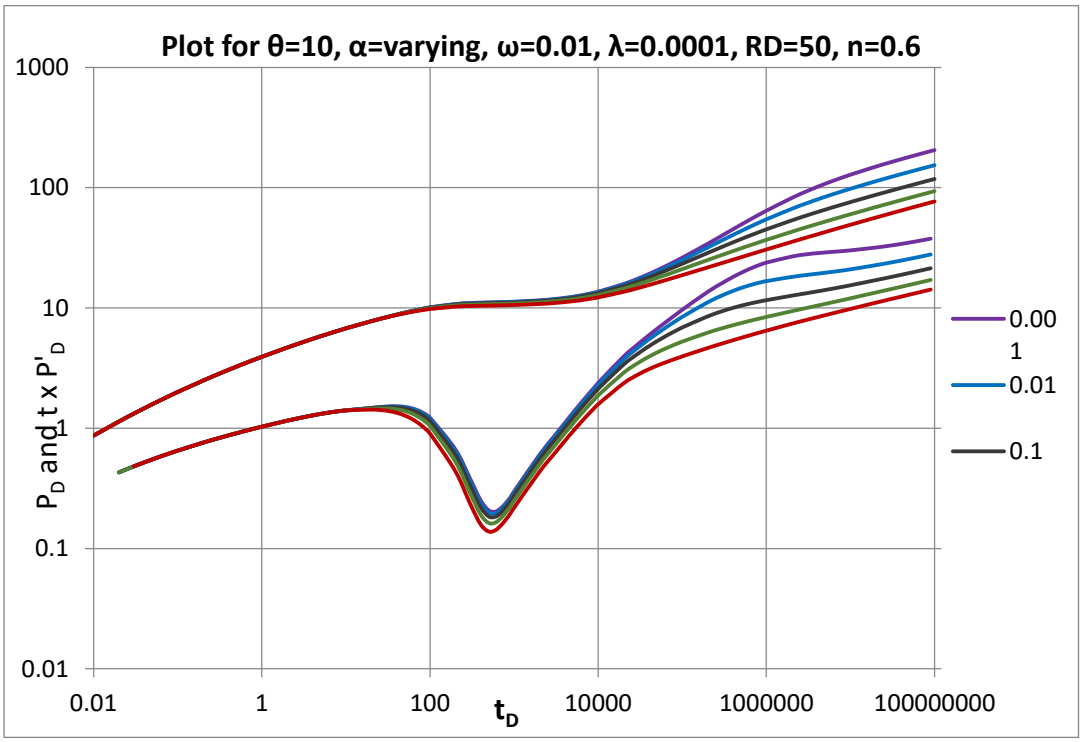

Figure 4.13: Dimensionless pressure and pressure derivative plot of radial flow behavior of power law fluid in composite system for S, CD=0, n=0.6, λ=0.0001, α=varying, ω=0.01, and θ=10

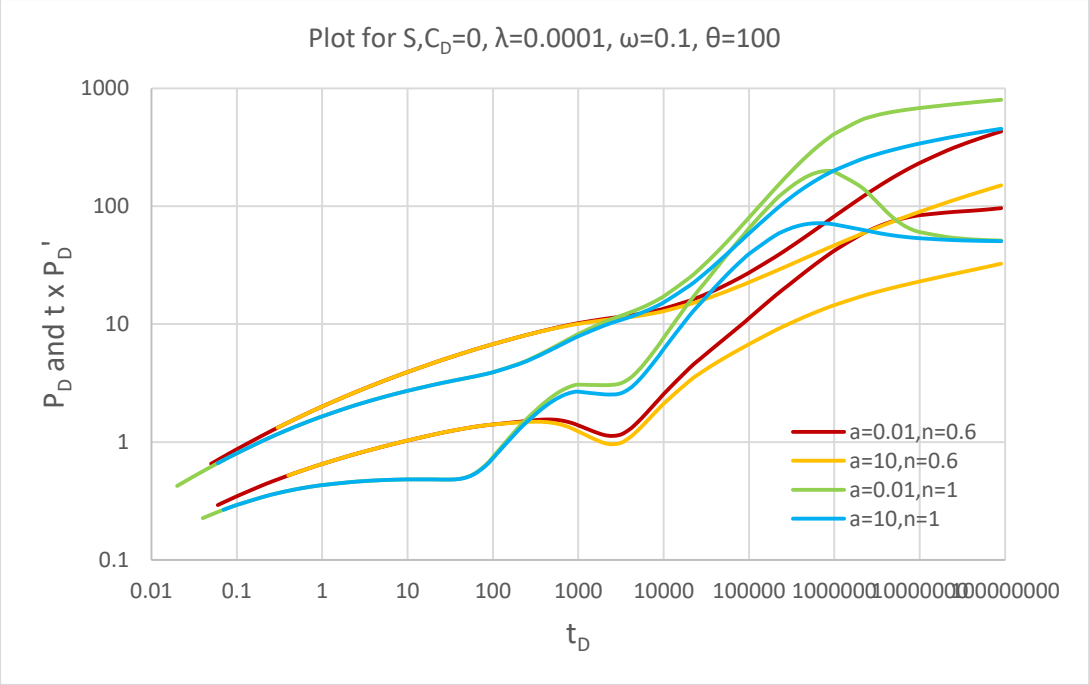

Fig 4.14: Pressure and Pressure derivative plot for radial flow behavior of non-Newtonian fluids in NFR. (Plot for S, C_D=0, λ=0.0001, ω=0.1, θ =100, α = 0.01, 10 and n = 0.6, 1)

4.5 Mathematical Development for Non-Newtonian/Non-Newtonian Composite Reservoir with different flow behavior index

Here, let region I flow behavior index be n, and

Region II flow behavior index be m.

Outer boundary condition

1. Infinite system

$$P_D(r_D = \infty, t_D) = 0$$

2. Closed (No-flow) boundary system

$$\frac{\partial \bar{P}_{D2}}{\partial r_D}(R_{eD} = 0) = 0$$

3. Constant pressure boundary system

$$\bar{P}_{D2}(R_{eD} = 0) = 0$$

Dimensionless parameter:

$$P_D = \frac{\Delta P}{\left(\frac{q}{2\pi h}\right)^n \left(\frac{\mu_1 r_W^{1-n}}{k_1}\right)}$$

Let,

$\mu_1 = \mu_{eff}$

Flow equation for non-Newtonian fluid (n) is:

$$\mu_1^n = -\frac{k_1}{\mu_1}\frac{\partial P_1}{\partial r} \tag{4.60}$$

$$\mu_1 = (-\frac{k_1}{\mu_1}\frac{\partial P_1}{\partial r})^{\frac{1}{n}} \tag{4.61}$$

$$q_1 = 2\pi rh(-\frac{k_1}{\mu_1}\frac{\partial P_1}{\partial r})^{\frac{1}{n}} \tag{4.62}$$

Taking the derivative of (4.60) with respect to radius r and re-arranging, we have:

$$\frac{\partial P_1}{\partial r} = (\frac{q}{2\pi h})^n \frac{\mu_1}{k_1} r_w^{1-n} \frac{\partial P_{D1}}{\partial r} \tag{4.63}$$

$$\frac{\partial P_1}{\partial r} = (\frac{q}{2\pi r_w h})^n \frac{\mu_1}{k_1} \frac{\partial P_{D1}}{\partial r_D} \tag{4.64}$$

From (4.62),

$$\frac{q_1}{2\pi rh} = \left(-\frac{k_1}{\mu_1}\frac{\partial P_1}{\partial r}\right)^{\frac{1}{n}} \tag{4.65}$$

Substituting (4.64) into (4.65), we have:

$$\frac{q_1}{2\pi rh} = \left(-\frac{k_1}{\mu_1}\left(\frac{q_1}{2\pi r_w h}\right)^n \frac{\mu_1}{k_1}\frac{\partial P_{D1}}{\partial r_D}\right)^{\frac{1}{n}} \tag{4.66}$$

$$\frac{2\pi r_w h q_1}{2\pi rh q_1} = \left(-\frac{\partial P_{D1}}{\partial r_D}\right)^{\frac{1}{n}} \tag{4.67}$$

$$\left(-\frac{\partial P_{D1}}{\partial r_D}\right)^{\frac{1}{n}} = \frac{r_w}{r} = \frac{1}{r_D} \tag{4.68}$$

And flow equation for non-Newtonian fluid (m) is:

$$\mu_2^m = -\frac{k_2}{\mu_2}\frac{\partial P_2}{\partial r} \tag{4.69}$$

$$q_2 = 2\pi rh(-\frac{k_2}{\mu_2}\frac{\partial P_2}{\partial r})^{\frac{1}{m}} \tag{4.70}$$

$$\frac{q_2}{2\pi rh} = \left(-\frac{k_2}{\mu_2}\frac{\partial P_2}{\partial r}\right)^{\frac{1}{m}} \tag{4.71}$$

But,

$$\frac{\partial P_2}{\partial r} = \left(\frac{q}{2\pi r_w h}\right)^n \frac{\mu_1}{k_1}\frac{\partial P_{D2}}{\partial r_D} \tag{4.72}$$

Adapting equation (12) in Lund and Ikoku (1981) to Non-Newtonian/Non-Newtonian fluid flow, at interface R or R_D:

$$\left[\lambda_{eff}\left(-\frac{\partial P_1}{\partial r}\right)\right]^{\frac{1}{n}} = \left[\lambda_2\left(-\frac{\partial P_2}{\partial r}\right)\right]^{\frac{1}{m}} \tag{4.73}$$

$$\left[\frac{k_1}{\mu_1}\left(-\left(\frac{q}{2\pi r_w h}\right)^n \frac{\mu_1}{k_1}\frac{\partial P_{D1}}{\partial r_D}\right)\right]^{\frac{1}{n}} = \left[-\frac{k_2}{\mu_2}\left(\left(\frac{q}{2\pi r_w h}\right)^n \frac{\mu_1}{k_1}\frac{\partial P_{D2}}{\partial r_D}\right)\right]^{\frac{1}{m}} \tag{4.74}$$

$$-\left(\frac{q}{2\pi r_w h}\right)\left[\left(\frac{\partial P_{D1}}{\partial r_D}\right)\right]^{\frac{1}{n}} = \left[-\frac{k_2}{\mu_2}\left(\left(\frac{q}{2\pi r_w h}\right)^n \frac{\mu_1}{k_1}\frac{\partial P_{D2}}{\partial r_D}\right)\right]^{\frac{1}{m}} \tag{4.75}$$

And so,

$$\left(-\frac{\partial P_{D1}}{\partial r_D}\right)^{\frac{1}{n}} = \left(\frac{q}{2\pi r_w h}\right)^{\frac{n}{m}-1}\left(-\frac{k_2}{\mu_2}\frac{\mu_1}{k_1}\frac{\partial P_{D2}}{\partial r_D}\right)^{\frac{1}{m}} \tag{4.76}$$

Substituting (4.68) into (4.76),

$$\frac{1}{R_D} = \left(\frac{q}{2\pi r_w h}\right)^{\frac{n}{m}-1}\left(-\frac{k_2}{\mu_2}\frac{\mu_1}{k_1}\frac{\partial P_{D2}}{\partial r_D}\right)^{\frac{1}{m}} \tag{4.77}$$

$$\frac{1}{R_D^m} = \left(\frac{q}{2\pi r_w h}\right)^{n-m}\left(-\frac{k_2}{\mu_2}\frac{\mu_1}{k_1}\frac{\partial P_{D2}}{\partial r_D}\right) \tag{4.78}$$

$$\frac{\partial P_{D2}}{\partial r_D} = \left(-\frac{k_1}{\mu_1}\frac{\mu_2}{k_2}\frac{q}{2\pi r_w h}\right)^{m-n}\frac{1}{R_D^m} \tag{4.79}$$

Set $\theta = \left(-\frac{k_1}{\mu_1}\frac{\mu_2}{k_2}\frac{q}{2\pi r_w h}\right)^{m-n}$,

$$\frac{\partial \bar{P}_{D2}}{\partial r_D} = \theta\frac{1}{sR_D^m} \tag{4.80}$$

A general Laplace solution for the dimensionless pressure drop for regions I is:

Region 1: $Non-Newtonian$ $(1 \le r_D \le R_D)$

$$\bar{P}_{D1}(1 \le r_D \le R_D) = r_D^{\frac{v_1}{\beta_1}}\left(C_1 I_{V1}\left(\beta_1 r_D^{\frac{1}{\beta_1}}\sqrt{sfs}\right) + C_2 K_{V1}\left(\beta_1 r_D^{\frac{1}{\beta_1}}\sqrt{sfs}\right)\right) \tag{4.81}$$

$$\frac{\partial \bar{P}_{D1}}{\partial r_D} = r_D^{\frac{1}{\beta}-1}\sqrt{sfs}\left(C_1 I_\beta\left(\beta\sqrt{sfs}r_D^{\frac{1}{\beta}}\right) - C_2 K_\beta\left(\beta\sqrt{sfs}r_D^{\frac{1}{\beta}}\right)\right) \tag{4.82}$$

Laplace solution for the dimensionless pressure drop in infinite (Non-Newtonian) flow for region II is:

$$\bar{P}_{D2}(R_D \le r_D \le \infty) = r_D^{\frac{v_2}{\beta_2}} C_3 K_{V2}\left(\beta_2 r_D^{\frac{1}{\beta_2}}\sqrt{\alpha sfs}\right) \tag{4.83}$$

$$\frac{\partial \bar{P}_{D2}}{\partial r_D} = -r_D^{\frac{v_2}{\beta_2}+\frac{1}{\beta_2}-1}\sqrt{\alpha sfs}C_3 K_{\beta_2}\left(\beta_2\sqrt{\alpha sfs}r_D^{\frac{1}{\beta_2}}\right) \tag{4.84}$$

Combining (4.80) and (4.84),

$$C_3 = \frac{R_D^{-\frac{v_2}{\beta_2}-\frac{1}{\beta_2}+1-m}\theta}{s\sqrt{\alpha sfs}K_{\beta 2}\left(\beta_2 R_D^{\frac{1}{\beta_2}}\sqrt{\alpha sfs}\right)} \tag{4.85}$$

At interface, $r_D = R_D, \bar{P}_{D1} = \bar{P}_{D2}$

Therefore,

$$C_3 = \frac{R_D^{\frac{v_1}{\beta_1}-\frac{v_2}{\beta_2}}\left(C_1 I_{V1}\left(\beta_1 R_D^{\frac{1}{\beta_1}}\sqrt{sfs}\right)+C_2 K_{V1}\left(\beta_1 R_D^{\frac{1}{\beta_1}}\sqrt{sfs}\right)\right)}{K_{V2}\left(\beta_2 R_D^{\frac{1}{\beta_2}}\sqrt{\alpha sfs}\right)} \tag{4.86}$$

Let:

$$s\sqrt{\alpha sfs}K_{\beta 2}\left(\beta_2 R_D^{\frac{1}{\beta_2}}\sqrt{\alpha sfs}\right) = A$$

$$K_{V2}\left(\beta_2 R_D^{\frac{1}{\beta_2}}\sqrt{\alpha sfs}\right) = B$$

$$p = -\frac{v_2}{\beta_2} - \frac{1}{\beta_2} + 1 - m$$

$$q = \frac{v_1}{\beta_1} - \frac{v_2}{\beta_2}$$

Where:

$$v_1 = \frac{1-n}{3-n}$$

$$v_2 = \frac{1-m}{3-m}$$

$$\beta_1 = \frac{2}{3-n}$$

$$\beta_2 = \frac{2}{3-m}$$

Equating (4.85) and (4.86), we have:

$$BR_D^p\theta = C_1 AR_D^q I_{V1}\left(\beta_1 r_D^{\frac{1}{\beta_1}}\sqrt{sfs}\right) + C_2 AR_D^q K_{V1}\left(\beta_1 r_D^{\frac{1}{\beta_1}}\sqrt{sfs}\right) \tag{4.87}$$

$$C_1 = \frac{B\theta R_D^p - C_2 A R_D^q K_{V1}\left(\beta_1 r_D^{\frac{1}{\beta_1}}\sqrt{sfs}\right)}{A R_D^q I_{V1}\left(\beta_1 r_D^{\frac{1}{\beta_1}}\sqrt{sfs}\right)} \tag{4.88}$$

At wellbore condition, $r_D = 1$:

$$\frac{\partial \bar{P}_{wD1}}{\partial r_D} = -\frac{1}{s} = \sqrt{sfs}\left(C_1 I_\beta\left(\beta\sqrt{sfs}\right) - C_2 K_\beta\left(\beta\sqrt{sfs}\right)\right) \tag{4.89}$$

$$C_1 = \frac{\frac{-1}{s\sqrt{sfs}} + C_2 K_{\beta 1}\left(\beta_1\sqrt{sfs}\right)}{I_{\beta 1}\left(\beta_1\sqrt{sfs}\right)} \tag{4.90}$$

Equating (4.88) and (4.90), we have:

$$B R_D^p \theta I_{\beta 1}\left(\beta_1\sqrt{sfs}\right) - C_2 A R_D^q I_{\beta 1}\left(\beta_1\sqrt{sfs}\right) K_{V1}\left(\beta_1 R_D^{\frac{1}{\beta_1}}\sqrt{sfs}\right) = \frac{-A R_D^q}{s\sqrt{sfs}} I_{V1}\left(\beta_1 R_D^{\frac{1}{\beta_1}}\sqrt{sfs}\right) +$$

$$C_2 A R_D^q I_{V1}\left(\beta_1 R_D^{\frac{1}{\beta_1}}\sqrt{sfs}\right) K_{\beta 1}\left(\beta_1\sqrt{sfs}\right) \tag{4.91}$$

$$C_2 = \frac{B\theta R_D^p I_{\beta 1}\left(\beta_1\sqrt{sfs}\right) + \frac{A R_D^q}{s\sqrt{sfs}} I_{V1}\left(\beta_1 R_D^{\frac{1}{\beta_1}}\sqrt{sfs}\right)}{A R_D^q I_{V1}\left(\beta_1 R_D^{\frac{1}{\beta_1}}\sqrt{sfs}\right) K_{\beta 1}\left(\beta_1\sqrt{sfs}\right) + I_{\beta 1}\left(\beta_1\sqrt{sfs}\right) K_{V1}\left(\beta_1 R_D^{\frac{1}{\beta_1}}\sqrt{sfs}\right)} \tag{4.92}$$

Laplace solution for the dimensionless pressure drops for constant pressure boundary system for region II is:

Region II: $Non - Newtonian$ $(R_D \le r_D \le \infty)$

$$\bar{P}_{D2} = \left[C_3 I_{V2}\left(\beta_2 r_D^{\frac{1}{\beta_2}}\sqrt{\alpha sfs}\right) + C_4 K_{V2}\left(\beta_2 r_D^{\frac{1}{\beta_2}}\sqrt{\alpha sfs}\right)\right] r_D^{\frac{V}{\beta}} \tag{4.93}$$

$$\frac{\partial \bar{P}_{D2}}{\partial r_D} = r_D^{\frac{v_2}{\beta_2}+\frac{1}{\beta_2}-1}\sqrt{\alpha sfs}\left[C_3 I_{\beta_2}\left(\beta_2\sqrt{\alpha sfs} r_D^{\frac{1}{\beta_2}}\right) - C_4 K_{\beta 2}\left(\beta_2 r_D^{\frac{1}{\beta_2}}\sqrt{\alpha sfs}\right)\right] \tag{4.94}$$

Since $\bar{P}_{D2} = 0$ @ R_{eD},

$$C_4 = \frac{-C_3 I_{V2}\left(\beta_2 R_{eD}^{\frac{1}{\beta_2}}\sqrt{\alpha sfs}\right)}{K_{V2}\left(\beta_2 R_{eD}^{\frac{1}{\beta_2}}\sqrt{\alpha sfs}\right)} \tag{4.95}$$

$$\frac{\partial \bar{P}_{D2}}{\partial r_D} = r_D^{\frac{v_2}{\beta_2}+\frac{1}{\beta_2}-1}\sqrt{\alpha sfs}[C_3 I_{\beta_2}\left(\beta_2\sqrt{\alpha sfs} r_D^{\frac{1}{\beta_2}}\right) + \frac{C_3 K_{V2}\left(\beta_2 R_{eD}^{\frac{1}{\beta_2}}\sqrt{\alpha sfs}\right)}{I_{V2}\left(\beta_2 R_{eD}^{\frac{1}{\beta_2}}\sqrt{\alpha sfs}\right)} K_{\beta 2}\left(\beta_2 r_D^{\frac{1}{\beta_2}}\sqrt{\alpha sfs}\right) \tag{4.96}$$

At interface R_D, $\frac{\partial \bar{P}_{D2}}{\partial r_D} = -\frac{\theta}{sR_D^m}$ and $\bar{P}_{D1} = \bar{P}_{D2}$

And so,

$$C_3 = \frac{-\theta}{R_D^{\frac{v_2}{\beta_2}-\frac{1}{\beta_2}+1+m} s\sqrt{\alpha sfs} I_{\beta_2}\left(\beta_2\sqrt{\alpha sfs}R_D^{\frac{1}{\beta_2}}\right) + \frac{K_{V2}\left(\beta_2 R_{eD}^{\frac{1}{\beta_2}}\sqrt{\alpha sfs}\right)}{I_{V2}\left(\beta_2 R_{eD}^{\frac{1}{\beta_2}}\sqrt{\alpha sfs}\right)} K_{\beta 2}\left(\beta_2 R_D^{\frac{1}{\beta_2}}\sqrt{\alpha sfs}\right)} \tag{4.97}$$

And,

$$C_3 = \frac{\left(C_1 I_{V1}\left(\beta_1 R_D^{\frac{1}{\beta_1}}\sqrt{sfs}\right) + C_2 K_{V1}\left(\beta_1 R_D^{\frac{1}{\beta_1}}\sqrt{sfs}\right)\right)}{R_D^{\frac{v_2}{\beta_2}-\frac{v_1}{\beta_1}}\left(I_{V2}\left(\beta_2 R_D^{\frac{1}{\beta_2}}\sqrt{sfs}\right) - \frac{K_{V2}\left(\beta_2 R_{eD}^{\frac{1}{\beta_2}}\sqrt{\alpha sfs}\right)}{I_{V2}\left(\beta_2 R_{eD}^{\frac{1}{\beta_2}}\sqrt{\alpha sfs}\right)} K_{V2}\left(\beta_2 R_D^{\frac{1}{\beta_2}}\sqrt{\alpha sfs}\right)\right)} \tag{4.98}$$

Let

$$R_D^{-\frac{v_2}{\beta_2}-\frac{1}{\beta_2}+1-m} s\sqrt{\alpha sfs} I_{\beta_2}\left(\beta_2\sqrt{\alpha sfs}R_D^{\frac{1}{\beta_2}}\right) + \frac{K_{V2}\left(\beta_2 R_{eD}^{\frac{1}{\beta_2}}\sqrt{\alpha sfs}\right)}{I_{V2}\left(\beta_2 R_{eD}^{\frac{1}{\beta_2}}\sqrt{\alpha sfs}\right)} K_{\beta 2}\left(\beta_2 R_D^{\frac{1}{\beta_2}}\sqrt{\alpha sfs}\right) = A$$

$$R_D^{\frac{v_2}{\beta_2}-\frac{v_1}{\beta_1}}\left(I_{V2}\left(\beta_2 R_D^{\frac{1}{\beta_2}}\sqrt{sfs}\right) - \frac{K_{V2}\left(\beta_2 R_{eD}^{\frac{1}{\beta_2}}\sqrt{\alpha sfs}\right)}{I_{V2}\left(\beta_2 R_{eD}^{\frac{1}{\beta_2}}\sqrt{\alpha sfs}\right)} K_{V2}\left(\beta_2 R_D^{\frac{1}{\beta_2}}\sqrt{\alpha sfs}\right)\right) = B$$

Combining (4.97) and (4.98),

$$-B\theta = C_1 A I_{V1}\left(\beta_1 R_D^{\frac{1}{\beta_1}}\sqrt{sfs}\right) + C_2 A K_{V1}\left(\beta_1 R_D^{\frac{1}{\beta_1}}\sqrt{sfs}\right) \tag{4.99}$$

$$C_1 = \frac{-\left[B\theta - C_2 A K_{V1}\left(\beta_1 R_D^{\frac{1}{\beta_1}}\sqrt{sfs}\right)\right]}{A I_{V1}\left(\beta_1 R_D^{\frac{1}{\beta_1}}\sqrt{sfs}\right)} \tag{4.100}$$

From (4.90),

$$C_1 = \frac{\frac{-1}{s\sqrt{sfs}} + C_2 K_{\beta 1}(\beta_1\sqrt{sfs})}{I_{\beta 1}(\beta_1\sqrt{sfs})}$$

Combining (4.100) and (4.90),

$$-B\theta I_{\beta 1}(\beta_1\sqrt{sfs}) - C_2 A I_{\beta 1}(\beta_1\sqrt{sfs})K_{V1}\left(\beta_1 R_D^{\frac{1}{\beta_1}}\sqrt{sfs}\right) =$$

$$\frac{-A}{s\sqrt{sfs}} I_{V1}\left(\beta_1 R_D^{\frac{1}{\beta_1}}\sqrt{sfs}\right) + C_2 A I_{V1}\left(\beta_1 R_D^{\frac{1}{\beta_1}}\sqrt{sfs}\right) K_{\beta 1}(\beta_1\sqrt{sfs})$$

(4.101)

$$C_2 = \frac{\frac{A}{s\sqrt{sfs}} I_{V1}\left(\beta_1 R_D^{\frac{1}{\beta_1}}\sqrt{sfs}\right) - B\theta I_{\beta 1}(\beta_1\sqrt{sfs})}{A\left[I_{V1}\left(\beta_1 R_D^{\frac{1}{\beta_1}}\sqrt{sfs}\right)K_{\beta 1}(\beta_1\sqrt{sfs}) + I_{\beta 1}(\beta_1\sqrt{sfs})K_{V1}\left(\beta_1 R_D^{\frac{1}{\beta_1}}\sqrt{sfs}\right)\right]} \quad (4.102)$$

Laplace solution for the dimensionless pressure drops for closed (no-flow) boundary system for region II is:

Region II: $Non - Newtonian\ (R_D \le r_D \le \infty)$

$$\frac{\partial \bar{P}_{D2}}{\partial r_D} = r_D^{\frac{v_2}{\beta_2}+\frac{1}{\beta_2}-1}\sqrt{\alpha sfs}\left[C_3 I_{\beta_2}\left(\beta_2\sqrt{\alpha sfs}\, r_D^{\frac{1}{\beta_2}}\right) - \frac{C_3 K_{\beta 2}\left(\beta_2 R_{eD}^{\frac{1}{\beta_2}}\sqrt{\alpha sfs}\right)}{I_{\beta 2}\left(\beta_2 R_{eD}^{\frac{1}{\beta_2}}\sqrt{\alpha sfs}\right)} K_{\beta 2}\left(\beta_2 r_D^{\frac{1}{\beta_2}}\sqrt{\alpha sfs}\right)\right.$$

(4.103)

At interface R_D, $\frac{\partial \bar{P}_{D2}}{\partial r_D} = -\frac{\theta}{sR_D^m}$ and $\bar{P}_{D1} = \bar{P}_{D2}$

$$C_3 = \frac{-\theta}{R_D^{-\frac{v_2}{\beta_2}-\frac{1}{\beta_2}+m-1} s\sqrt{\alpha sfs} I_{\beta_2}\left(\beta_2\sqrt{\alpha sfs} R_D^{\frac{1}{\beta_2}}\right) + \frac{K_{\beta 2}\left(\beta_2 R_{eD}^{\frac{1}{\beta_2}}\sqrt{\alpha sfs}\right)}{I_{\beta 2}\left(\beta_2 R_{eD}^{\frac{1}{\beta_2}}\sqrt{\alpha sfs}\right)} K_{\beta 2}\left(\beta_2 R_D^{\frac{1}{\beta_2}}\sqrt{\alpha sfs}\right)} \quad (4.104)$$

$$C_3 = \frac{\left(C_1 I_{V1}\left(\beta_1 R_D^{\frac{1}{\beta_1}}\sqrt{sfs}\right) + C_2 K_{V1}\left(\beta_1 R_D^{\frac{1}{\beta_1}}\sqrt{sfs}\right)\right)}{R_D^{\frac{v_2}{\beta_2}-\frac{v_1}{\beta_1}}\left(I_{V2}\left(\beta_2 R_D^{\frac{1}{\beta_2}}\sqrt{\alpha sfs}\right) + \frac{K_{\beta 2}\left(\beta_2 R_{eD}^{\frac{1}{\beta_2}}\sqrt{\alpha sfs}\right)}{I_{\beta 2}\left(\beta_2 R_{eD}^{\frac{1}{\beta_2}}\sqrt{\alpha sfs}\right)} K_{V2}\left(\beta_2 R_D^{\frac{1}{\beta_2}}\sqrt{\alpha sfs}\right)\right)} \quad (4.105)$$

Let

$$R_D^{-\frac{v_2}{\beta_2}-\frac{1}{\beta_2}+m-1} s\sqrt{\alpha sfs} I_{\beta_2}\left(\beta_2\sqrt{\alpha sfs} R_D^{\frac{1}{\beta_2}}\right) + \frac{K_{\beta 2}\left(\beta_2 R_{eD}^{\frac{1}{\beta_2}}\sqrt{\alpha sfs}\right)}{I_{\beta 2}\left(\beta_2 R_{eD}^{\frac{1}{\beta_2}}\sqrt{\alpha sfs}\right)} K_{\beta 2}\left(\beta_2 R_D^{\frac{1}{\beta_2}}\sqrt{\alpha sfs}\right) = A$$

$$R_D^{\frac{v_2}{\beta_2}-\frac{v_1}{\beta_1}}\left(I_{V2}\left(\beta_2 R_D^{\frac{1}{\beta_2}}\sqrt{\alpha sfs}\right)+\frac{K_{\beta 2}\left(\beta_2 R_{eD}^{\frac{1}{\beta_2}}\sqrt{\alpha sfs}\right)}{I_{\beta 2}\left(\beta_2 R_{eD}^{\frac{1}{\beta_2}}\sqrt{\alpha sfs}\right)}\right)K_{V2}\left(\beta_2 R_D^{\frac{1}{\beta_2}}\sqrt{\alpha sfs}\right)=B$$

Equating (4.104) and (4.105), we have:

$$-B\theta = C_1 A I_{V1}\left(\beta_1 R_D^{\frac{1}{\beta_1}}\sqrt{sfs}\right)+C_2 A K_{V1}\left(\beta_1 R_D^{\frac{1}{\beta_1}}\sqrt{sfs}\right) \quad (4.106)$$

$$C_1 = \frac{-\left[B\theta - C_2 A K_{V1}\left(\beta_1 R_D^{\frac{1}{\beta_1}}\sqrt{sfs}\right)\right]}{A I_{V1}\left(\beta_1 R_D^{\frac{1}{\beta_1}}\sqrt{sfs}\right)} \quad (4.107)$$

From (4.90),

$$C_1 = \frac{\frac{-1}{s\sqrt{sfs}}+C_2 K_{\beta 1}\left(\beta_1\sqrt{sfs}\right)}{I_{\beta 1}\left(\beta_1\sqrt{sfs}\right)}$$

Equating (4.90) and (4.107),

$$-B\theta I_{\beta 1}\left(\beta_1\sqrt{sfs}\right)-C_2 A I_{\beta 1}\left(\beta_1\sqrt{sfs}\right)K_{V1}\left(\beta_1 R_D^{\frac{1}{\beta_1}}\sqrt{sfs}\right)=$$

$$\frac{-A}{s\sqrt{sfs}}I_{V1}\left(\beta_1 R_D^{\frac{1}{\beta_1}}\sqrt{sfs}\right)+C_2 A I_{V1}\left(\beta_1 R_D^{\frac{1}{\beta_1}}\sqrt{sfs}\right)K_{\beta 1}\left(\beta_1\sqrt{sfs}\right) \quad (4.108)$$

$$C_2 = \frac{\frac{A}{s\sqrt{sfs}}I_{V1}\left(\beta_1 R_D^{\frac{1}{\beta_1}}\sqrt{sfs}\right)-B\theta I_{\beta 1}\left(\beta_1\sqrt{sfs}\right)}{A\left[I_{V1}\left(\beta_1 R_D^{\frac{1}{\beta_1}}\sqrt{sfs}\right)K_{\beta 1}\left(\beta_1\sqrt{sfs}\right)+I_{\beta 1}\left(\beta_1\sqrt{sfs}\right)K_{V1}\left(\beta_1 R_D^{\frac{1}{\beta_1}}\sqrt{sfs}\right)\right]} \quad (4.109)$$

4.6 Development of type curves

The equations developed above were inverted using the Stehfest algorithm (1970). Dimensionless pressures were computed for homogeneous infinite and constant pressure conditions on MATLAB simulation platform for different values of flow behavior index (m and n) as well as for naturally fractured reservoirs. The pressure and pressure derivative type curves were developed and plotted.

Figure 4.15 shows the pressure and pressure derivative for varying flow behavior index, n (region 1) with constant m (region 2) at infinite boundary conditions. Figure 4.16 shows the pressure and pressure derivative for varying flow behavior index, m (region 2) with constant n (region 1) at infinite boundary conditions. Figs 4.17-4.18 also show the pressure and pressure derivative for varying flow behavior index, n (region 1) with constant m (region 2) at constant pressure boundary conditions. Figures 4.19-4.21 show the same plots as above, but for naturally fractured reservoirs as indicated by the trough between the pressure derivative curves.

4.6.1 Homogeneous Reservoir

(A) Infinite boundary condition

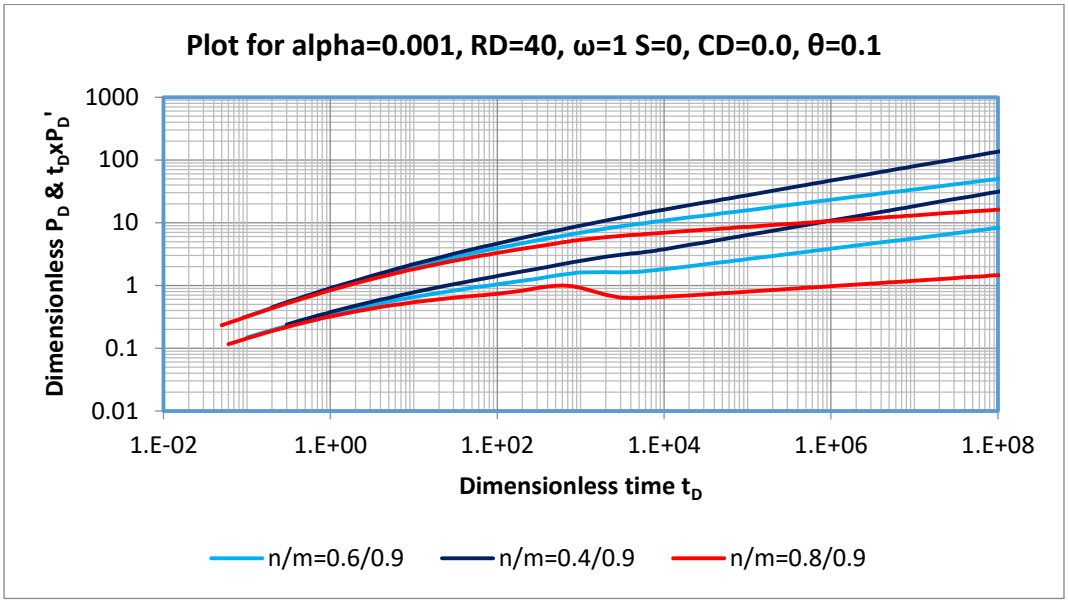

Figure 4.15: Pressure and Pressure derivative plot for radial flow behavior of non-Newtonian fluids. (Skin = 0, varying flow index (n), m=0.9, RD=40, ω = 1, α=0.001, θ =0.1)

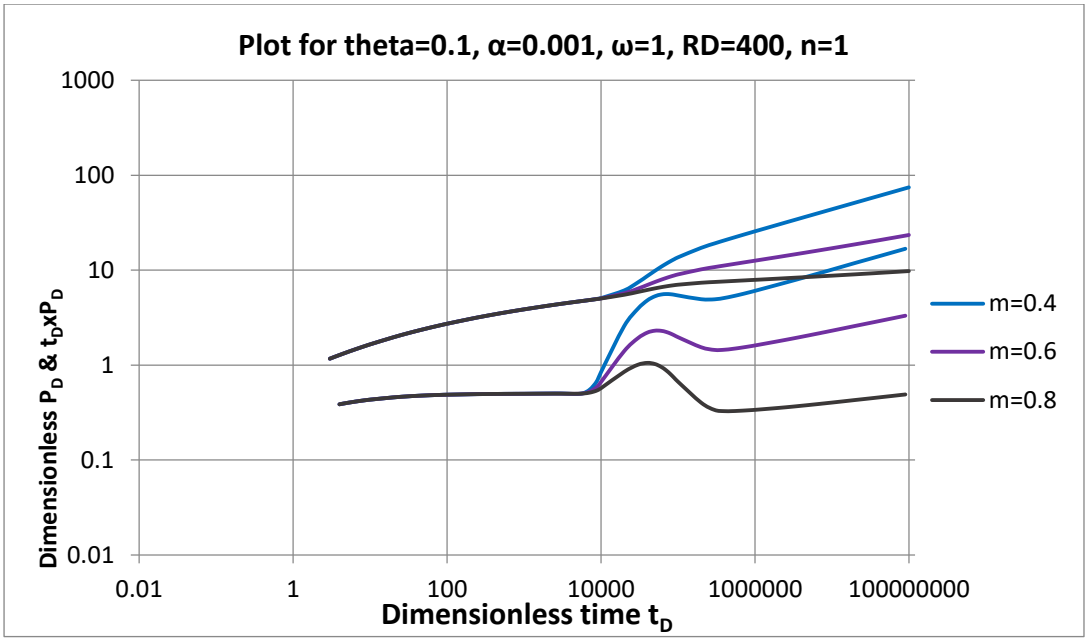

Figure 4.16: Pressure and Pressure derivative plot for radial flow behavior of non-Newtonian fluids. (Skin = 0, varying m, n=1.0, RD=400, ω = 1, α=0.001, θ =0.1)

(B) Constant pressure boundary

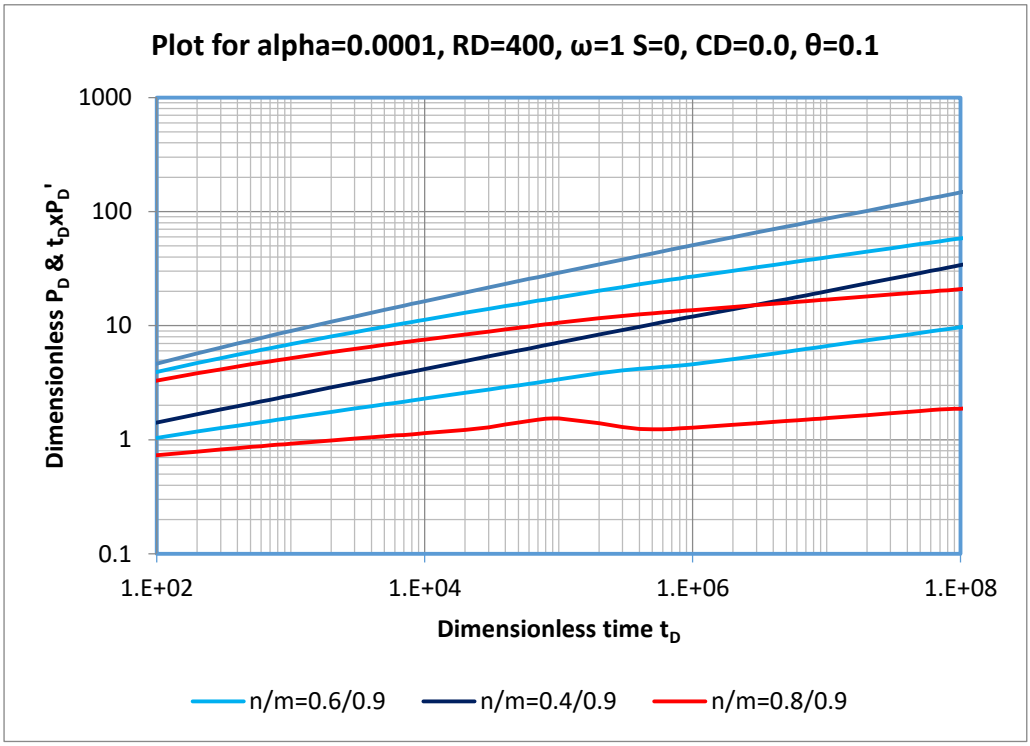

Figure 4.17: Pressure and Pressure derivative plot for radial flow behavior of non-Newtonian fluids. (Skin = 0, varying flow index (n), m=0.9, RD=400, ReD=10000, ω = 1, α=0.0001, θ =0.1)

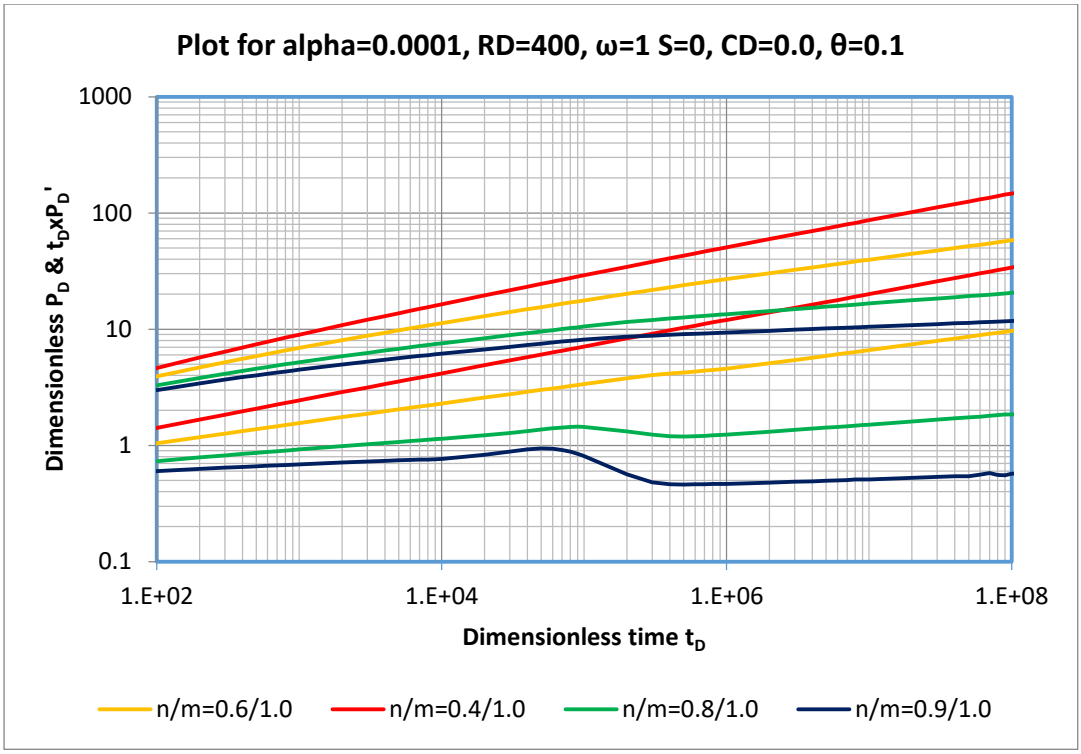

Figure 4.18: Pressure and Pressure derivative plot for radial flow behavior of non-Newtonian fluids. (Skin = 0, varying flow index (n), m=1.0, RD=400, ω = 1, α=0.0001, θ =0.1)

4.6.2 Naturally Fractured Reservoir (NFR)

(A) Infinite boundary system

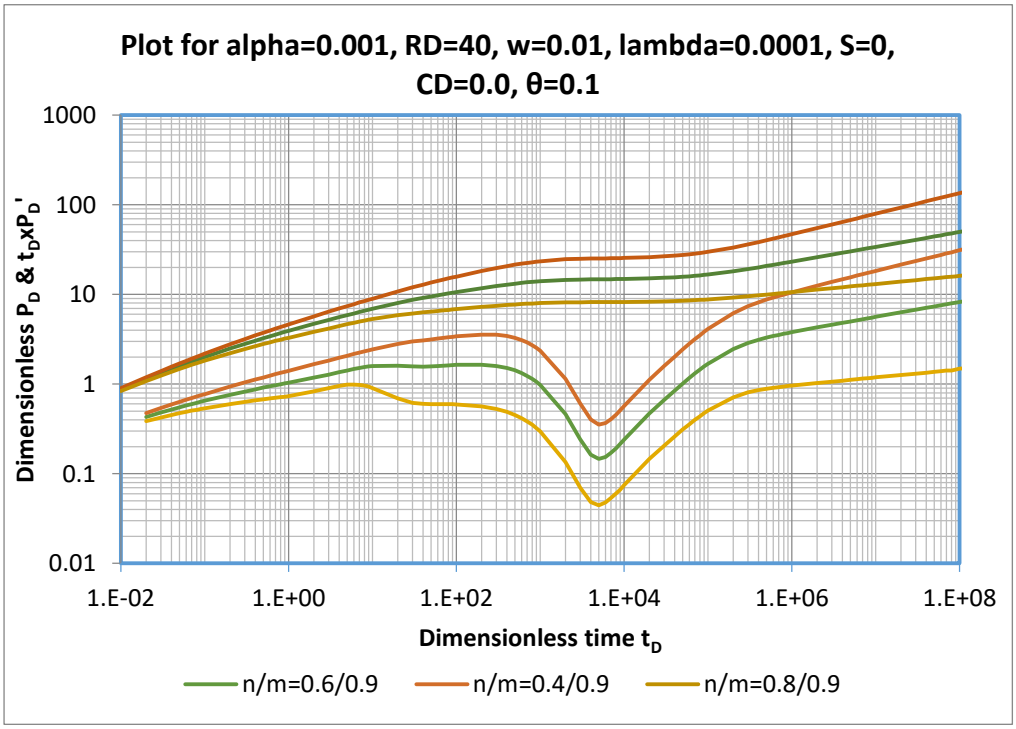

Figure 4.19: Pressure and Pressure derivative plot for radial flow behavior of non-Newtonian fluids. (Skin = 0, varying flow index (n), m=0.9, RD=40, ω = 0.01, λ=0.0001, α=0.001, θ =0.1)

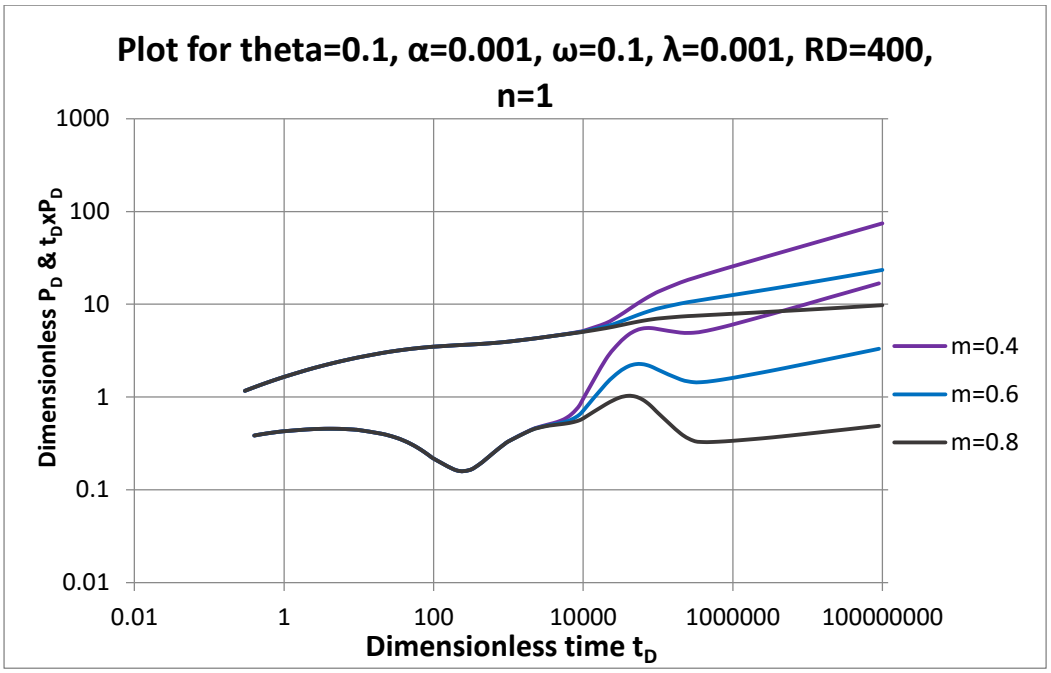

Figure 4.20: Pressure and Pressure derivative plot for radial flow behavior of non-Newtonian fluids. (Skin = 0, varying m, n=1.0, RD=400, ω = 0.1, λ=0.001, α=0.001, θ =0.1, inner boundary Newtonian, outer boundary non-Newtonian)

(B) Constant pressure boundary

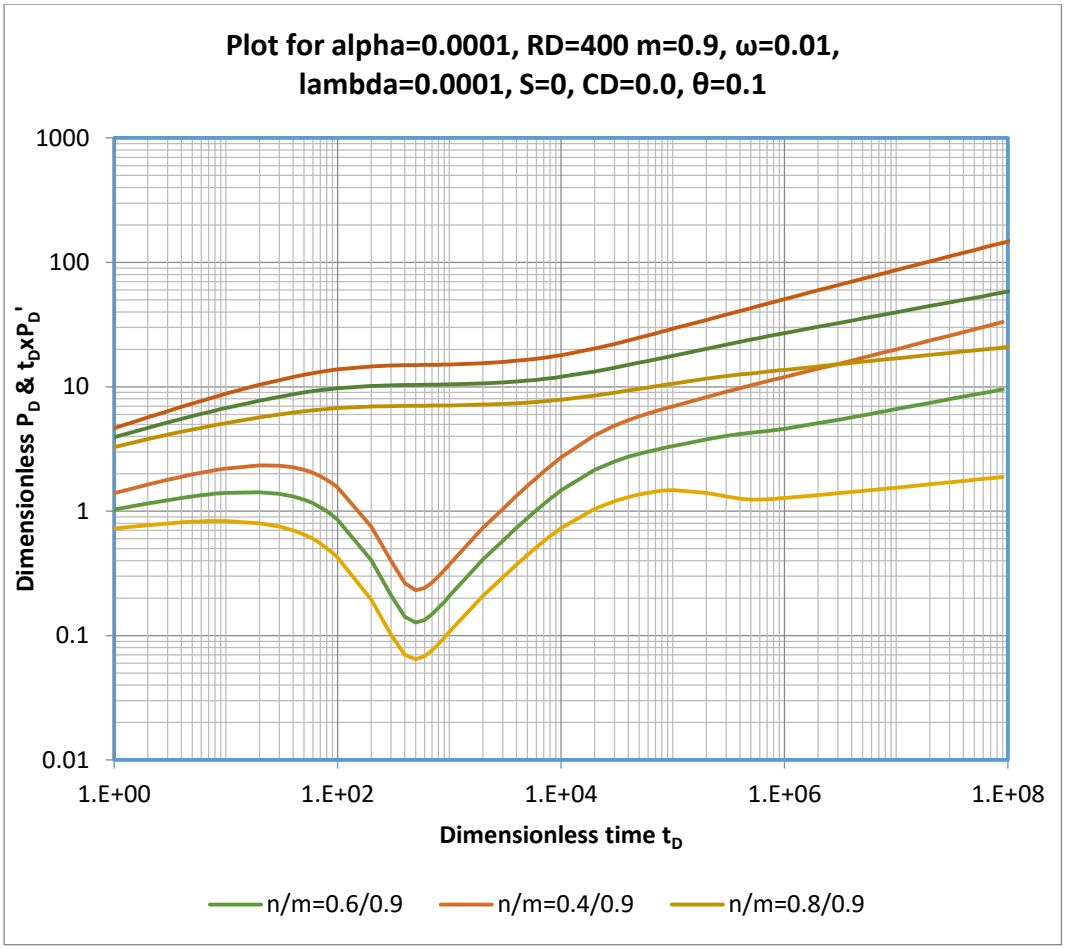

Figure 4.21: Pressure and Pressure derivative plot for radial flow behavior of non-Newtonian fluids. (Skin = 0, varying flow index (n), m=0.9, RD=400, ReD=10000, ω = 0.01, λ=0.0001, α=0.0001, θ =0.1)

4.7 Verification of model using n=1 and m=1 at θ=1 and α=0.1, 1, 10

The purpose of this section is to use the mathematical model developed in replicating the behavior observed in the Abbaszadeh and Kamal (1989) work. The results obtained as shown in Figures 4.22 to 4.25 predict similar behavior as presented by Abbaszadeh and Kamal (1989).

4.7.1 Type curves for homogeneous reservoir

Infinite boundary system

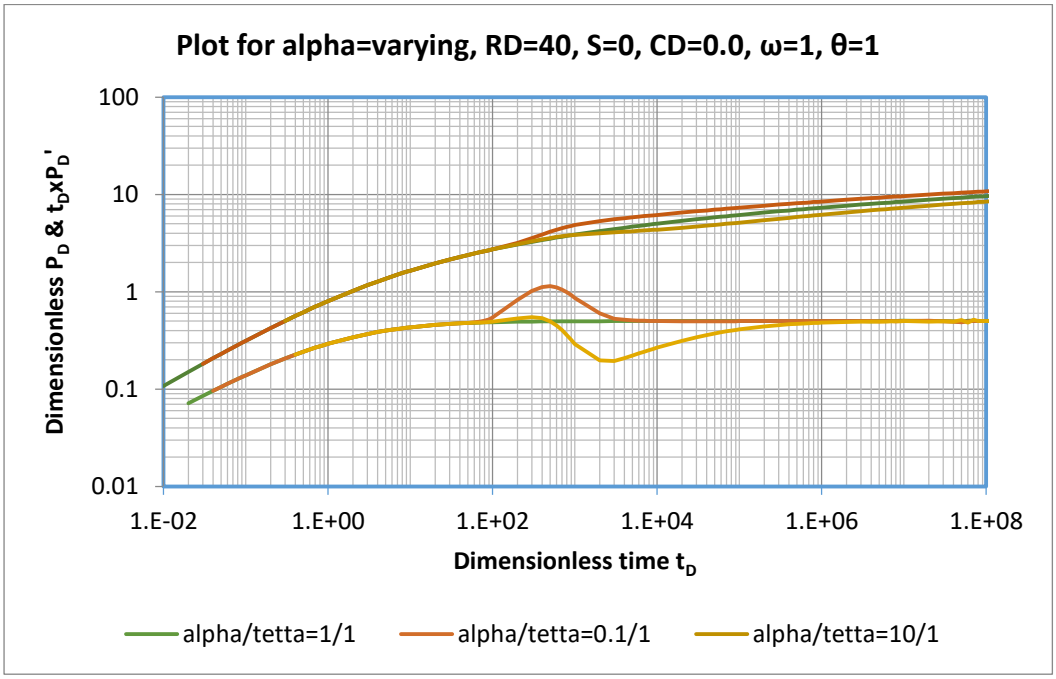

Figure 4.22: Pressure and Pressure derivative plot for radial flow behavior of non-Newtonian fluids. (Skin = 0, n=m=1.0, RD=40, ω = 1, α=varying, θ =1)

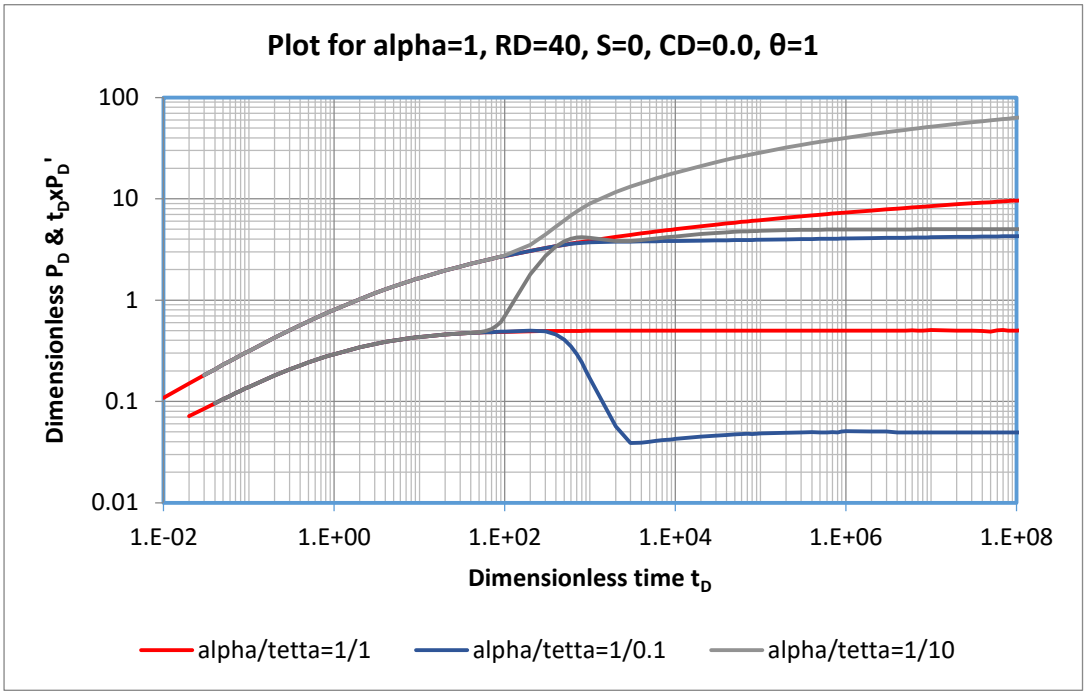

Figure 4.23: Pressure and Pressure derivative plot for radial flow behavior of non-Newtonian fluids. (Skin = 0, n=m=1.0, RD=40, ω = 1, α=1.0, θ =varying)

4.7.2 Type curve verification for naturally fractured reservoir (NFRs)

Infinite reservoir boundary system

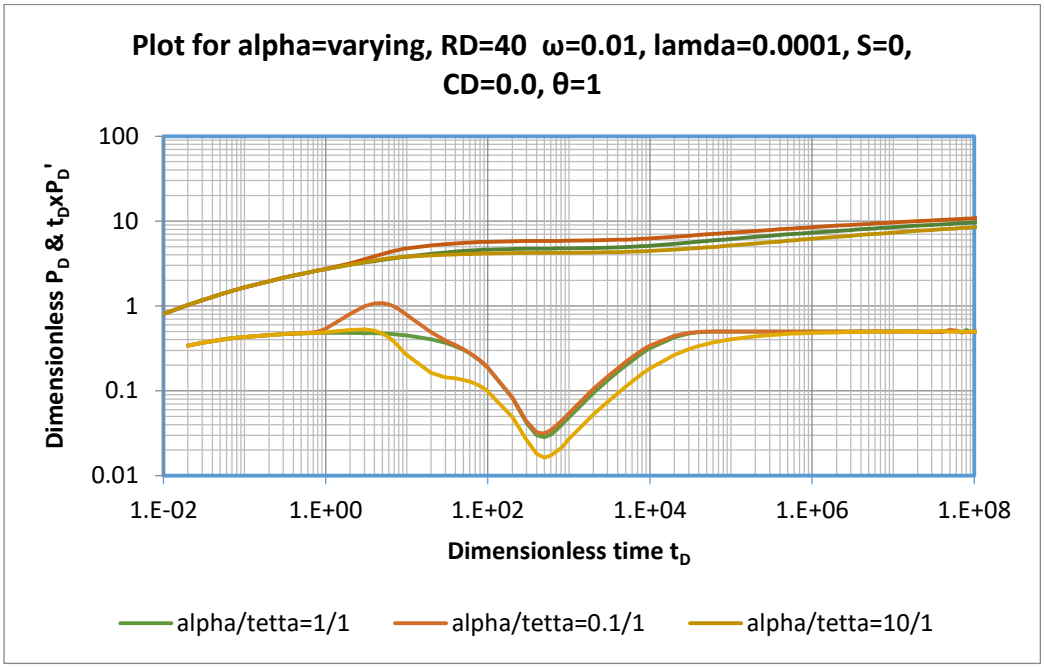

Figure 4.24: Pressure and Pressure derivative plot for radial flow behavior of non-Newtonian fluids. (Skin = 0, n=m=1.0, RD=40, ω =0.01, λ=0.001, α=varying, θ =1.0)

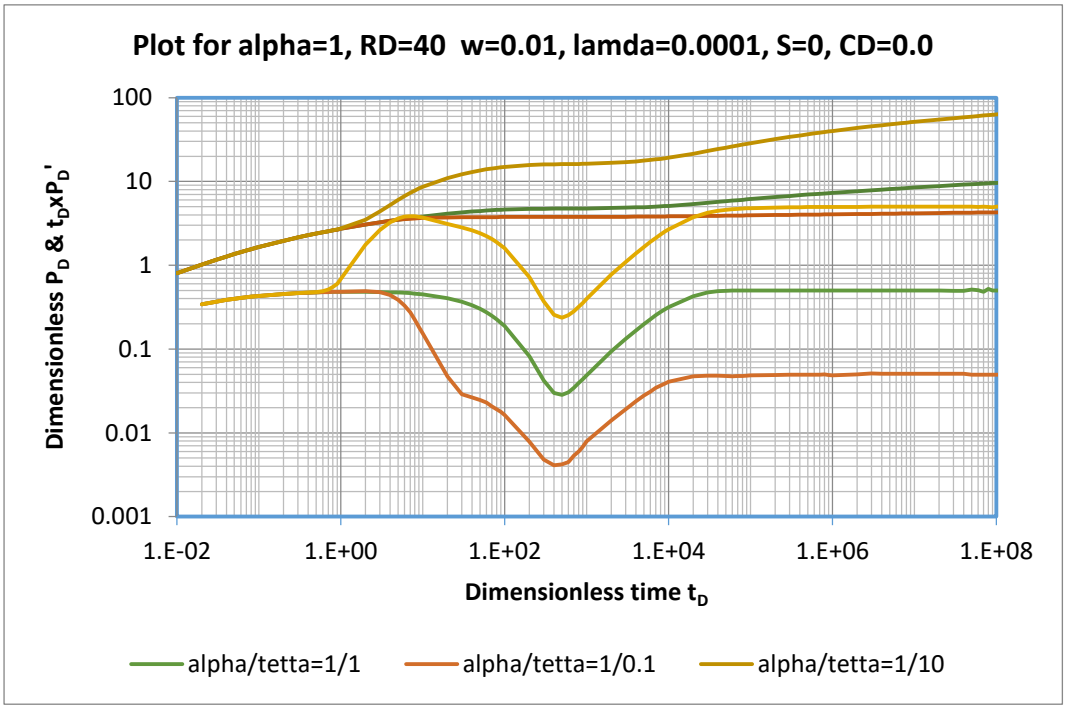

Figure 4.25: Pressure and Pressure derivative plot for radial flow behavior of non-Newtonian fluids. (Skin = 0, n=m=1.0, RD=40, ω =0.01, λ=0.001, α=1.0, θ =varying)

CHAPTER 5

NON-NEWTONIAN/NEWTONIAN COMPOSITE RADIAL FLUID FLOW IN A TWO-REGION, HOMOGENEOUS, AND NATURALLY FRACTURED RESERVOIR SYSTEM

This chapter shows the step-by-step analysis for developing the mathematical model for the interface boundary conditions of two-region radial composite reservoir system with wellbore storage and skin at the active (injection or production) well for non-Newtonian/Newtonian fluid flow. It considers the situation whereby non-Newtonian power-law fluid (polymer solutions) is injected into a reservoir and comes in contact with a Newtonian fluid (crude oil).

5.1 Model Assumptions

1. Fluid flow is radial
2. Laminar and Darcy's flow is valid
3. Isothermal, single phase and slightly compressible fluids with constant properties in each region
4. Pseudoplastic (non-Newtonian) fluid obeys Ostwald de Waele power-law relationship
5. Newtonian fluid is a constant viscosity fluid
6. Non-Newtonian fluid displaces Newtonian fluid in a piston-like displacement
7. Effect of gravity is negligible
8. Infinite, constant –pressure, and closed (no-flow) outer boundaries

5.2 Mathematical Model Development

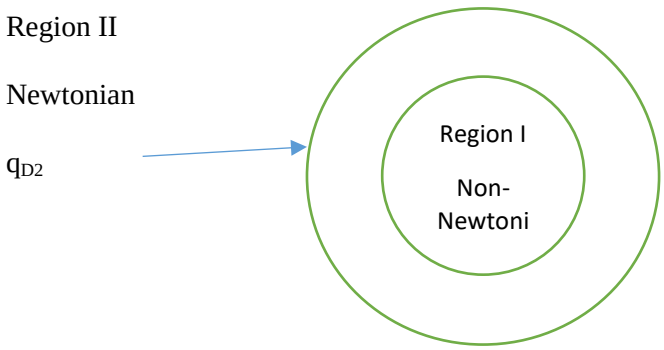

Figure 5.1: A diagram of a two-region (Non-Newtonian/Newtonian) radial composite reservoir

The linearized approximation of the partial differential equation for radial flow of Newtonian fluids through a porous media is given by the diffusivity equation as:

$$\frac{\partial^2 P_2}{\partial r^2} + \frac{1}{r}\frac{\partial P_2}{\partial r} = \left(\frac{\varphi c_t \mu}{k}\right)_2 \frac{\partial P_2}{\partial t} \tag{5.1}$$

The dimensionless form is given as:

$$\frac{\partial^2 P_{D2}}{\partial r_D^2} + \frac{1}{r_D}\frac{\partial P_{D2}}{\partial r_D} = \left(\frac{\varphi c_t r_w^2 \mu}{k}\right)_2 \frac{\partial P_{D2}}{\partial t_D} \tag{5.2}$$

Initial and boundary conditions for regions I and II (subscript 1 and 2 refers to non-Newtonian and Newtonian regions respectively) are:

Initial condition:

$$P_D(r_D, t_D = 0) = 0 \; for \; 1 < r_D < \infty \tag{5.3}$$

At wellbore, $r_D = 1$ and inner boundary condition is:

$$\frac{\partial P_{D1}}{\partial r_D} = -\frac{1}{s} \tag{5.4}$$

Outer boundary condition:

- For an infinite system:

$$P_D(r_D = \infty, t_D) = 0 \tag{5.5}$$

- No-flow (closed) boundary system:

$$\frac{\partial \bar{P}_{D2}}{\partial r_D}(\, R_{eD} = 0) = 0 \tag{5.6}$$

- Constant pressure boundary system:

$$\bar{P}_{D2}(\, R_{eD} = 0) = 0 \tag{5.7}$$

Solution

Flow equation for non-Newtonian fluid is given as:

$$q_1 = -2\pi r h \left(\frac{k_1}{\mu_{eff}}\frac{\partial P_1}{\partial r}\right)^{\frac{1}{n}} \tag{5.8}$$

Re-arranging, we have:

$$\left(-\frac{\partial P_1}{\partial r}\right) = \frac{\mu_{eff}}{k_1}\left(\frac{q_1}{2\pi r h}\right)^n \tag{5.9}$$

Dimensionless parameters:

$$P_D = \frac{P - P_i}{\left(\frac{q}{2\pi h}\right)^n \left(\frac{\mu_{eff} r_w^{1-n}}{k}\right)} \tag{5.10}$$

$$t_D = \frac{t}{n\left(\frac{\varphi c_t \mu_{eff}}{k}\right)_1 \left(\frac{2\pi h}{q}\right)^{1-n} r_w^{3-n}} \tag{5.11}$$

Therefore from equation (5.10), we get

$$\frac{k_r}{\mu_{eff}} = \frac{P_D \left(\frac{q}{2\pi h}\right)^n r_w^{1-n}}{P - P_i} \tag{5.12}$$

And from equation (5.11),

$$\varphi c_t = \frac{k_r}{\mu_{eff}} \frac{t}{t_D n \left(\frac{2\pi h}{q}\right)^{1-n} r_w^{3-n}} \tag{5.13}$$

Taking the derivative of (5.10) with respect to radius r, we have:

$$\frac{\partial P_D}{\partial r} = -\frac{\partial P}{\partial r} \frac{k_1}{\left(\frac{q}{2\pi h}\right)^n \mu_{eff} r_w^{1-n}} \tag{5.14}$$

Re-arranging,

$$\frac{\partial P}{\partial r} = -\left(\frac{q}{2\pi h}\right)^n \frac{\mu_{eff} r_w^{1-n}}{k_1} \frac{\partial P_D}{\partial r} \tag{5.15}$$

$$\frac{\partial P}{\partial r} = -\left(\frac{q}{2\pi h}\right)^n \frac{\mu_{eff} r_w^{1-n}}{k_1 r_w} \frac{\partial P_{D1}}{\partial r_D} \tag{5.16}$$

$$\frac{\partial P}{\partial r} = -\left(\frac{q}{2\pi r_w h}\right)^n \frac{\mu_{eff}}{k_1} \frac{\partial P_D}{\partial r_D} \tag{5.17}$$

From equation (12) in Lund and Ikoku (1981), at interface R or R_D:

$$\left[\lambda_{eff}\left(-\frac{\partial P_1}{\partial r}\right)\right]^{\frac{1}{n}} = \lambda_2\left(-\frac{\partial P_2}{\partial r}\right) \tag{5.18}$$

Where,

$$\lambda_{eff} = \frac{k_1}{\mu_{eff}}, \tag{5.19}$$

And,

$$\lambda_2 = \frac{k_2}{\mu_2} \tag{5.20}$$

Substituting (5.17) into (5.18), we have:

$$\left[\frac{k_1}{\mu_{eff}}\left(-\left(\frac{q}{2\pi r_w h}\right)^n \frac{\mu_{eff}}{k_1}\frac{\partial P_{D1}}{\partial r_D}\right)\right]^{\frac{1}{n}} = \frac{k_2}{\mu_2}\left(-\left(\frac{q}{2\pi r_w h}\right)^n \frac{\mu_{eff}}{k_1}\frac{\partial P_{D2}}{\partial r_D}\right) \tag{5.21}$$

$$\left(\frac{q}{2\pi r_w h}\right)^{1-n}\left[\frac{k_1}{\mu_{eff}}\left(-\frac{\mu_{eff}}{k_1}\frac{\partial P_{D1}}{\partial r_D}\right)\right]^{\frac{1}{n}} = \frac{k_2}{\mu_2}\left(-\frac{\mu_{eff}}{k_1}\frac{\partial P_{D2}}{\partial r_D}\right) \tag{5.22}$$

$$\left(\frac{q}{2\pi r_w h}\right)^{1-n}\left[\left(-\frac{\partial P_{D1}}{\partial r_D}\right)\right]^{\frac{1}{n}} = \frac{k_2}{\mu_2}\left(-\frac{\mu_{eff}}{k_1}\frac{\partial P_{D2}}{\partial r_D}\right) \tag{5.23}$$

$$\left(\frac{q}{2\pi r_w h}\right)^{1-n}\left(\frac{k_1}{\mu_{eff}}/\frac{k_2}{\mu_2}\right)\left[-\frac{\partial P_{D1}}{\partial r_D}\right]^{\frac{1}{n}} = \left(-\frac{\partial P_{D2}}{\partial r_D}\right) \tag{5.24}$$

Combining equation (5.9) and (5.17),

$$\left(\frac{\partial P}{\partial r}\right) = \left(-\left(\frac{q}{2\pi r_w h}\right)^n \frac{\mu_{eff}}{k_1}\frac{\partial P_{D1}}{\partial r_D}\right) = \frac{\mu_{eff}}{k_1}\left(\frac{q}{2\pi r h}\right)^n \tag{5.25}$$

$$-\frac{\partial P_{D1}}{\partial r_D} = \left(\frac{r_w}{r}\right)^n = \left(\frac{1}{r_D}\right)^n \tag{5.26}$$

$$\left[-\frac{\partial P_{D1}}{\partial r_D}\right]^{\frac{1}{n}} = \left(\frac{1}{r_D}\right) \tag{5.27}$$

Substituting (5.27) into (5.24), we get:

$$\left(\frac{q}{2\pi r_w h}\right)^{1-n}\left(\frac{k_1}{\mu_{eff}}/\frac{k_2}{\mu_2}\right)\left(\frac{1}{r_D}\right) = \left(-\frac{\partial P_{D2}}{\partial r_D}\right) \tag{5.28}$$

$$\left(\frac{q}{2\pi r_w h}\right)^{1-n}\left(\frac{\lambda_{eff}}{\lambda_2}\right)\left(\frac{1}{r_D}\right) = \left(-\frac{\partial P_{D2}}{\partial r_D}\right) \tag{5.29}$$

Set $\theta = \left(\frac{\lambda_{eff}}{\lambda_2}\right)\left(\frac{q}{2\pi r_w h}\right)^{1-n}$,

And (5.29) becomes:

$$\frac{\partial P_{D2}}{\partial r_D} = \left(-\frac{\theta}{r_D}\right) \tag{5.30}$$

$$\frac{\partial \bar{P}_{D2}}{\partial r_D} = \left(-\frac{\theta}{sR_D}\right) \tag{5.31}$$

When n is approximately 1 (Newtonian fluid) or for higher values of n, equation (5.24) becomes:

$$\left(\frac{\lambda_{eff}}{\lambda_2}\right)\frac{\partial P_{D1}}{\partial r_D} = \frac{\partial P_{D2}}{\partial r_D} \tag{5.32}$$

A general Laplace solution for the dimensionless pressure drop for regions I is:

Region I: $Non-Newtonian\ (1 \le r_D \le R_D)$

$$\bar{P}_{D1}(1 \le r_D \le R_D) = r_D^{\frac{V}{\beta}}\left(C_1 I_V\left(\beta r_D^{\frac{1}{\beta}}\sqrt{sfs}\right) + C_2 K_V\left(\beta r_D^{\frac{1}{\beta}}\sqrt{sfs}\right)\right) \tag{5.33}$$

Differentiating P_{D1}, we get:

$$\frac{\partial \bar{P}_{D1}}{\partial r_D} = r_D^{\frac{1}{\beta}-1}\sqrt{sfs}\left(C_1 I_\beta\left(\beta\sqrt{sfs}r_D^{\frac{1}{\beta}}\right) - C_2 K_\beta\left(\beta\sqrt{sfs}r_D^{\frac{1}{\beta}}\right)\right) \tag{5.34}$$

At wellbore condition, $r_D = 1$:

$$\bar{P}_{wD1}(r_D = 1) = C_1 I_V\left(\beta\sqrt{sfs}\right) + C_2 K_V\left(\beta\sqrt{sfs}\right) \tag{5.35}$$

$$\frac{\partial \bar{P}_{wD1}}{\partial r_D} = -\frac{1}{s} = \sqrt{sfs}\left(C_1 I_\beta\left(\beta\sqrt{sfs}\right) - C_2 K_\beta\left(\beta\sqrt{sfs}\right)\right) \tag{5.36}$$

$$C_1 = \frac{-\frac{1}{s\sqrt{sfs}} + C_2 K_\beta\left(\beta\sqrt{sfs}\right)}{I_\beta\left(\beta\sqrt{sfs}\right)} \tag{5.37}$$

Laplace solution for the dimensionless pressure drop in infinite flow for region II is:

Region II: $Newtonian\ (R_D \le r_D \le \infty)$

$$\bar{P}_{D2} = C_3 K_o\left(r_D\sqrt{\alpha sfs}\right) \tag{5.38}$$

At interface, $r_D = R_D$ and, $P_{D1} = P_{D2}$:

$$r_D^{\frac{V}{\beta}}\left(C_1 I_V\left(\beta r_D^{\frac{1}{\beta}}\sqrt{sfs}\right) + C_2 K_V\left(\beta r_D^{\frac{1}{\beta}}\sqrt{sfs}\right)\right) = C_3 K_o\left(r_D\sqrt{\alpha sfs}\right) \tag{5.39}$$

Making C_3 the subject, we have:

$$C_3 = \frac{R_D^{\frac{V}{\beta}}\left(C_1 I_V\left(\beta R_D^{\frac{1}{\beta}}\sqrt{sfs}\right) + C_2 K_V\left(\beta R_D^{\frac{1}{\beta}}\sqrt{sfs}\right)\right)}{K_O\left(R_D\sqrt{\alpha sfs}\right)} = \frac{R_D^{\frac{V}{\beta}}\left(C_1 I_V\left(\beta R_D^{\frac{1}{\beta}}\sqrt{sfs}\right) + C_2 K_V\left(\beta R_D^{\frac{1}{\beta}}\sqrt{sfs}\right)\right)}{B} \tag{5.40}$$

Differentiating P_{D2}, and applying, n = 1, β = 1, and v = 0 for Newtonian fluid, we get:

$$\frac{\partial \bar{P}_{D2}}{\partial r_D} = -C_3\sqrt{\alpha sfs}K_1\left(R_D\sqrt{\alpha sfs}\right) \tag{5.41}$$

Substituting $\frac{\partial \bar{P}_{D2}}{\partial r_D}$ from equation (5.30),

$$\left(-\frac{\theta}{R_D}\right) = -C_3\sqrt{\alpha sfs}K_1\left(R_D\sqrt{\alpha sfs}\right) \tag{5.42}$$

$$C_3 = \frac{\theta}{R_D\sqrt{\alpha sfs}K_1\left(R_D\sqrt{\alpha sfs}\right)} = \frac{\theta}{A} \tag{5.43}$$

Equating (5.40) and (5.43),

$$\frac{R_D^{\frac{V}{\beta}}\left(C_1 I_V\left(\beta R_D^{\frac{1}{\beta}}\sqrt{sfs}\right)+C_2 K_V\left(\beta R_D^{\frac{1}{\beta}}\sqrt{sfs}\right)\right)}{B} = \frac{\theta}{A} \tag{5.44}$$

$$B\theta = AR_D^{\frac{V}{\beta}}C_1 I_V\left(\beta R_D^{\frac{1}{\beta}}\sqrt{sfs}\right) + AR_D^{\frac{V}{\beta}}C_2 K_V\left(\beta R_D^{\frac{1}{\beta}}\sqrt{sfs}\right) \tag{5.45}$$

$$AR_D^{\frac{V}{\beta}}C_1 I_V\left(\beta R_D^{\frac{1}{\beta}}\sqrt{sfs}\right) = B\theta - AR_D^{\frac{V}{\beta}}C_2 K_V\left(\beta R_D^{\frac{1}{\beta}}\sqrt{sfs}\right) \tag{5.46}$$

$$C_1 = \frac{B\theta - AR_D^{\frac{V}{\beta}}C_2 K_V\left(\beta R_D^{\frac{1}{\beta}}\sqrt{sfs}\right)}{AR_D^{\frac{V}{\beta}}I_V\left(\beta R_D^{\frac{1}{\beta}}\sqrt{sfs}\right)} \tag{5.47}$$

Equating (5.37) and (5.39),

$$\frac{-\frac{1}{s\sqrt{sfs}}+C_2 K_\beta\left(\beta\sqrt{sfs}\right)}{I_\beta\left(\beta\sqrt{sfs}\right)} = \frac{B\theta - AR_D^{\frac{V}{\beta}}C_2 K_V\left(\beta R_D^{\frac{1}{\beta}}\sqrt{sfs}\right)}{AR_D^{\frac{V}{\beta}}I_V\left(\beta R_D^{\frac{1}{\beta}}\sqrt{sfs}\right)} \tag{5.48}$$

$$-\frac{AR_D^{\frac{V}{\beta}}I_V\left(\beta R_D^{\frac{1}{\beta}}\sqrt{sfs}\right)}{s\sqrt{sfs}} + AR_D^{\frac{V}{\beta}}I_V\left(\beta R_D^{\frac{1}{\beta}}\sqrt{sfs}\right)C_2 K_\beta\left(\beta\sqrt{sfs}\right) =$$

$$I_\beta\left(\beta\sqrt{sfs}\right)B\theta - A\,R_D^{\frac{V}{\beta}}C_2 K_V\left(\beta R_D^{\frac{1}{\beta}}\sqrt{sfs}\right)I_\beta\left(\beta\sqrt{sfs}\right) \tag{5.49}$$

$$C_2\left[AR_D^{\frac{V}{\beta}}I_V\left(\beta R_D^{\frac{1}{\beta}}\sqrt{sfs}\right)K_\beta\left(\beta\sqrt{sfs}\right) + AR_D^{\frac{V}{\beta}}K_V\left(\beta R_D^{\frac{1}{\beta}}\sqrt{sfs}\right)I_\beta\left(\beta\sqrt{sfs}\right)\right] = I_\beta\left(\beta\sqrt{sfs}\right)B\theta +$$

$$\frac{AR_D^{\frac{V}{\beta}}I_V\left(\beta R_D^{\frac{1}{\beta}}\sqrt{sfs}\right)}{s\sqrt{sfs}} \tag{5.50}$$

$$C_2 = \frac{I_\beta(\beta\sqrt{sfs})B\theta + \frac{AR_D^{\frac{V}{\beta}} I_V\left(\beta R_D^{\frac{1}{\beta}}\sqrt{sfs}\right)}{s\sqrt{sfs}}}{\left[AR_D^{\frac{V}{\beta}} I_V\left(\beta R_D^{\frac{1}{\beta}}\sqrt{sfs}\right)K_\beta(\beta\sqrt{sfs}) + AR_D^{\frac{V}{\beta}} K_V\left(\beta R_D^{\frac{1}{\beta}}\sqrt{sfs}\right)I_\beta(\beta\sqrt{sfs})\right]} = \frac{E}{D} \quad (5.51)$$

Laplace solution for the dimensionless pressure drops for closed (no-flow) boundary system for region II is:

Region II: $Newtonian\ (R_D \le r_D \le \infty)$

$$\bar{P}_{D2} = \left[C_3 I_0\left(r_D\sqrt{\alpha sfs}\right) + C_4 K_O\left(r_D\sqrt{\alpha sfs}\right)\right] \quad (5.52)$$

Differentiating P_{D2}:

$$\frac{\partial \bar{P}_{D2}}{\partial r_D}(r_D \to R_D) = \left[C_3\sqrt{\alpha sfs} I_1\left(R_D\sqrt{\alpha sfs}\right) - C_4\sqrt{\alpha sfs} K_1\left(R_D\sqrt{\alpha sfs}\right)\right] \quad (5.53)$$

Substituting (5.6) into (5.53), we get:

$$C_4 = C_3 \frac{I_1\left(R_{eD}\sqrt{\alpha sfs}\right)}{K_1\left(R_{eD}\sqrt{\alpha sfs}\right)} \quad (5.54)$$

And so, (5.47) and (5.48) becomes:

$$\bar{P}_{D2} = C_3\left[\frac{I_1\left(R_{eD}\sqrt{\alpha sfs}\right)}{K_1\left(R_{eD}\sqrt{\alpha sfs}\right)} K_O\left(R_D\sqrt{\alpha sfs}\right) + \left(I_0 R_D\sqrt{\alpha sfs}\right)\right] \quad (5.55)$$

$$\frac{\partial \bar{P}_{D2}}{\partial r_D}(r_D \to R_D) = C_3\sqrt{\alpha sfs}\left[\left(I_1 R_D\sqrt{\alpha sfs}\right) - \frac{I_1\left(R_{eD}\sqrt{\alpha sfs}\right)K_1\left(R_D\sqrt{\alpha sfs}\right)}{K_1\left(R_{eD}\sqrt{\alpha sfs}\right)}\right] \quad (5.56)$$

At interface $r_D = R_D$, and $P_{D1} = P_{D2}$:

$$r_D^{\frac{V}{\beta}}\left(C_1 I_V\left(\beta r_D^{\frac{1}{\beta}}\sqrt{sfs}\right) + C_2 K_V\left(\beta r_D^{\frac{1}{\beta}}\sqrt{sfs}\right)\right) = C_3\left[\frac{I_1\left(R_{eD}\sqrt{\alpha sfs}\right)}{K_1\left(R_{eD}\sqrt{\alpha sfs}\right)} K_O\left(R_D\sqrt{\alpha sfs}\right) + \left(I_0 R_D\sqrt{\alpha sfs}\right)\right] \quad (5.57)$$

Making C_3 the subject from (5.57), we have:

$$C_3 = \frac{R_D^{\frac{V}{\beta}}\left(C_1 I_V\left(\beta R_D^{\frac{1}{\beta}}\sqrt{sfs}\right) + C_2 K_V\left(\beta R_D^{\frac{1}{\beta}}\sqrt{sfs}\right)\right)}{\frac{I_1\left(R_{eD}\sqrt{\alpha sfs}\right)}{K_1\left(R_{eD}\sqrt{\alpha sfs}\right)} K_O\left(R_D\sqrt{\alpha sfs}\right) + \left(I_0 R_D\sqrt{\alpha sfs}\right)} = \frac{R_D^{\frac{V}{\beta}}\left(C_1 I_V\left(\beta R_D^{\frac{1}{\beta}}\sqrt{sfs}\right) + C_2 K_V\left(\beta R_D^{\frac{1}{\beta}}\sqrt{sfs}\right)\right)}{B} \quad (5.58)$$

Combining (5.33) and (5.58) and re-arranging, we have:

$$C_3 = \frac{\theta}{R_D\sqrt{\alpha sfs}\left[\frac{I_1(R_{eD}\sqrt{\alpha sfs})K_1(R_D\sqrt{\alpha sfs})}{K_1(R_{eD}\sqrt{\alpha sfs})} - (I_1 R_D\sqrt{\alpha sfs})\right]} = \frac{\theta}{A} \tag{5.59}$$

Equating (5.58) and (5.59),

$$B\theta = A\,R_D^{\frac{V}{\beta}}\left(C_1 I_V\left(\beta R_D^{\frac{1}{\beta}}\sqrt{sfs}\right) + A\,R_D^{\frac{V}{\beta}}\,C_2 K_V\left(\beta R_D^{\frac{1}{\beta}}\sqrt{sfs}\right)\right) \tag{5.60}$$

$$C_1 = \frac{B\theta - AR_D^{\frac{V}{\beta}}C_2 K_V\left(\beta R_D^{\frac{1}{\beta}}\sqrt{sfs}\right)}{AR_D^{\frac{V}{\beta}} I_V\left(\beta R_D^{\frac{1}{\beta}}\sqrt{sfs}\right)} \tag{5.61}$$

Equating (5.37) and (5.61), we get an equation same as (5.48). Therefore, C_2 is same as (5.51) and is:

$$C_2 = \frac{I_\beta(\beta\sqrt{sfs})B\theta + \frac{AR_D^{\frac{V}{\beta}} I_V\left(\beta R_D^{\frac{1}{\beta}}\sqrt{sfs}\right)}{s\sqrt{sfs}}}{\left[AR_D^{\frac{V}{\beta}} I_V\left(\beta R_D^{\frac{1}{\beta}}\sqrt{sfs}\right)K_\beta(\beta\sqrt{sfs}) + AR_D^{\frac{V}{\beta}} K_V\left(\beta R_D^{\frac{1}{\beta}}\sqrt{sfs}\right)I_\beta(\beta\sqrt{sfs})\right]} = \frac{E}{D}$$

Laplace solution for the dimensionless pressure drops for constant pressure boundary system for region II is:

Region II: $Newtonian\ (R_D \le r_D \le \infty)$

$$\bar{P}_{D2} = \left[C_3 I_0\left(r_D\sqrt{\alpha sfs}\right) + C_4 K_O\left(r_D\sqrt{\alpha sfs}\right)\right] \tag{5.62}$$

Differentiating P_{D2}, and applying, n = 1, β = 1, and v = 0 for Newtonian fluid, we get:

$$\frac{\partial \bar{P}_{D2}}{\partial r_D}(r_D \to R_D) = \sqrt{\alpha sfs}\left[C_3 I_1\left(R_D\sqrt{\alpha sfs}\right) - C_4 K_1\left(R_D\sqrt{\alpha sfs}\right)\right] \tag{5.63}$$

So, substituting (5.7) into (5.62), we get:

$$C_4 = -C_3\frac{I_0\left(R_{eD}\sqrt{\alpha sfs}\right)}{K_0\left(R_{eD}\sqrt{\alpha sfs}\right)} \tag{5.64}$$

Therefore at interface $r_D = R_D$,

$$\bar{P}_{D2} = C_3\left[\frac{I_0\left(R_{eD}\sqrt{\alpha sfs}\right)}{K_0\left(R_{eD}\sqrt{\alpha sfs}\right)}K_O\left(R_D\sqrt{\alpha sfs}\right) + \left(I_0 R_D\sqrt{\alpha sfs}\right)\right] \tag{5.65}$$

$$\frac{\partial \bar{P}_{D2}}{\partial r_D}(r_D \to R_D) = C_3\sqrt{\alpha sfs}\left[I_1\left(R_D\sqrt{\alpha sfs}\right) - \frac{I_0\left(R_{eD}\sqrt{\alpha sfs}\right)K_1\left(R_D\sqrt{\alpha sfs}\right)}{K_0\left(R_{eD}\sqrt{\alpha sfs}\right)}\right] \tag{5.66}$$

And $P_{D1} = P_{D2}$ becomes:

$$r_D^{\frac{V}{\beta}}\left(C_1 I_V\left(\beta r_D^{\frac{1}{\beta}}\sqrt{sfs}\right) + C_2 K_V\left(\beta r_D^{\frac{1}{\beta}}\sqrt{sfs}\right)\right) = C_3\left[\frac{I_0(R_{eD}\sqrt{\alpha sfs})}{K_0(R_{eD}\sqrt{\alpha sfs})}K_O(R_D\sqrt{\alpha sfs}) - (I_0 R_D\sqrt{\alpha sfs})\right] \tag{5.67}$$

Making C_3 the subject of (5.65), we have:

$$C_3 = \frac{R_D^{\frac{V}{\beta}}\left(C_1 I_V\left(\beta R_D^{\frac{1}{\beta}}\sqrt{sfs}\right)+C_2 K_V\left(\beta R_D^{\frac{1}{\beta}}\sqrt{sfs}\right)\right)}{\frac{I_1(R_{eD}\sqrt{\alpha sfs})}{K_1(R_{eD}\sqrt{\alpha sfs})}K_O(R_D\sqrt{\alpha sfs})-I_0(R_D\sqrt{\alpha sfs})} = \frac{R_D^{\frac{V}{\beta}}\left(C_1 I_V\left(\beta R_D^{\frac{1}{\beta}}\sqrt{sfs}\right)+C_2 K_V\left(\beta R_D^{\frac{1}{\beta}}\sqrt{sfs}\right)\right)}{B} \tag{5.68}$$

Combining (5.31) with (5.66) and re-arranging,

$$C_3 = \frac{\theta}{R_D\sqrt{\alpha sfs}\left[\frac{I_0(R_{eD}\sqrt{\alpha sfs})K_1(R_D\sqrt{\alpha sfs})}{K_0(R_{eD}\sqrt{\alpha sfs})}+I_1(R_D\sqrt{\alpha sfs})\right]} = \frac{\theta}{A} \tag{5.69}$$

Equating (5.68) and (5.69), and re-arranging,

$$B\theta = A\,R_D^{\frac{V}{\beta}}\left(C_1 I_V\left(\beta R_D^{\frac{1}{\beta}}\sqrt{sfs}\right) + A\,R_D^{\frac{V}{\beta}}\,C_2 K_V\left(\beta R_D^{\frac{1}{\beta}}\sqrt{sfs}\right)\right) \tag{5.70}$$

$$C_1 = \frac{B\theta - AR_D^{\frac{V}{\beta}}C_2 K_V\left(\beta R_D^{\frac{1}{\beta}}\sqrt{sfs}\right)}{AR_D^{\frac{V}{\beta}}I_V\left(\beta R_D^{\frac{1}{\beta}}\sqrt{sfs}\right)} \tag{5.71}$$

Combining (5.37) and (5.71), we get an equation which is same as (5.48). Therefore, C_2 is same as (5.51) and is:

$$C_2 = \frac{I_\beta(\beta\sqrt{sfs})B\theta + \frac{AR_D^{\frac{V}{\beta}}I_V\left(\beta R_D^{\frac{1}{\beta}}\sqrt{sfs}\right)}{s\sqrt{sfs}}}{\left[AR_D^{\frac{V}{\beta}}I_V\left(\beta R_D^{\frac{1}{\beta}}\sqrt{sfs}\right)K_\beta(\beta\sqrt{sfs})+AR_D^{\frac{V}{\beta}}K_V\left(\beta R_D^{\frac{1}{\beta}}\sqrt{sfs}\right)I_\beta(\beta\sqrt{sfs})\right]} = \frac{E}{D}$$

Substituting (5.51) into (5.71), we have:

$$C_1 = \frac{-\frac{1}{s\sqrt{sfs}}+\frac{D}{E}K_\beta(\beta\sqrt{sfs})}{I_\beta(\beta\sqrt{sfs})} \tag{5.72}$$

5.3 Development of Type Curves

The different pressure and pressure derivative type curves are generated on MATLAB simulation platform. This section gives the summary of the developed type curves. Section 5.3.1 applies to the homogeneous formation when the flow index is not approximate to 1.0 or greater.

5.3.1 General solution type curves

5.3.1.1. Infinite Reservoir

These type curves are for infinite homogeneous and NFR system. Figure 5.2 illustrates the effect of mobility ratio on a Non-Newtonian/Newtonian flow. The curve for mobility ≤ 1 show a smooth straight line, while that of $\theta=100$ show the greatest shift from a straight line. Figure 5.3 shows the effect of α at other constant parameters. A shift is noticed between t_D=300 to 70000. Figure 5.4 shows log-log pressure and pressure derivative behavior for several dimensionless front radii with mobility ratio of 10 and storativity ratio of 1. Curves for R_D=50, 100, 500 and 1000 form almost a single curve at all times, while that for R_D=5 shows a difference from tD≥1.0. This is valid with observations made by Ambastha (1988).

Figs 5.5-5.6 show plots for varying storativity ratios, while Figs 5.7-5.8 show plot for several interporosity parameters at a constant storativity and mobility ratio with an arbitrary dimensionless radius. At smaller values of storativity ratio, the trough is seen to deepen, however, the appearance of the trough is a curve is seen to shift further to the right with decreasing interporosity parameter.

Figure 5.9-5.11 illustrates the effect of mobility ratio, alpha and dimensionless radius for NFRs; same observation as Fig 5.2-5.4 is made with a dip due to the low storativity.

Homogeneous

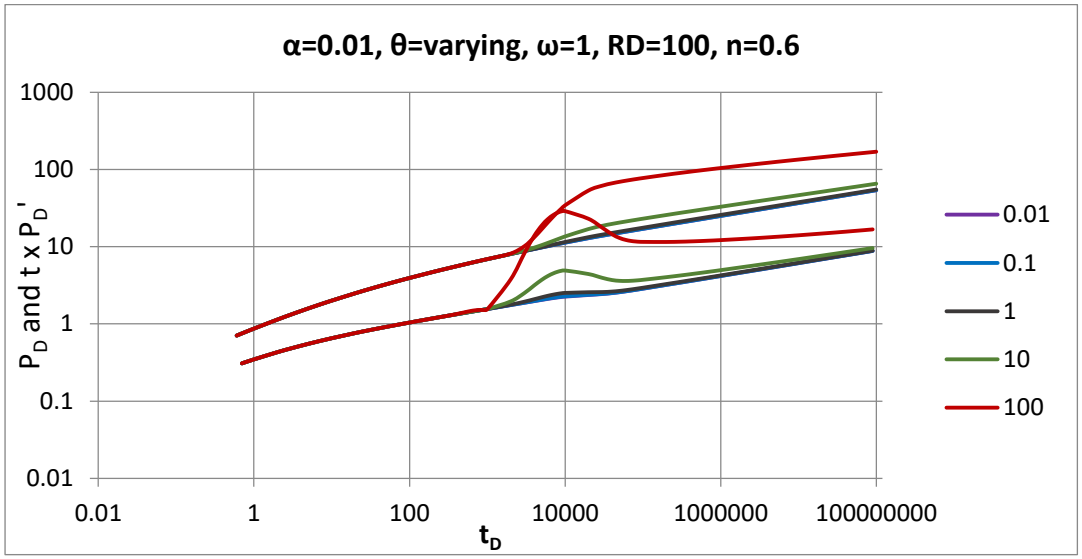

Figure 5.2: Effect of mobility ratio on interface-boundary conditions of Non-Newtonian/Newtonian flow (θ = varying, α = 0.01, ω = 1, R_D = 100, n = 0.6)

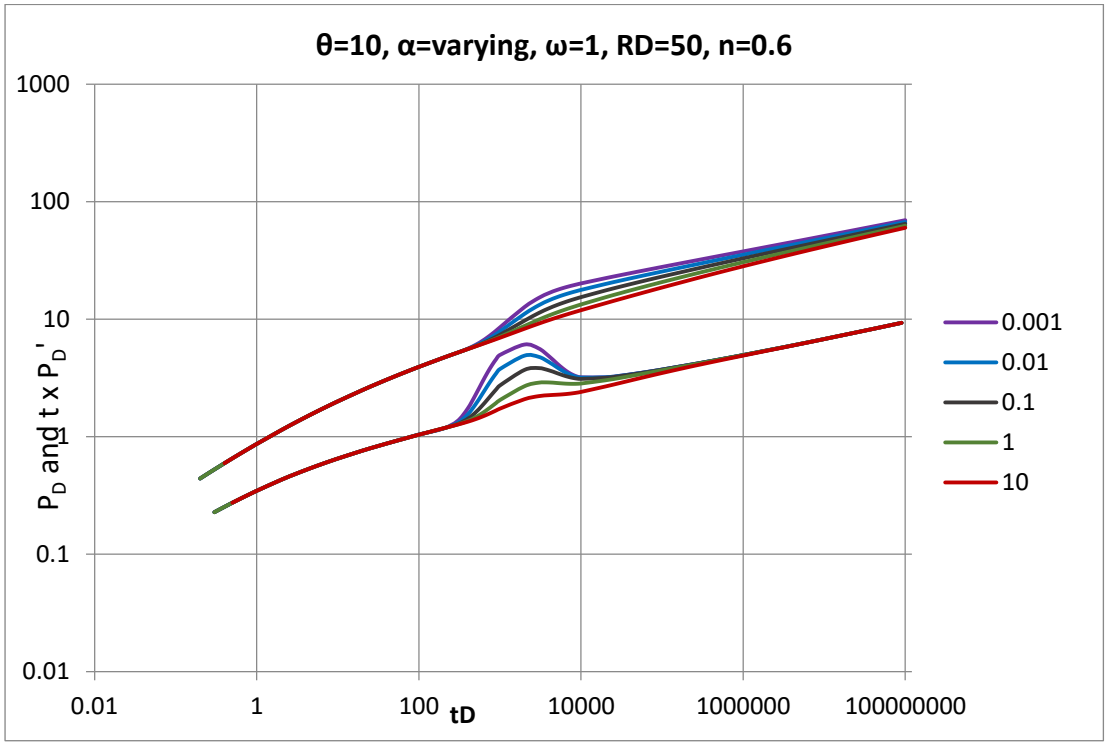

Figure 5.3: Effect of alpha on interface-boundary conditions of Non-Newtonian/Newtonian flow (θ=10, α = varying, ω = 1, R_D = 50, n = 0.6)

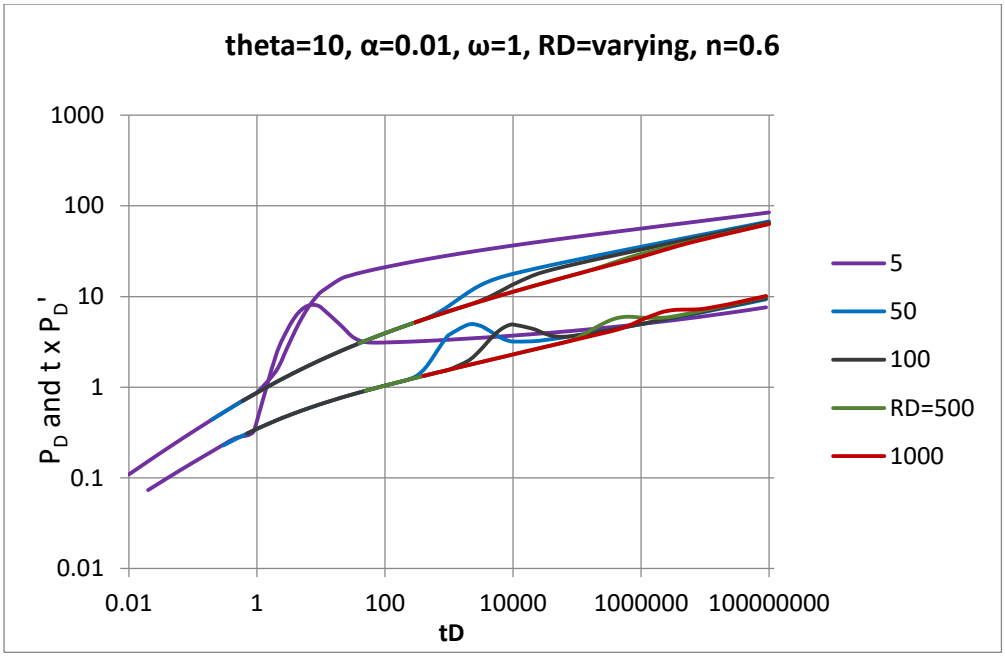

Figure 5.4: Effect of polymer front on interface-boundary conditions of Non-Newtonian/Newtonian flow (θ = 10, α = 0.01, ω = 1, R_D = varying, n = 0.6)

Naturally Fractured Reservoirs

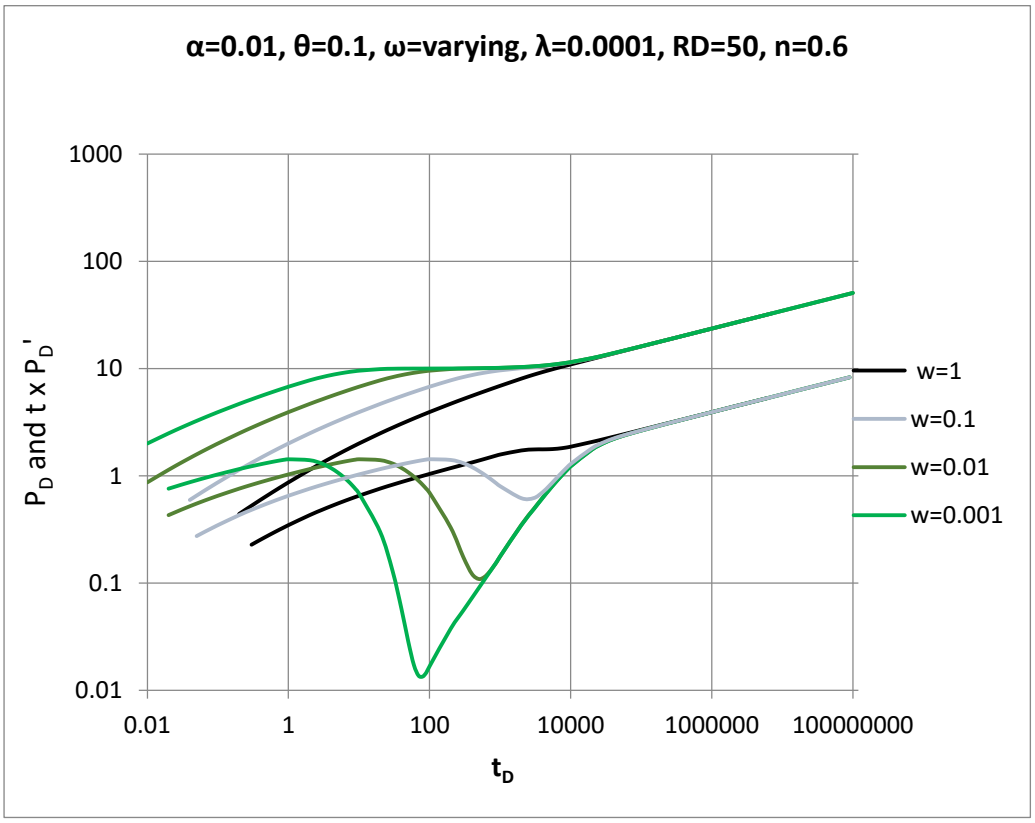

Figure 5.5: Effect of storage capacity ratio on interface-boundary conditions of Non-Newtonian/Newtonian flow (θ = 0.1, α = 0.01, ω = varying, λ=0.0001, R_D = 50, n = 0.6)

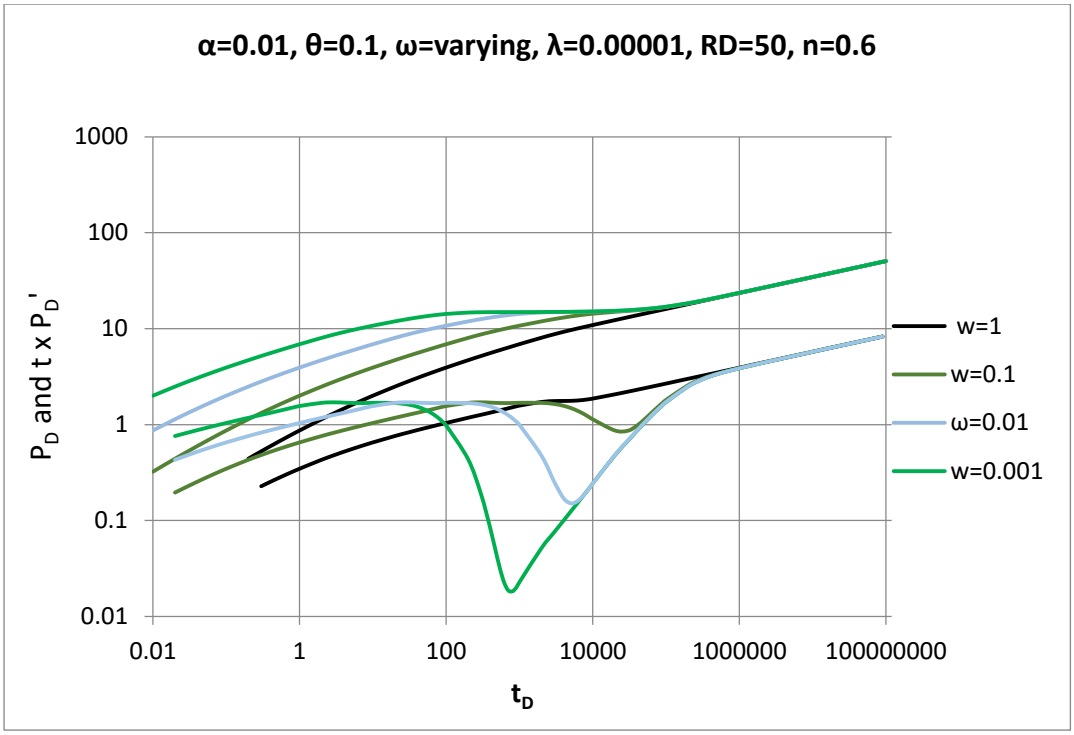

Figure 5.6: Effect of storage capacity ratio on interface-boundary conditions of Non-Newtonian/Newtonian flow (θ = 0.1, α = 0.01, ω = varying, λ=0.00001, R_D = 50, n = 0.6)

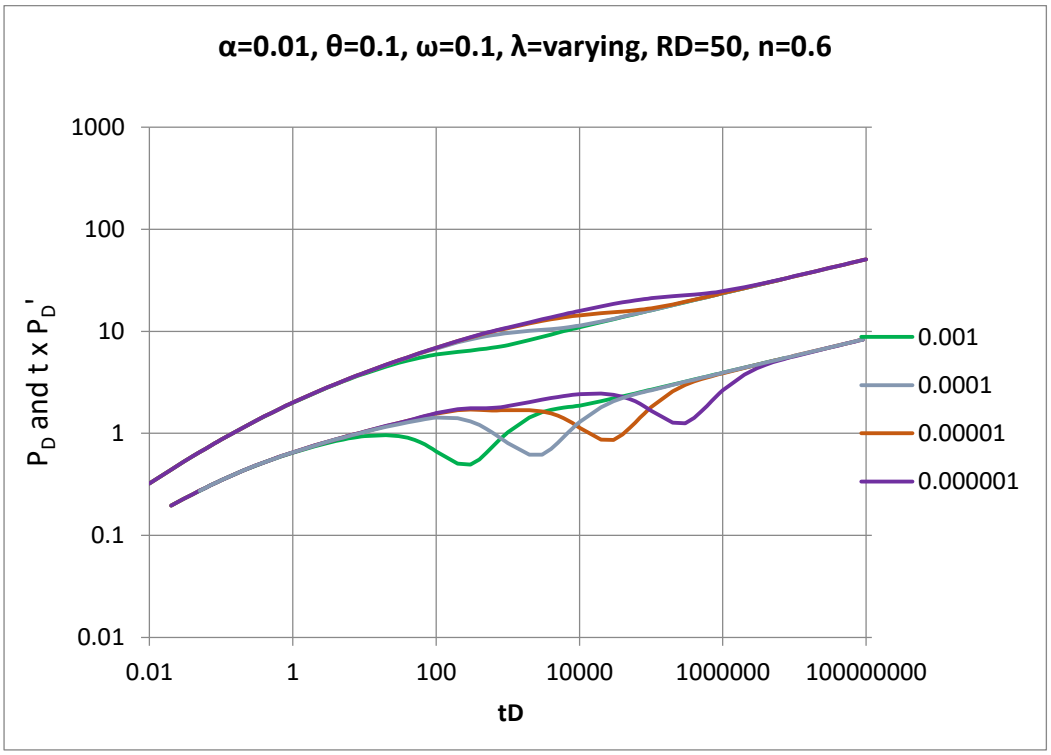

Figure 5.7: Effect of interporosity parameter on interface-boundary conditions of Non-Newtonian/Newtonian flow (θ = 0.1, α = 0.01, ω = 0.1, λ=varying, R_D = 50, n = 0.6)

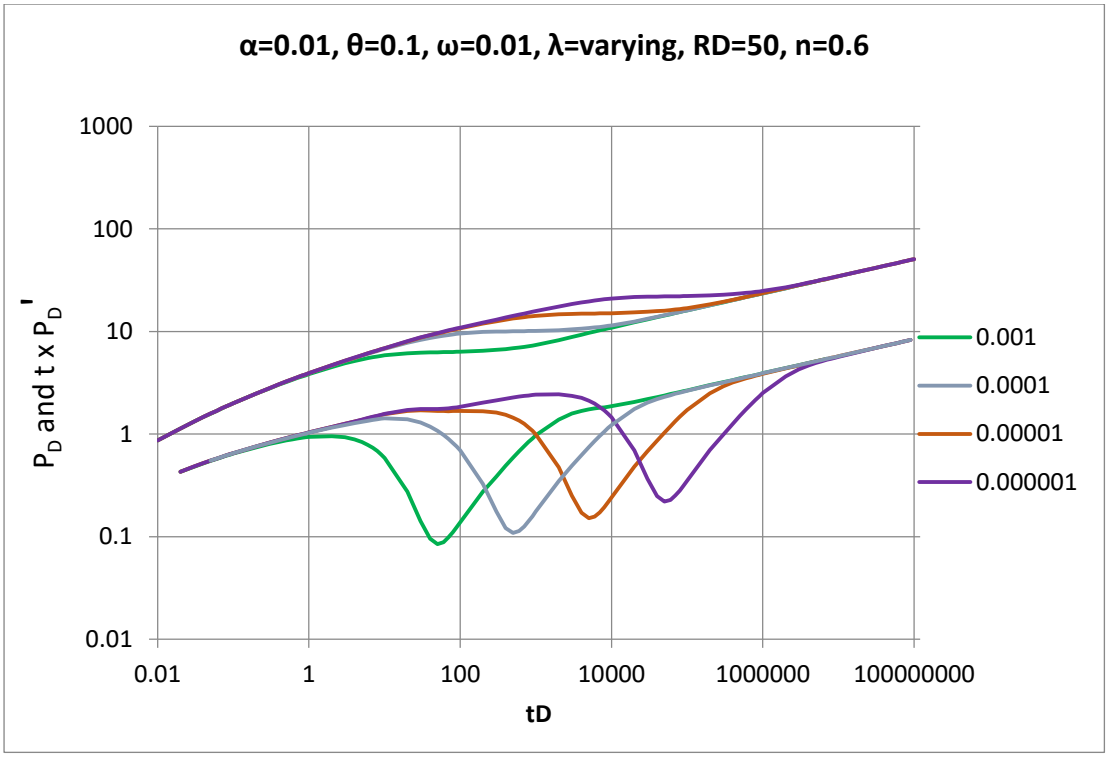

Figure 5.8: Effect of interporosity parameter on interface-boundary conditions of Non-Newtonian/Newtonian flow (θ = 0.1, α = 0.01, ω = 0.01, λ=varying, R_D = 50, n = 0.6)

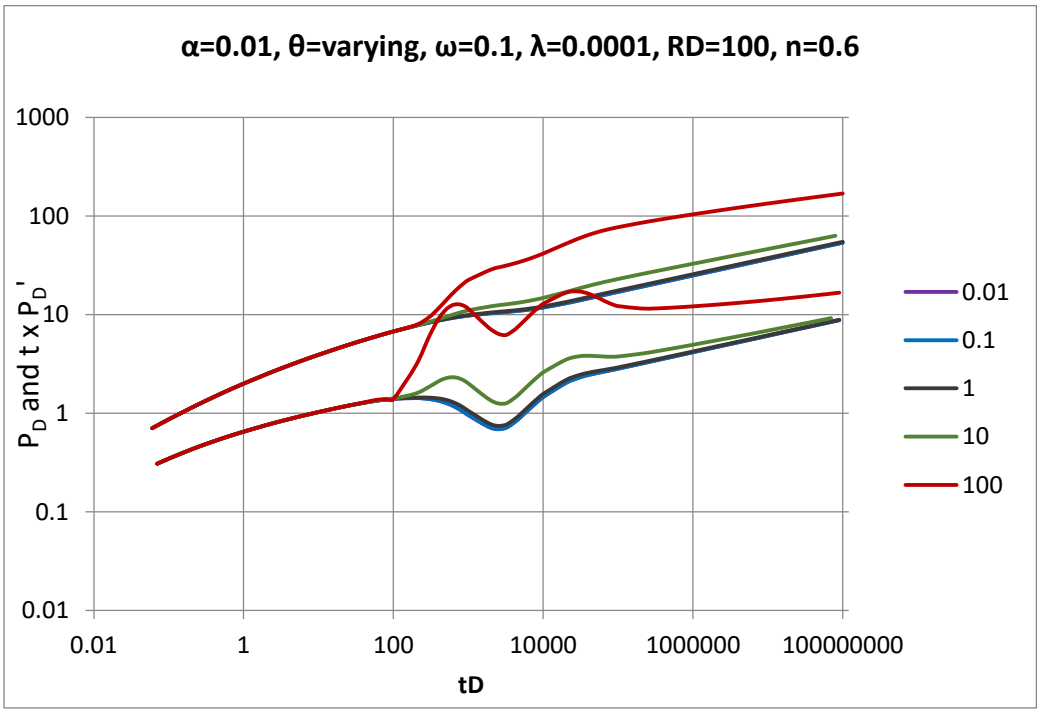

Figure 5.9: Effect of mobility ratio on interface-boundary conditions of Non-Newtonian/Newtonian flow (θ = varying, α = 0.01, ω=0.1, λ=0.0001, R_D = 100, n = 0.6)

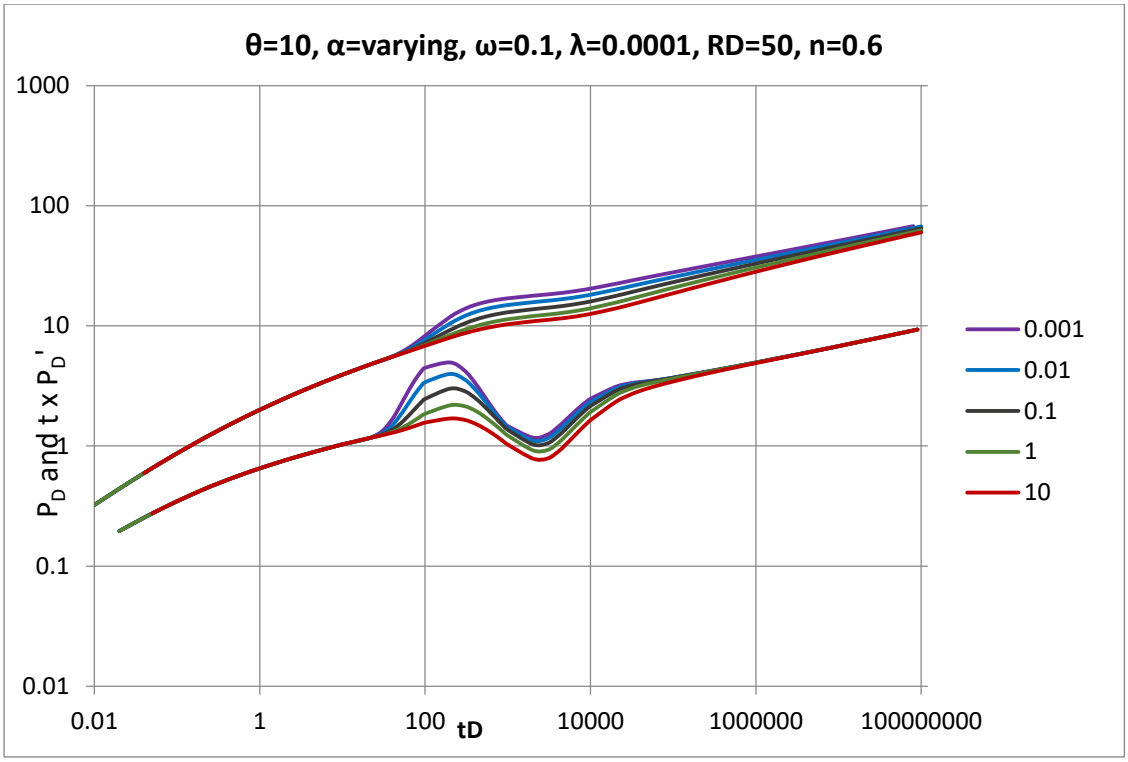

Figure 5.10: Effect of alpha on interface-boundary conditions of Non-Newtonian/Newtonian flow (θ=10, α = varying, ω = 0.1, λ=0.0001, R_D = 50, n = 0.6)

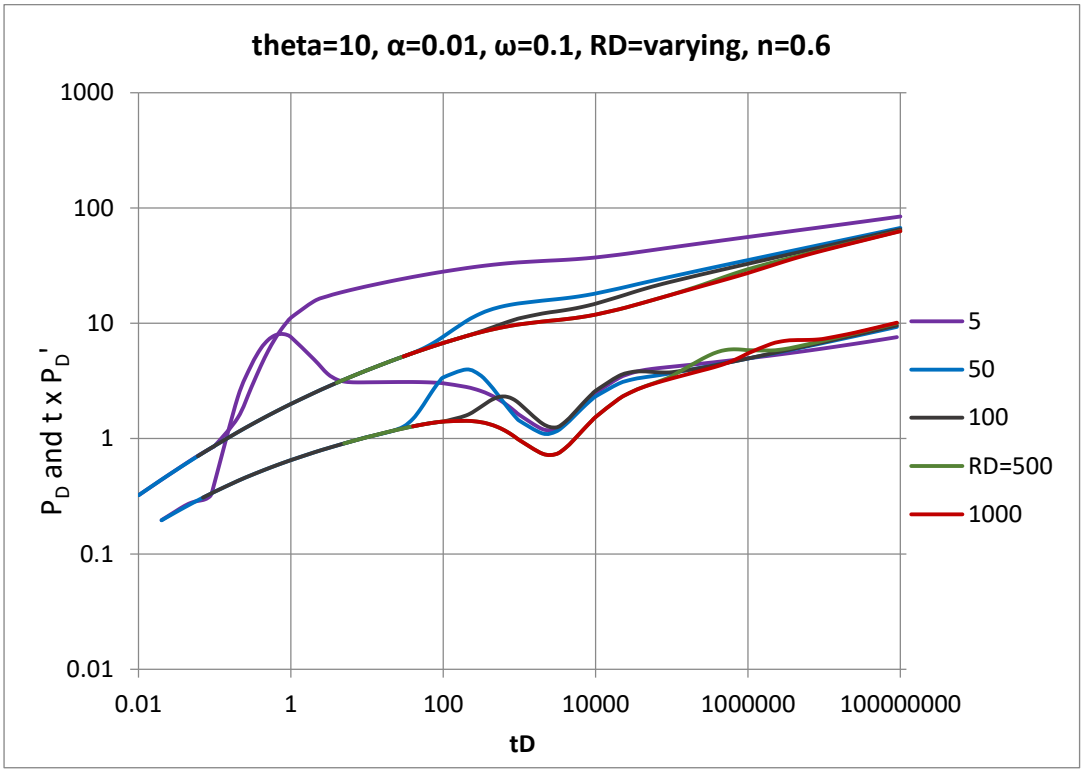

Figure 5.11: Effect of polymer front on interface-boundary conditions of Non-Newtonian/Newtonian flow (θ = 10, α = 0.01, ω =0.1, R_D = varying, n = 0.6)

5.3.1.2. Constant Pressure Boundary Reservoir

The type curves below are for constant pressure homogeneous and NFR system. Figure 5.12 illustrates the effect of change in interporosity parameter on a Non-Newtonian/Newtonian flow. Fig 5.13 shows effect of change in storage capacity ratio. A hump is observed at the left part of the derivative curves before the effect of the storage value is noticed. Changes in alpha at Fig 5.14-5.15 shows a single curve at all times. In Figs 5.16 and 5.17, on the pressure derivative part, the curves for mobility ratio converge to form a single straight line at t_D= 70000 and 80000 respectively. Curves for R_D=50, 100 and 1000 differ from that of R_D=5 in Figs 5.18-5.19.

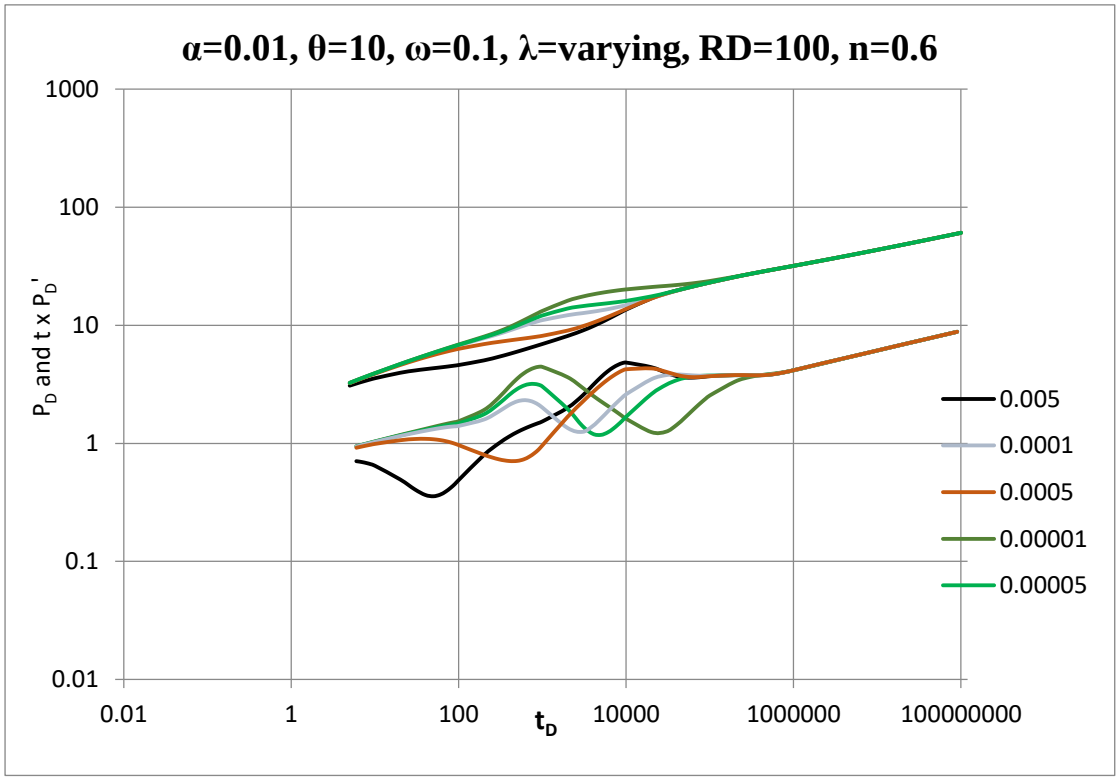

Figure 5.12: Effect of interporosity parameter on interface-boundary conditions of Non-Newtonian/Newtonian flow (θ = 10, α = 0.01, ω = 0.1, λ=varying, R_D = 100, n = 0.6)

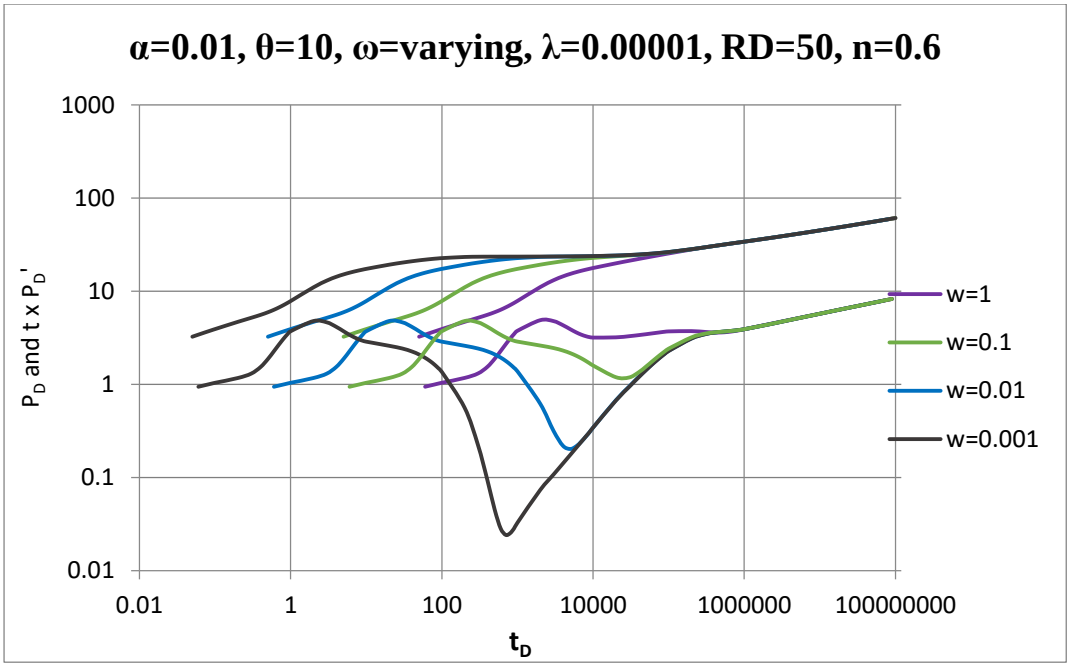

Figure 5.13: Effect of storage capacity ratio on interface-boundary conditions of Non-Newtonian/Newtonian flow (θ = 10, α = 0.01, ω = varying, λ=0.00001, R_D = 50, n = 0.6)

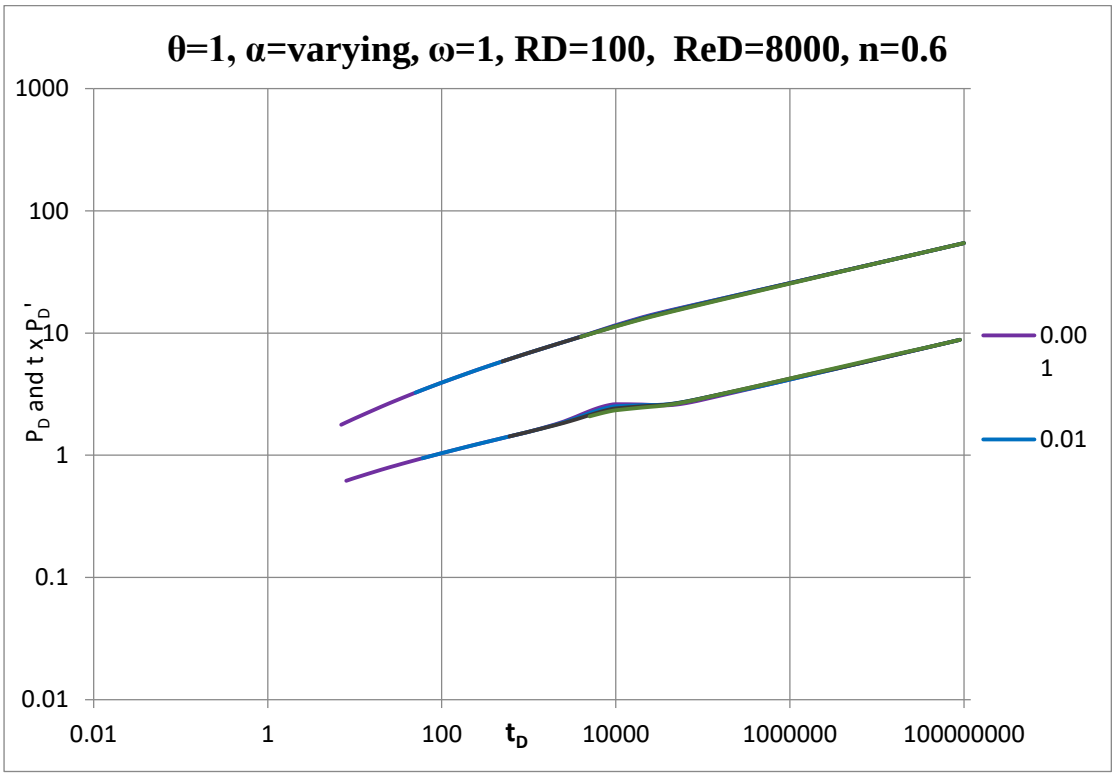

Figure 5.14: Effect of alpha on interface-boundary conditions of Non-Newtonian/Newtonian flow (θ=1, α = varying, ω = 1, R_D = 100, Re_D = 8000, n = 0.6)

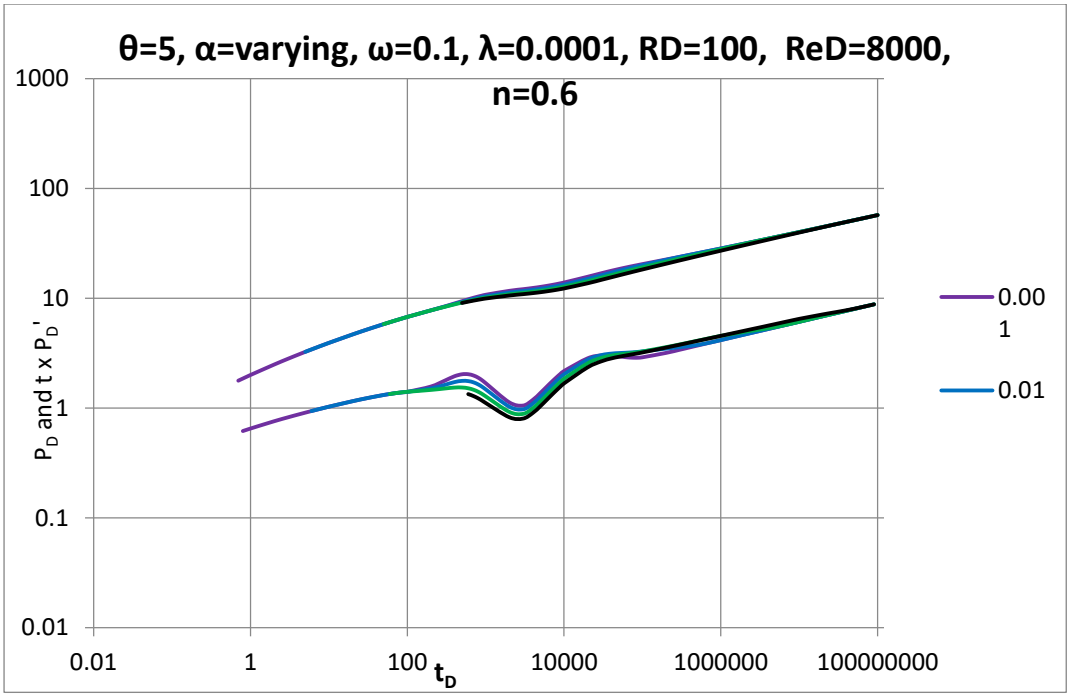

Figure 5.15: Effect of alpha on interface-boundary conditions of Non-Newtonian/Newtonian flow (θ=5, α = varying, ω = 0.1, R_D = 100, Re_D = 8000, n = 0.6)

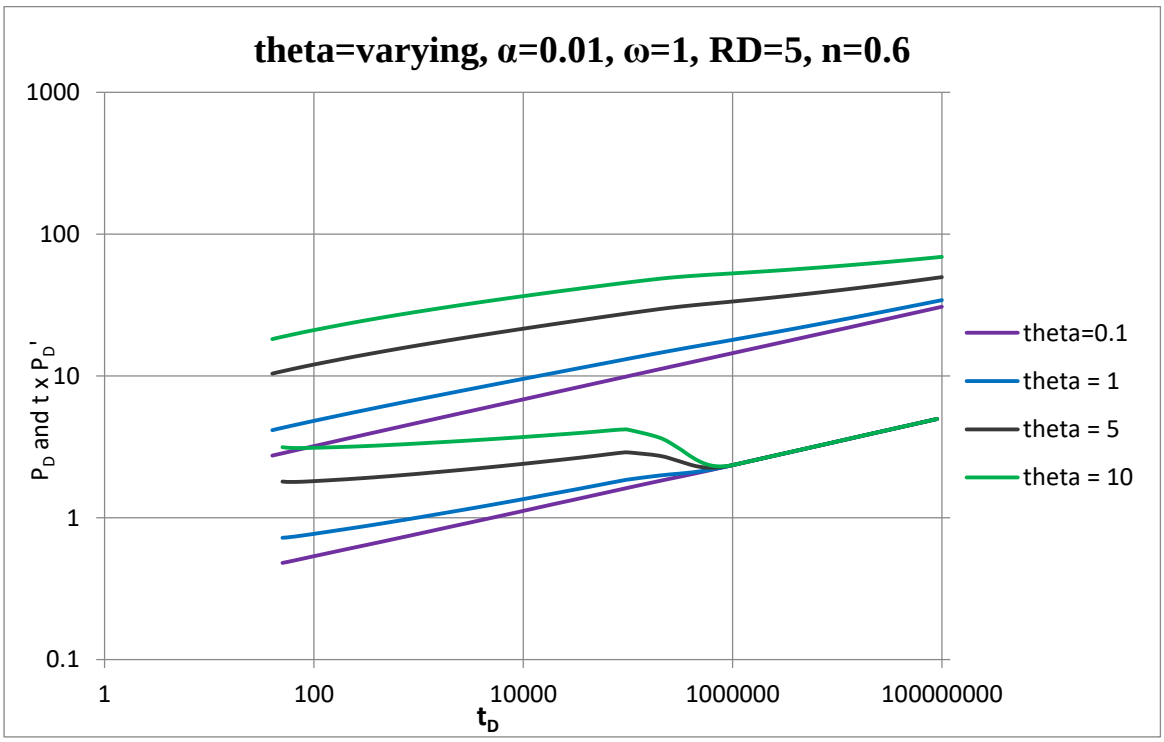

Figure 5.16: Effect of mobility ratio on interface-boundary conditions of Non-Newtonian/Newtonian flow (θ=varying, α = 0.01, ω = 1, R_D = 5, Re_D = 8000, n = 0.6)

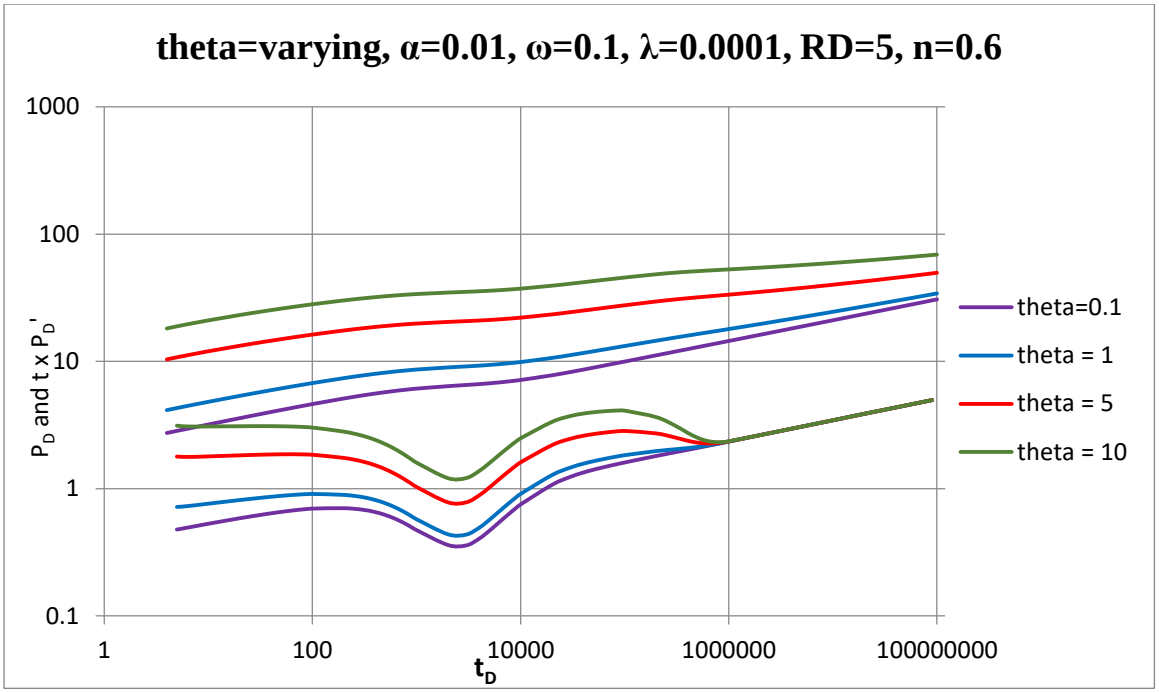

Figure 5.17: Effect of mobility ratio on interface-boundary conditions of Non-Newtonian/Newtonian flow (θ=varying, α = 0.01, ω = 0.1, λ=0.0001, R_D = 5, Re_D = 8000, n = 0.6)

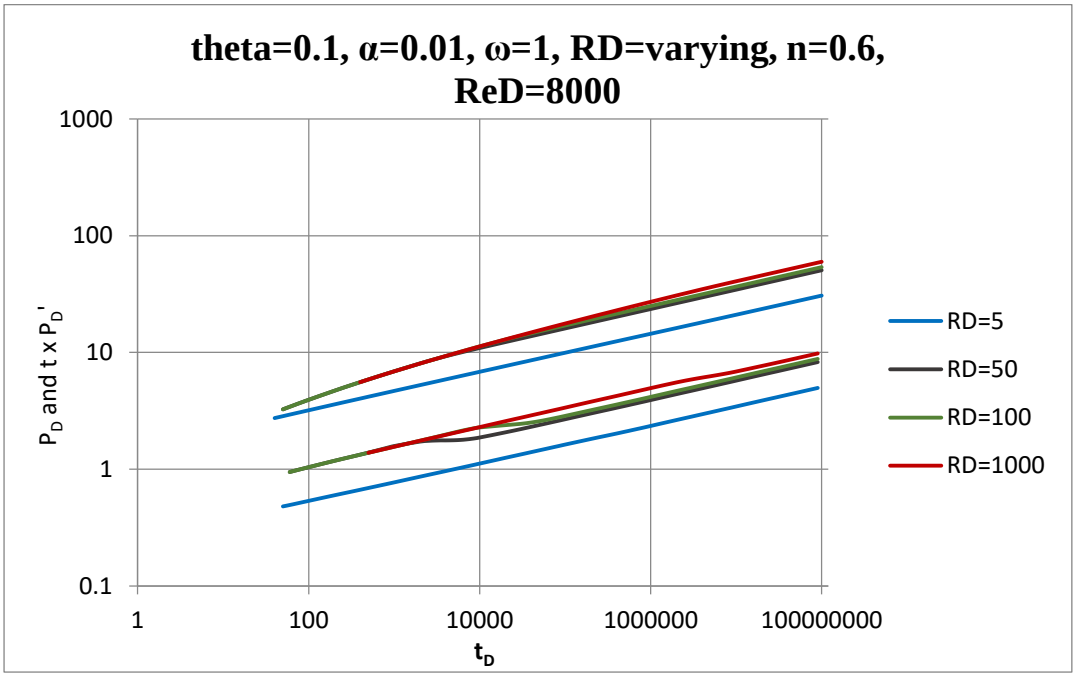

Figure 5.18: Effect of polymer front on interface-boundary conditions of Non-Newtonian/Newtonian flow (θ = 0.1, α = 0.01, ω =1, R_D = varying, Re_D = 8000, n = 0.6)

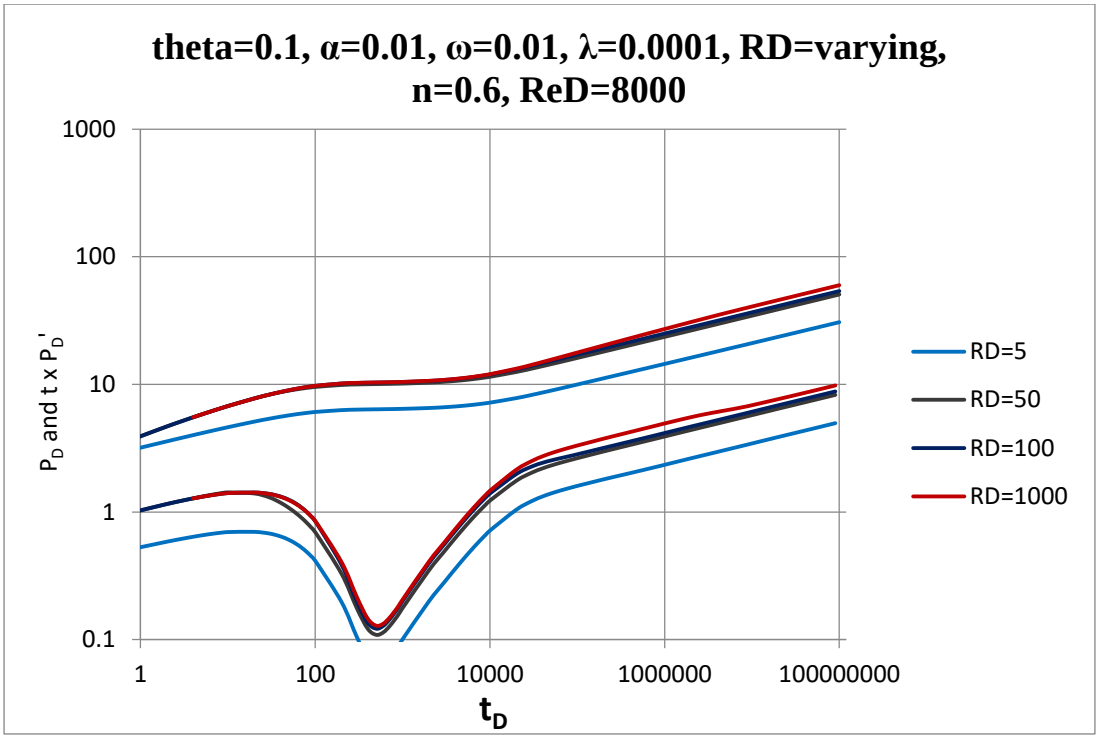

Figure 5.19: Effect of polymer front on interface-boundary conditions of Non-Newtonian/Newtonian flow ($\theta = 0.1$, $\alpha = 0.01$, $\omega = 0.01$, $\lambda = 0.0001$, R_D = varying, $Re_D = 8000$, $n = 0.6$)

5.3.1.3. Closed (No-Flow) Boundary Reservoir

These type curves are for closed (no flow) boundary homogeneous and NFR system. Effect of the closed system is seen at the steep incline of the curves towards the right in each plot. The characteristics fingerprints of each plot is observed using the dimensionless pressure derivative curves which are below the dimensionless pressure curves. In Fig 5.21, a decrease in storage capacity ratio leads to an increase in the trough size for the pressure derivative curves. Figure 5.22-5.23 illustrate the effect of alpha on a Non-Newtonian/Newtonian flow, which is a steeper curve with decrease in alpha value. The curves for mobility ≥ 1 in Fig 5.24 show a hump between t_D=2000 to 70000 and a steep incline towards the right of the curves. A dip is seen after the hump in Fig 5.25 due to the low storativity value.

Curves for R_D=50, 100, 500 and 1000 in Figs 5.26-5.27 form almost a single curve at all times, while that for R_D=5 shows a complete curve.

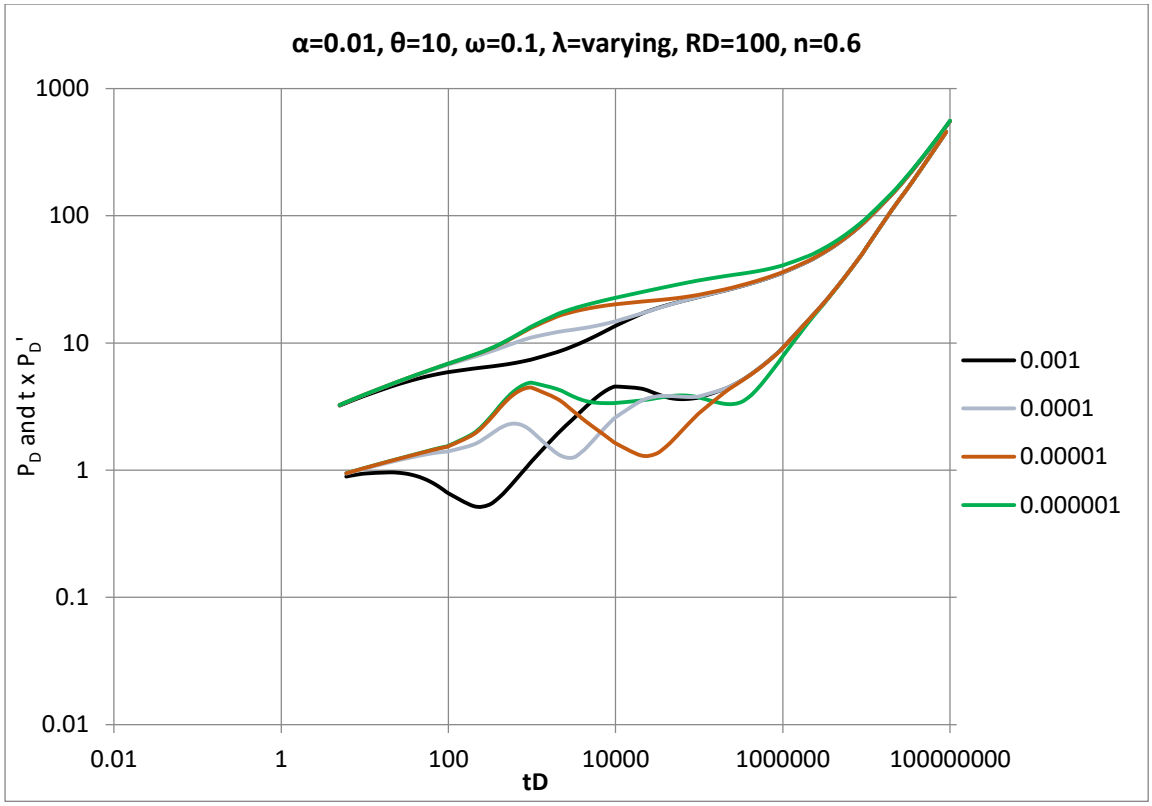

Figure 5.20: Effect of interporosity parameter on interface-boundary conditions of Non-Newtonian/Newtonian flow (θ = 10, α = 0.01, ω = 0.1, λ=varying, R_D = 100, n = 0.6)

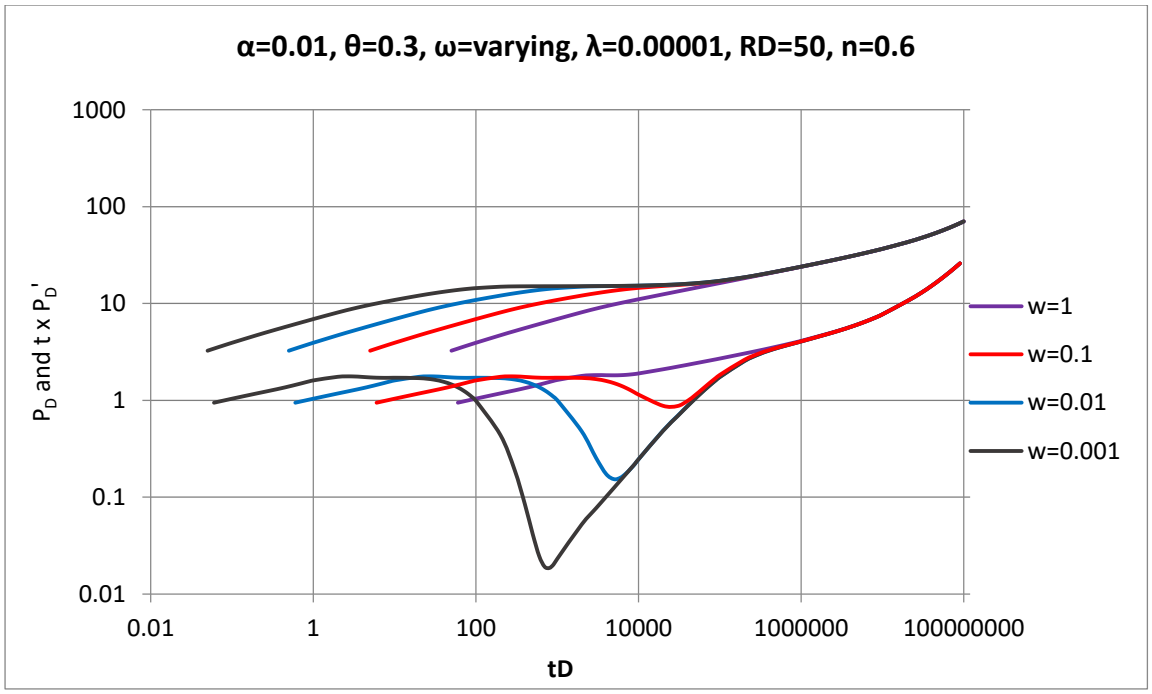

Figure 5.21: Effect of storage capacity ratio on interface-boundary conditions of Non-Newtonian/Newtonian flow (θ = 0.03, α = 0.01, ω = varying, λ=0.00001, R_D = 50, n = 0.6)

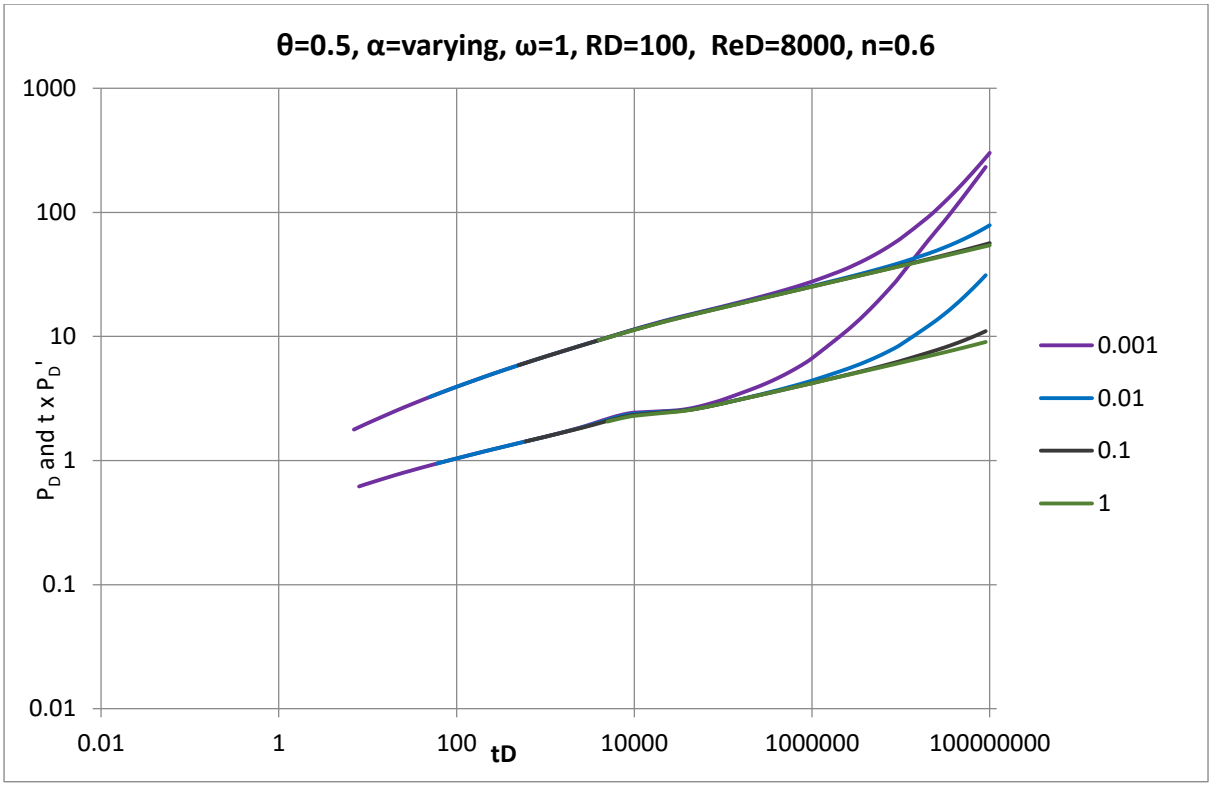

Figure 5.22: Effect of alpha on interface-boundary conditions of Non-Newtonian/Newtonian flow (θ=0.5, α = varying, ω = 1, R_D = 100, Re_D=8000, n = 0.6)

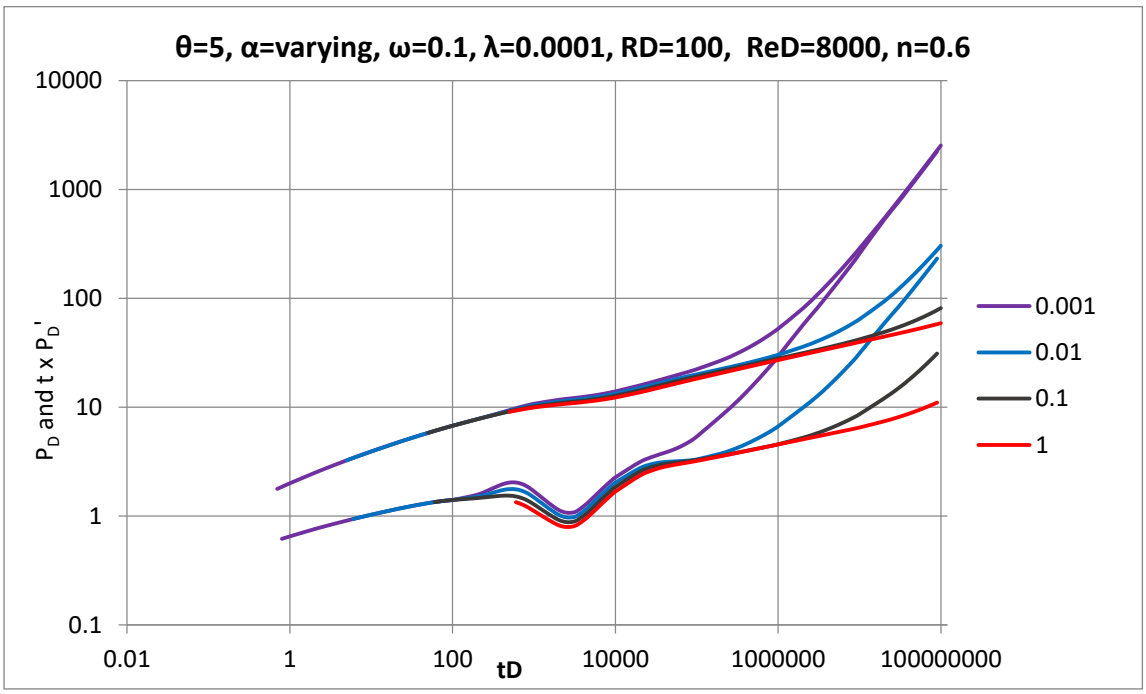

Figure 5.23: Effect of alpha on interface-boundary conditions of Non-Newtonian/Newtonian flow (θ=5, α = varying, ω = 0.1, λ=0.0001, R_D = 100, Re_D=8000, n = 0.6)

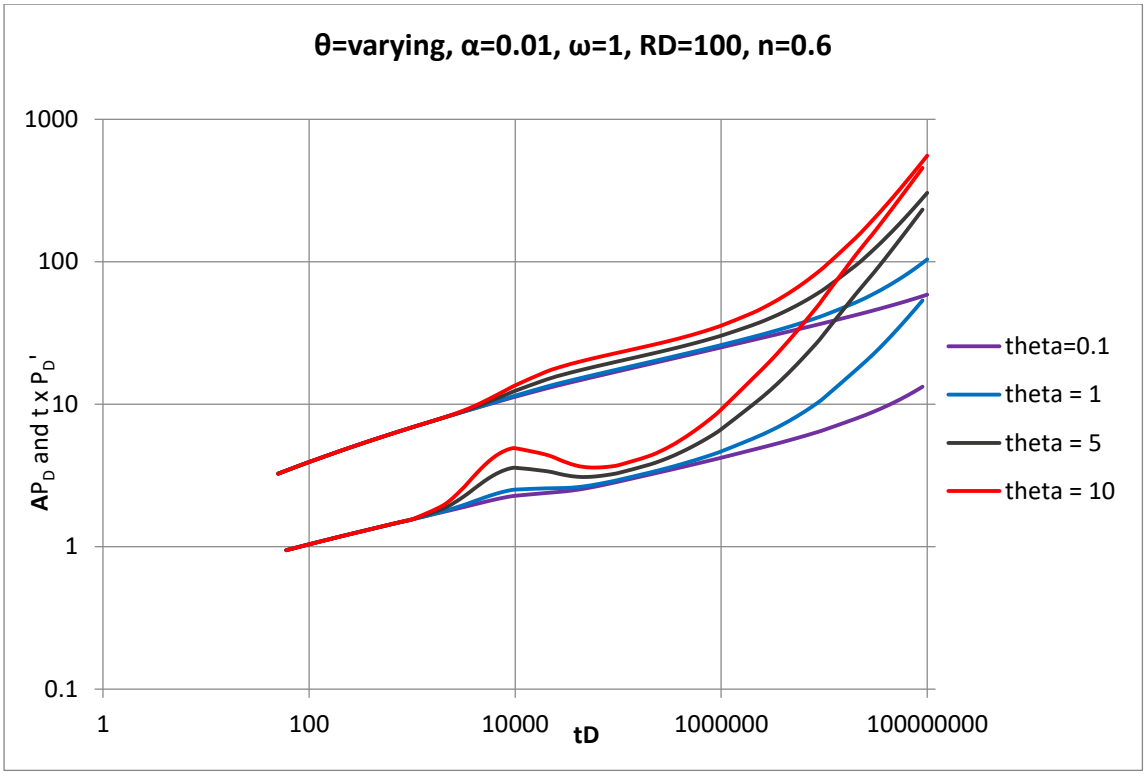

Figure 5.24: Effect of mobility ratio on interface-boundary conditions of Non-Newtonian/Newtonian flow (θ = varying, α = 0.01, ω = 1, R_D = 100, n = 0.6)

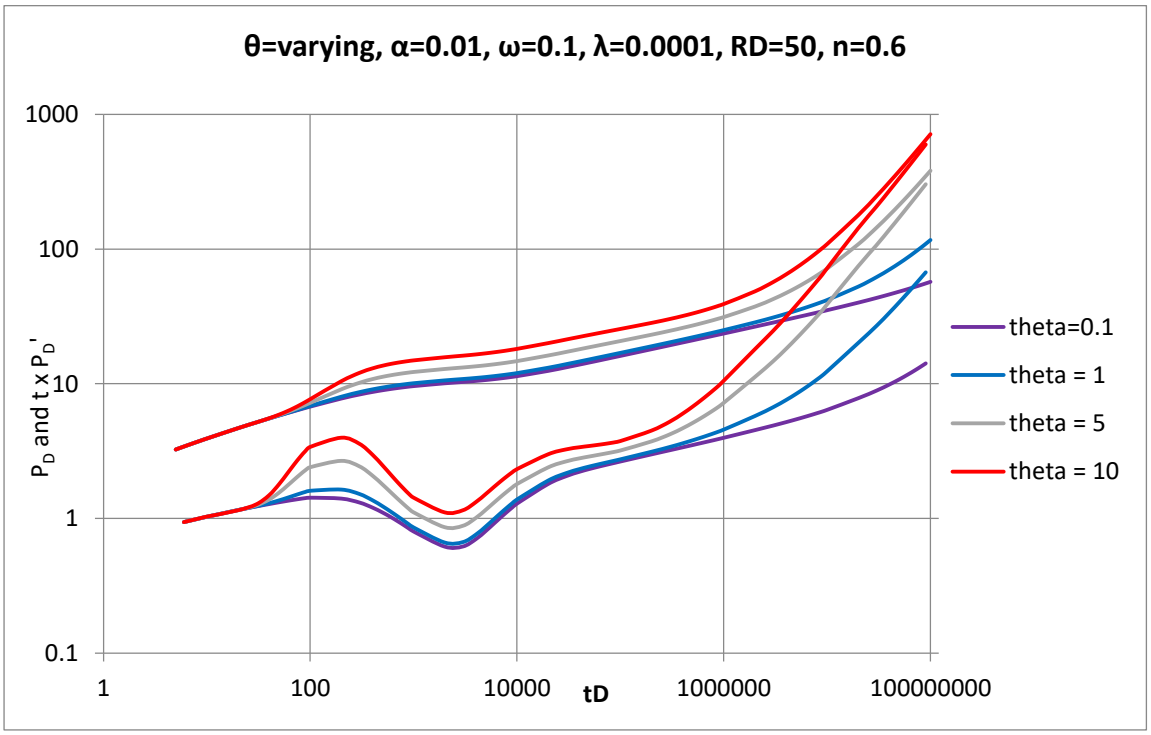

Figure 5.25: Effect of mobility ratio on interface-boundary conditions of Non-Newtonian/Newtonian flow (θ = varying, α = 0.01, ω = 0.1, λ=0.0001, R_D = 50, n = 0.6)

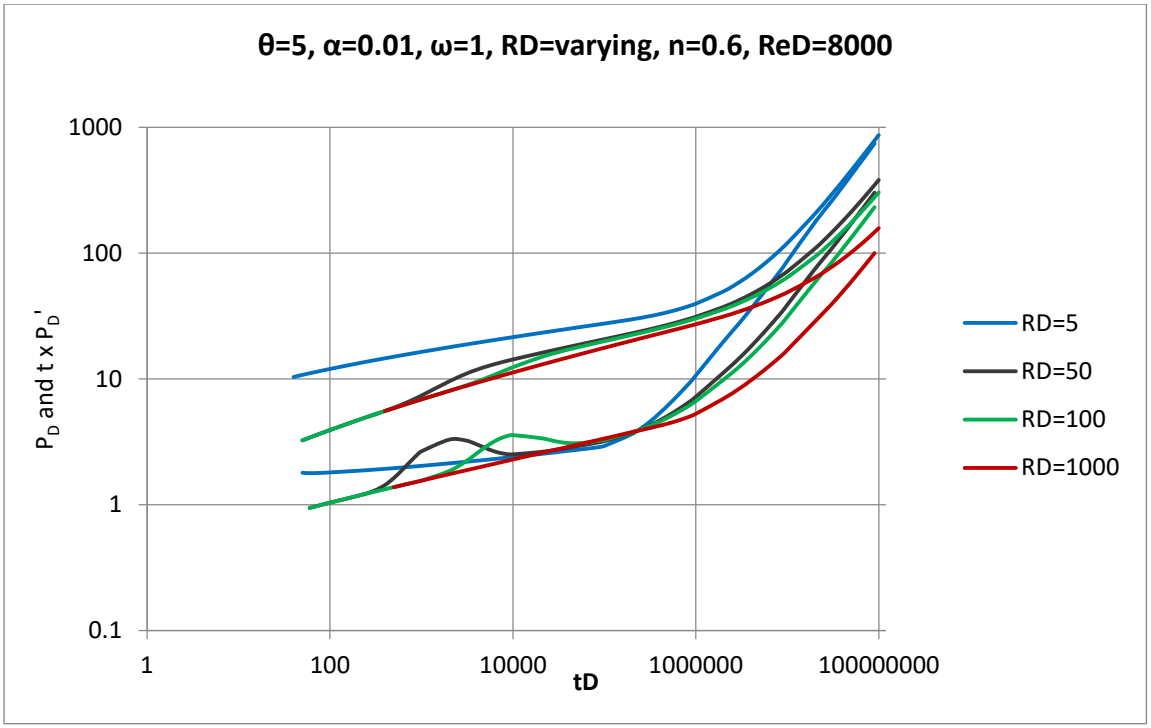

Figure 5.26: Effect of polymer front on interface-boundary conditions of Non-Newtonian/Newtonian flow ($\theta = 5$, $\alpha = 0.01$, $\omega = 1$, R_D = varying, $Re_D = 8000$, $n = 0.6$)

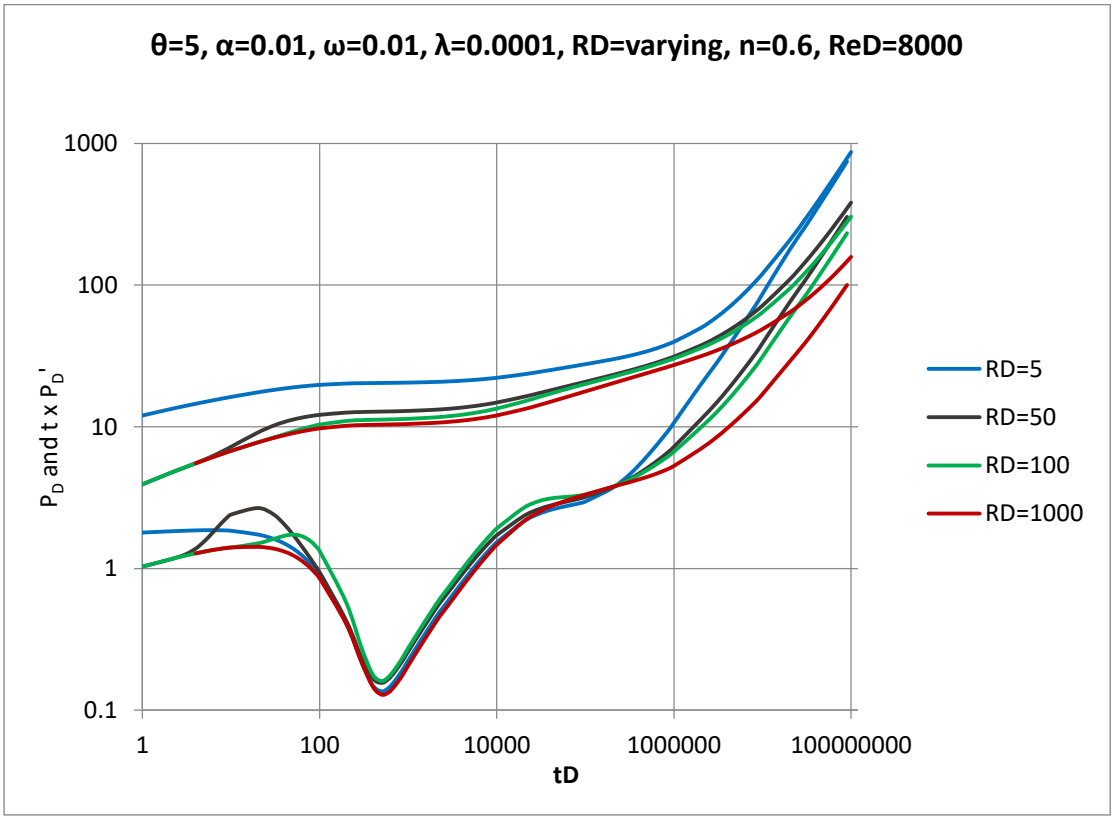

Figure 5.27: Effect of polymer front on interface-boundary conditions of Non-Newtonian/Newtonian flow ($\theta = 5$, $\alpha = 0.01$, $\omega = 0.01$, R_D = varying, $\lambda = 0.0001$, $Re_D = 8000$, $n = 0.6$)

5.3.2 Type curves for when flow index behavior (n) is approximately 1.0

5.3.2.1 Homogeneous System

Whereas the previous curves were for $0.1 \leq n \leq 0.99$, the below curves are for when $n \approx 1.0$. The type curves are for infinite homogeneous and NFR system. In figure 5.28, the mobility ratio curves remain same until t_D=600,000 for the pressure derivative and t_D=4,000,000 for the pressure curves with the most deviation occurring at a mobility ratio of 100. Curves for R_D=50, 100, 500 and 1000 in Figs 5.30-5.31 form almost a single curve up to t_D=5, while that for R_D=5 shows a complete curve. It is observed that at the interface, a transition zone is noted and then when the pressure reaches the Newtonian phase, the pressure derivative forms a flat line. At longer R_D, the Newtonian zone takes a long time in appearing.

Figures 5.32-5.34 are the pressure and pressure derivative type curves for the cases of varying storativity ratios at constant values of θ, α, λ, R_D, and n. Figures 5.35-5.39 illustrate the effect of alpha, mobility ratio and polymer front on a Non-Newtonian/Newtonian flow in a naturally fractured reservoir (NFR).

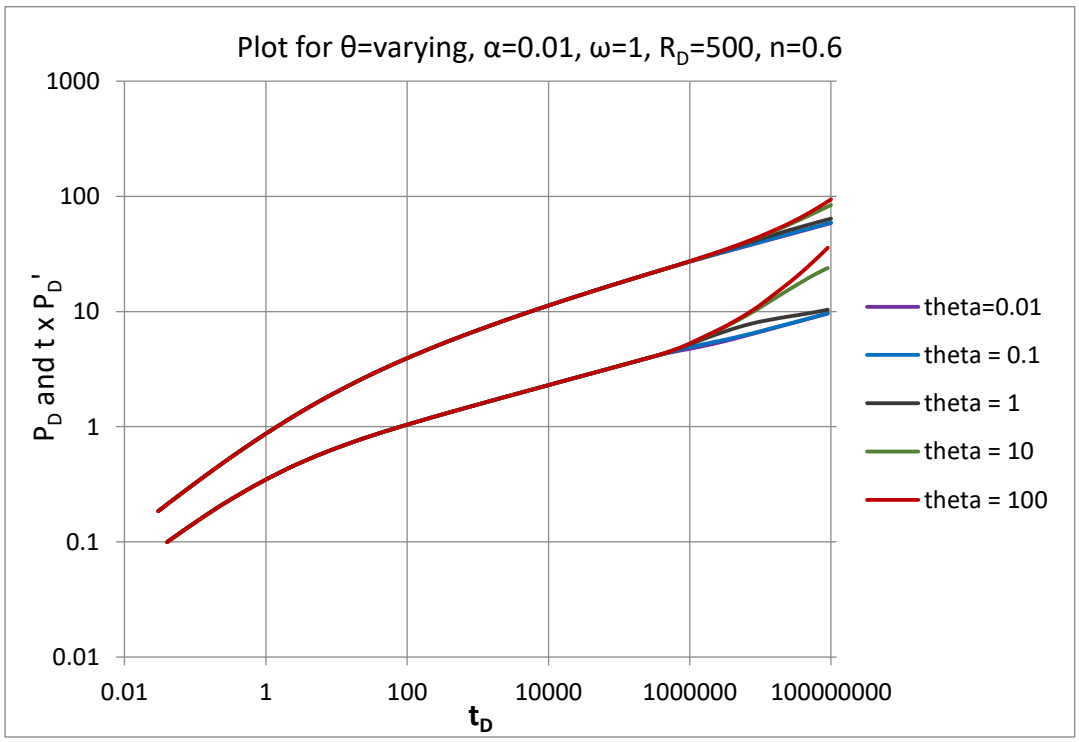

Figure 5.28: Effect of mobility ratio on interface-boundary conditions of Non-Newtonian/Newtonian flow (θ = varying, α = 0.01, ω = 1, R_D = 500, n = 0.6)

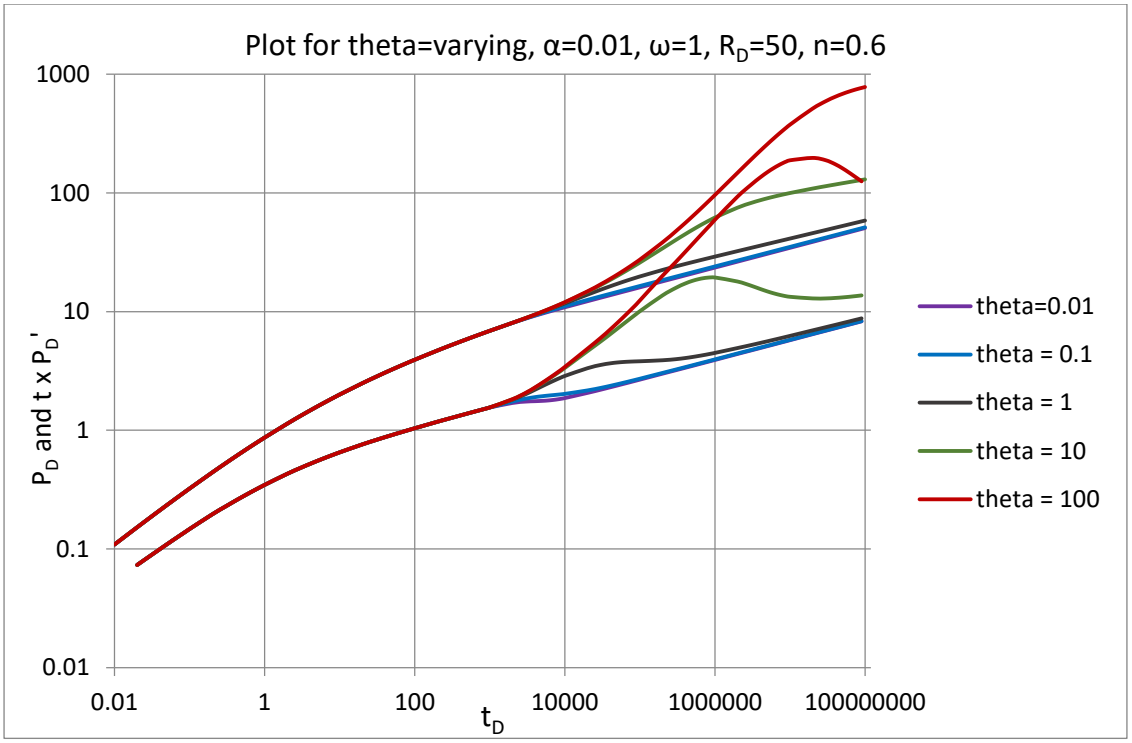

Figure 5.29: Effect of mobility ratio on interface-boundary conditions of Non-Newtonian/Newtonian flow (theta=varying, α=0.01, ω=1, R_D=50, n=0.6)

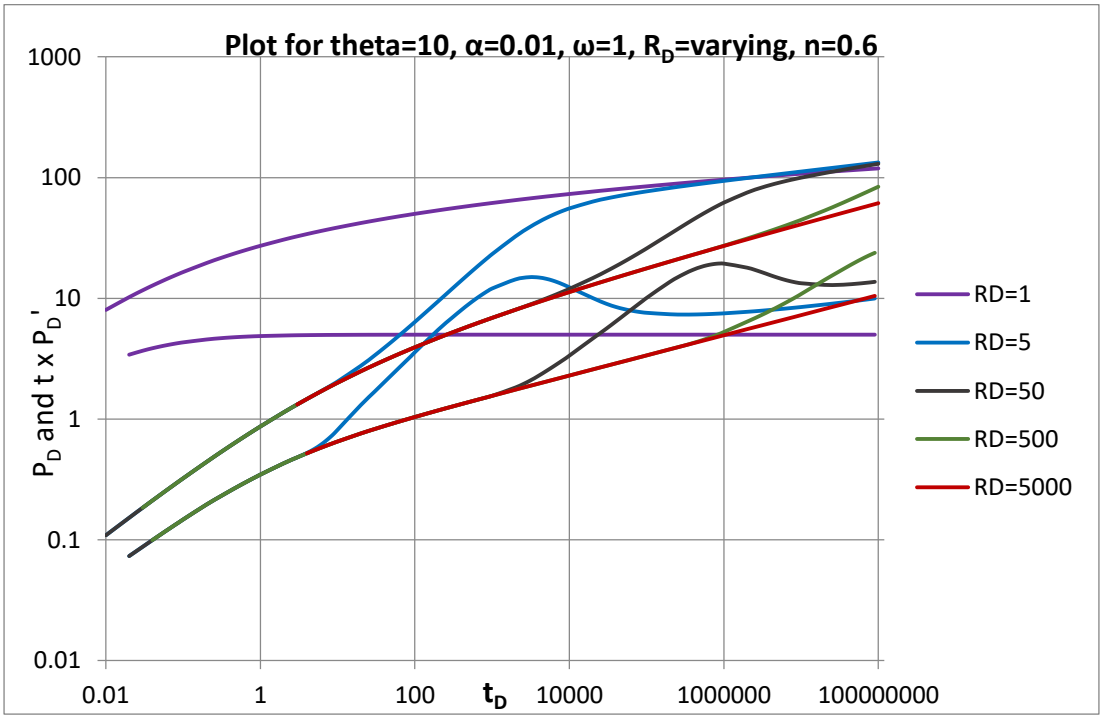

Figure 5.30: Effect of polymer front on interface-boundary conditions of Non-Newtonian/Newtonian flow (theta= 10, α= 0.01, ω= 1, R_D= varying, n= 0.6)

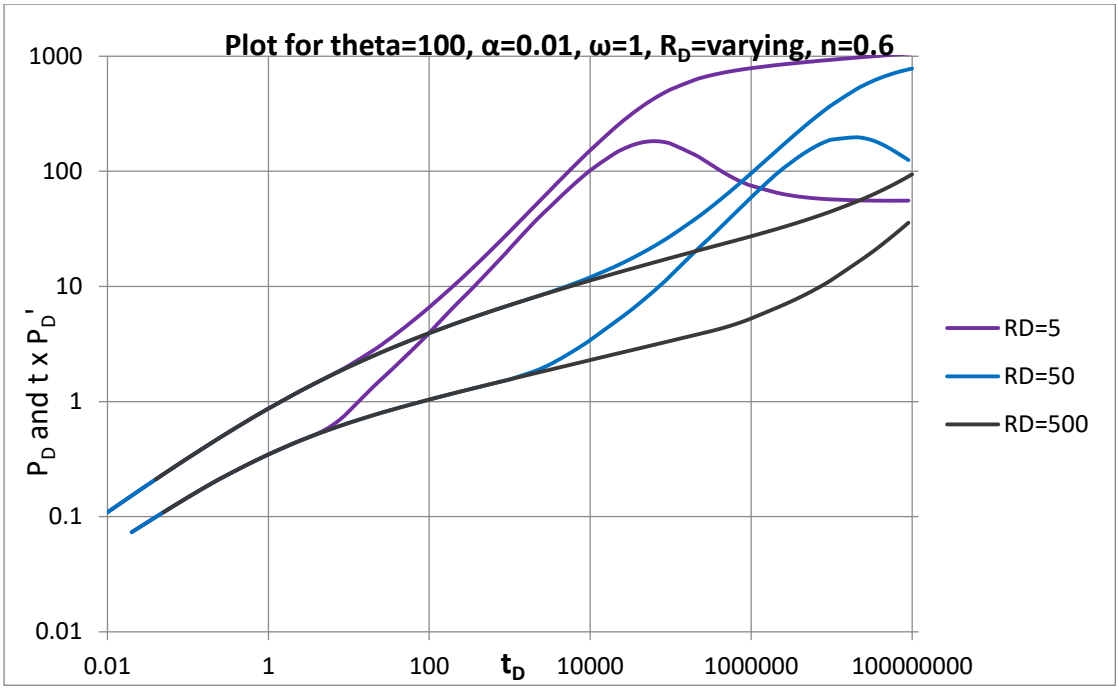

Figure 5.31: Effect of polymer front on interface-boundary conditions of Non-Newtonian/Newtonian flow (theta= 100, α= 0.01, ω= 1, R_D= varying, n= 0.6)

5.3.2.2 Naturally Fractured Reservoir

Figures 5.5-5.7 are the pressure and pressure derivative type curves for the cases of varying storativity ratio. Figure 5.8 is the type curve at α=0.001-10 for values of θ, λ, R_D, and n. Figure 5.9 shows the graph for varying R_D. Figures 5.10-5.12 are the plots for theta varying from 0.01-100.

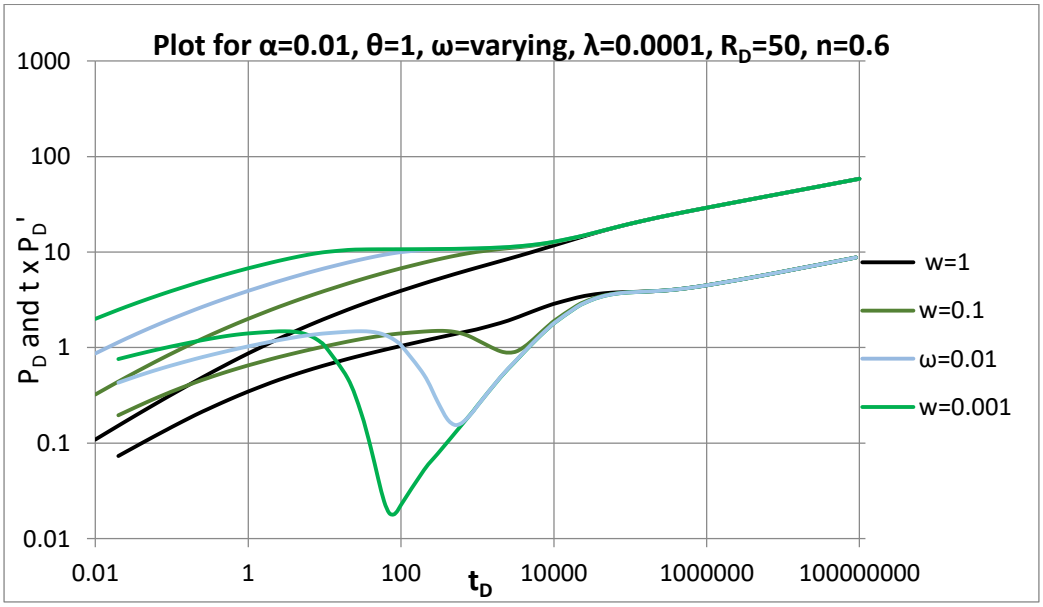

Figure 5.32: Effect of storage capacity ratio on interface-boundary conditions of Non-Newtonian/Newtonian flow (α=0.01, theta=1, ω=varying, λ=0.0001, R_D=50, n=0.6)

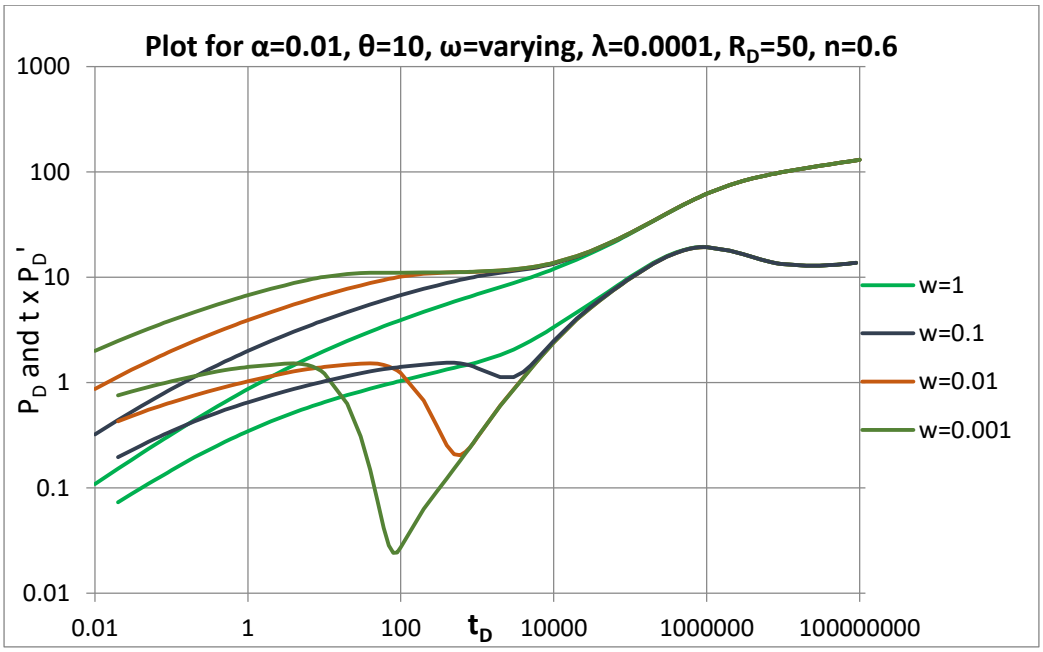

Figure 5.33: Effect of dimensionless storage co-efficient on interface-boundary conditions of Non-Newtonian/Newtonian flow (α=0.01, θ=10, ω=varying, λ=0.0001, R_D=50, n=0.6)

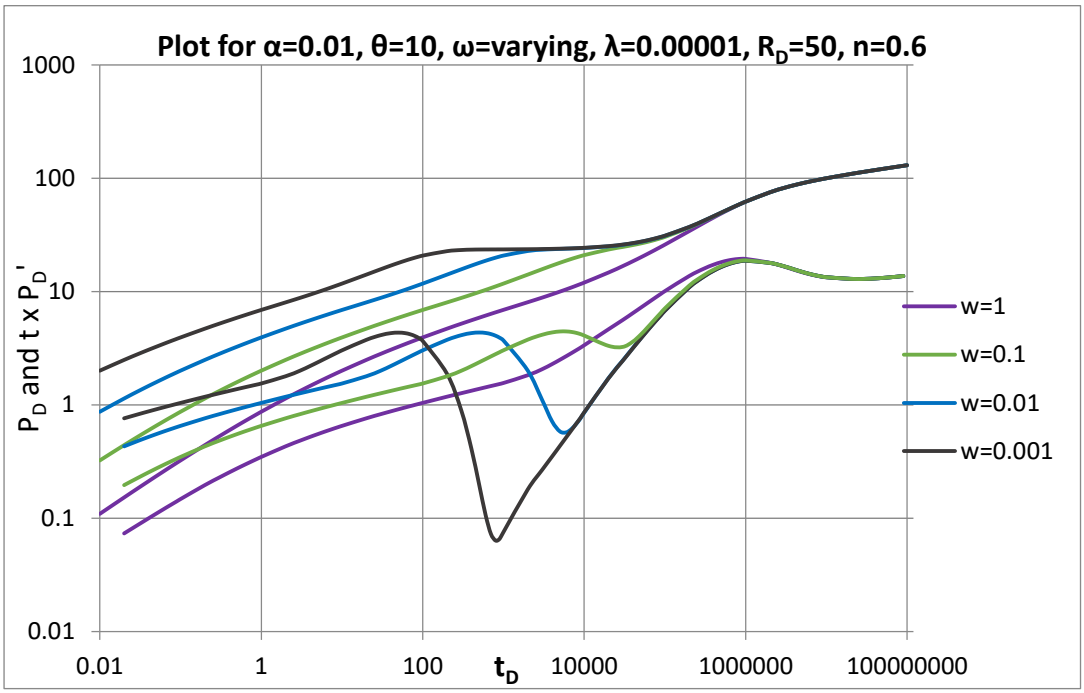

Figure 5.34: Effect of storage capacity ratio on interface-boundary conditions of Non-Newtonian/Newtonian flow (α=0.01, θ=10, ω=varying, λ=0.00001, R_D=50, n=0.6)

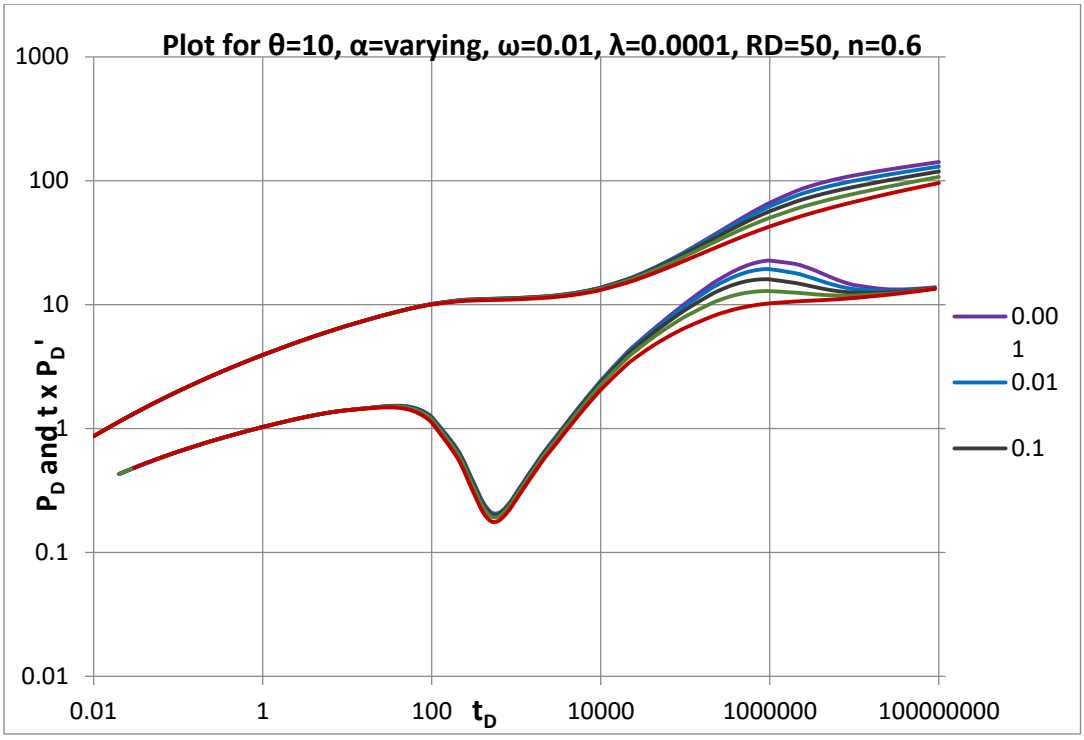

Figure 5.35: Effect of alpha on interface-boundary conditions of Non-Newtonian/Newtonian flow (α=varying, θ=10, ω=0.01, λ=0.0001, R_D=50, n=0.6)

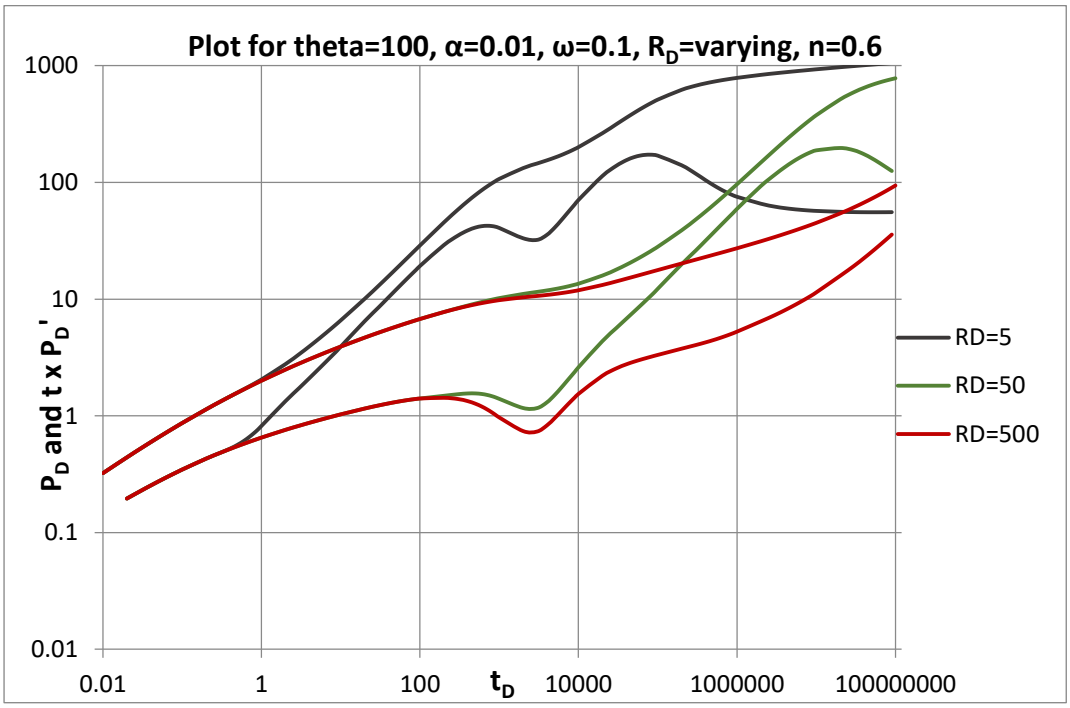

Figure 5.36: Effect of polymer front on interface-boundary conditions of Non-Newtonian/Newtonian flow (theta=100, α=0.01, ω=0.1, R_D=varying, n=0.6)

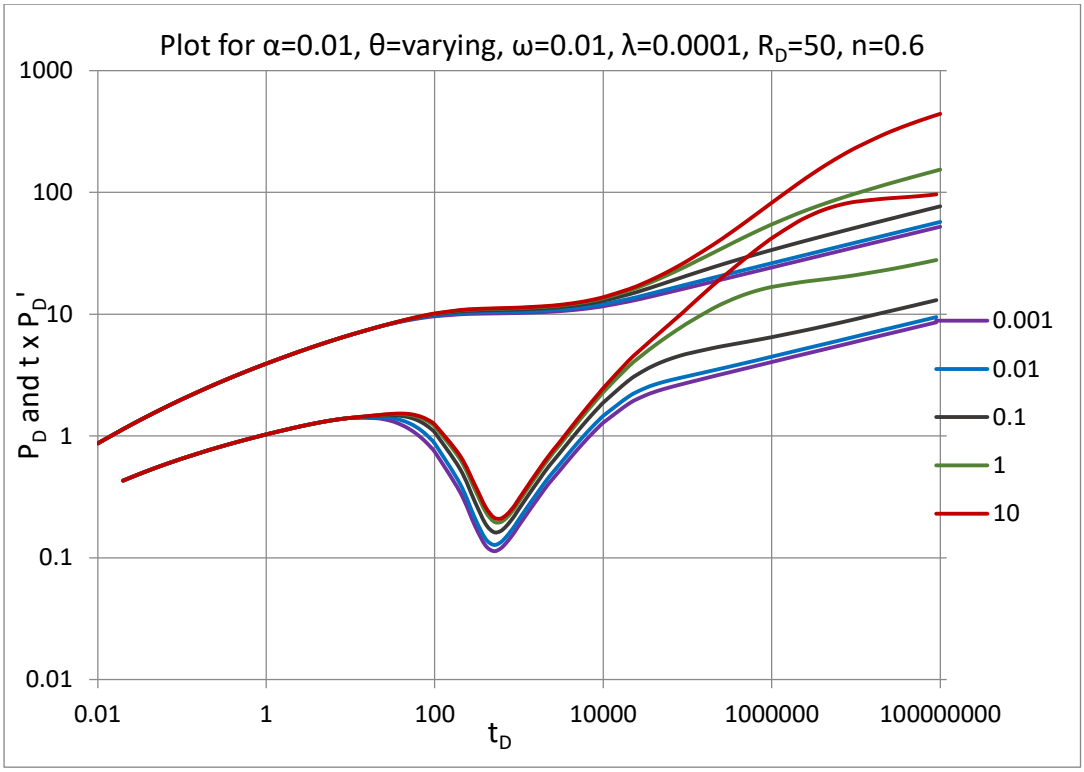

Figure 5.37: Effect of mobility ratio on interface-boundary conditions of Non-Newtonian/Newtonian flow (α=0.01, θ=varying, ω=0.01, λ=0.0001, R_D=50, n=0.6)

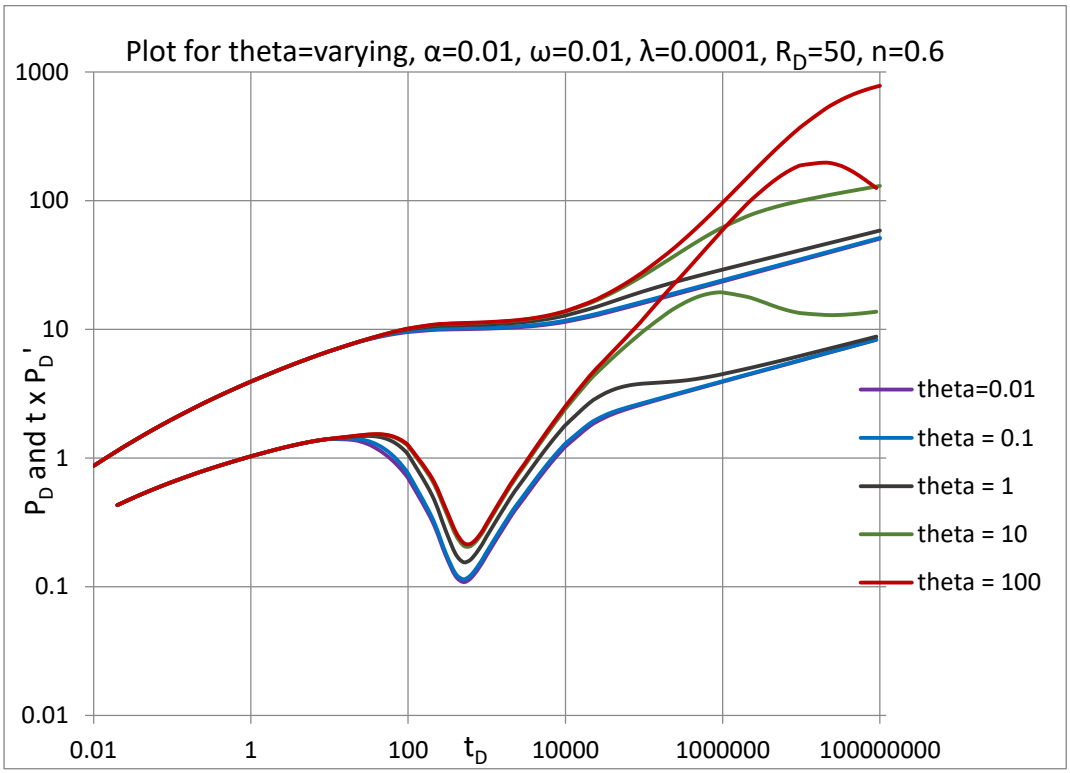

Figure 5.38: Effect of mobility ratio on interface-boundary conditions of Non-Newtonian/Newtonian flow (α=0.01, θ=varying, ω=0.01, λ=0.0001, R_D=50, n=0.6)

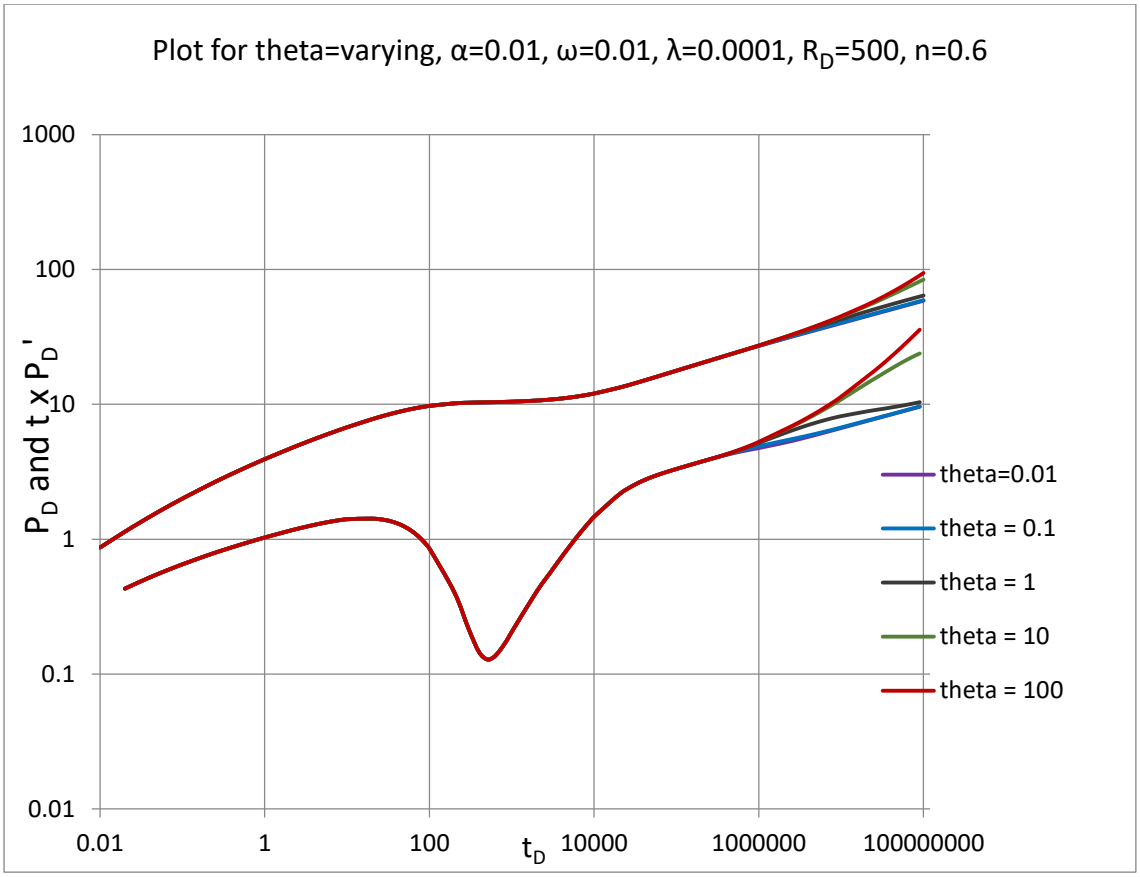

Figure 5.39: Effect of mobility ratio on interface-boundary conditions of Non-Newtonian/Newtonian flow (theta=varying, α=0.01, ω=0.01, λ=0.0001, R_D=500, n=0.6)

CHAPTER 6

TIAB DIRECT SYNTHESIS (TDS) TECHNIQUE DEVELOPMENT

A two region reservoir means that the two media have different mobilities and so, the use of a conventional straight line method for the data interpretation could be erroneous (Escobar et al, 2010). Tiab Direct Synthesis (TDS) technique offers pressure transient test interpretation without the use of type curves.

It relies on unique flow characteristics revealed on log-log pressure and pressure derivative plots to develop analytical equations for estimating formation and fluid properties. In this study, the unique intersection of the characteristic line on the log-log plot of the type curves developed is combined with long time solutions to develop the TDS method for well test interpretation.

At the infinite acting radial flow regime of non-Newtonian fluid, the log-log plot of the pressure derivative versus time will give a straight line with slope, *v*. The value n can then be determined from the slope. By substituting the dimensionless equations (3.2-3.5) into the pressure derivative equation (3.18), the mobility ratio (effective permeability-viscosity ratio) is calculated by Igbokoyi and Tiab (2007) as:

$$\frac{k}{\mu_{eff}} = \left(\frac{0.5\left(\frac{q}{2\pi h}\right)^{\frac{1+n}{3-n}} t_{IARF}^{\frac{1-n}{3-n}}}{(tx\Delta P'_w)_{IARF}(n\varphi c_t)^{\frac{1-n}{3-n}}} \right)^{\frac{3-n}{2}} \tag{6.1}$$

At t_{IARF} = 1sec,

$$\frac{k}{\mu_{eff}} = \left(\frac{0.5\left(\frac{q}{2\pi h}\right)^{\frac{1+n}{3-n}}}{(tx\Delta P'_w)_{IARF1sec}(n\varphi c_t)^{\frac{1-n}{3-n}}} \right)^{\frac{3-n}{2}} \tag{6.2}$$

The skin factor is best estimated from the infinite-acting flow regime line and by substituting (3.2) and (3.18) into (3.17), the following equation from Igbokoyi and Tiab (2007) is obtained:

$$S = \frac{k}{\mu_{eff}} \left(\frac{2\pi h}{q}\right)^n r_w^{1-n} \left[(\Delta P_w)_{IARF} - \frac{3-n}{1-n} (tx\Delta P'_w)_{IARF} \right] + \frac{1}{1-n} \tag{6.3}$$

6.1 Radius of Investigation

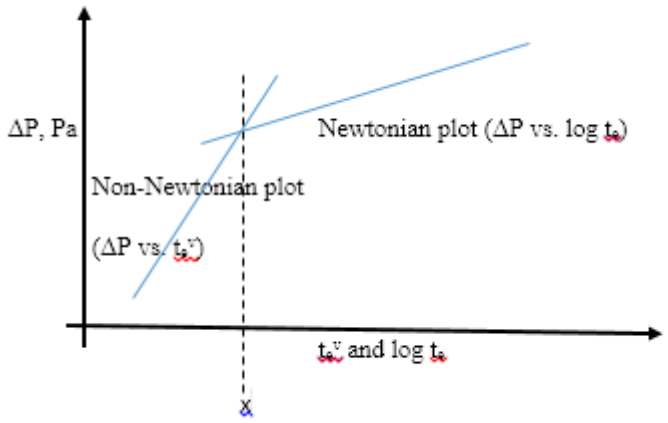

Figure 6.1: A schematic plot showing intersection of Newtonian and Non-Newtonian fluid flow.

Assuming a sharp interface without transition, at intersection of Newtonian and non-Newtonian plot, the pressure of both fluids are same and time for intersection can be gotten as:

1. For non-Newtonian fluid,

$$t_e = x^{\frac{1}{v}}\, sec \tag{6.4}$$

Radius of investigation for non-Newtonian flow in porous media is given by Ikoku and Ramey (1979) as:

$$r_{inv}(meter) = \left(\Gamma\left(\frac{2}{3-n}\right)\right)^{\frac{1}{n-1}}\left[\frac{(3-n)^2 t}{G}\right]^{\frac{1}{3-n}} \tag{6.5}$$

From dimensionless parameters,

$$t_{DNN} = \frac{t}{G(r)^{3-n}} \tag{6.6}$$

$$r_{inv}(meter) = \left(\frac{t_e}{G}\right)^{\frac{1}{3-n}} \tag{6.7}$$

2. For Newtonian fluid, when n is unity (1.0):

$$t_e = 10^x\, sec \tag{6.8}$$

$$r_{inv}(feet) = \sqrt{\frac{k(md)t(hr)}{948\varphi c_t \mu_w(cp)}} \tag{6.9}$$

Or

$$r_{inv}(feet) = 0.029\sqrt{\frac{kt}{\varphi c_t \mu_w}} \quad (6.10)$$

Where

$\varphi = fraction$

$k = mD$

$t = hr$

$\mu_w = cp$

6.2 Step by Step Procedure of Applying TDS Technique

1. Compute the pressure difference ΔP_w for injection or falloff test, and determine the pressure derivative $t \times \Delta P_w'$.

2. On a log-log scale, plot the ΔP_w and $t \times \Delta P_w'$ versus injection time for the injection test, or versus Δt for falloff test.

3. Identify the unit slope line at the early time of the plot showing the wellbore storage effect. At any point (t, ΔP_w) on the unit slope line, compute the wellbore storage effect using equation below

$$C = qB\left(\frac{t}{\Delta P_w}\right) \quad (6.11)$$

4. Obtain the equation of a straight line (power equation) drawn through the infinite-acting flow regime of the non-Newtonian region and determine its slope v. Using $n = \frac{3v-1}{v-1}$, estimate the value of the flow behavior index, n of the power-law fluid.

5. Select any values of $(\Delta P_w)_{IARF}$, $(t * \Delta P'_w)_{IARF}$ and t_{IARF} in the non-Newtonian infinite acting radial flow region of the plot.

6. Compute non-Newtonian mobility $\frac{k}{\mu_{eff}}$ using equation 6.1 and 6.2. If μ_{eff} is known, then the permeability can be computed.

7. Compute skin factor of the non-Newtonian region using equation (6.3)

8. Radius of investigation is calculated at the intersection of the non-Newtonian/Newtonian radial flow lines using equations 6.4 to 6.10.

9. The mobility of the Newtonian region can be calculated by setting n=1 in equations 6.1 and 6.2. The skin factor equation is obtained as in Tiab (1995).

$$\left(\frac{k}{\mu_{eff}}\right)_2 = \frac{0.5qB}{2\pi h(t*\Delta P')_{IARF}} \tag{6.12}$$

$$s_2 = \frac{1}{2}\left[\left(\frac{\Delta P}{t*\Delta P'}\right)_{r2} - \ln\left(\frac{k_2 t_{r2}}{\varphi\mu_N c_t r_w^2}\right) + 7.43\right] \tag{6.13}$$

6.3 Estimating Reservoir Parameters for NFR

10. Mobility in NFR is given as in homogeneous system in equation 6.1 and 6.2, and skin as in equation (6.3).

11. Select the value of $(t \times \Delta P_w)_{min}$ and t_{min} from pressure derivative at the lowest point of the trough.

12. Calculate the inter-porosity flow parameter using equation (3.34) presented by Tiab et al. (2006), also given below:

$$\lambda = \frac{42.5\mu r_w^2 h(\varphi c_t)_{m+f}}{qB}\frac{(t \times \Delta P_w)_{min}}{(t)_{min}} \tag{6.15}$$

13. Obtain a relationship, R between $(t \times \Delta P_w)_{min}$ and $(t \times \Delta P_w)_{IARF}$ where

$$R = \left(\frac{(t \times \Delta P_w)_{min}}{(t \times \Delta P_w)_{IARF}}\right) \tag{6.14}$$

14. Calculate the storage ratio using

$$\omega = 0.5604R^6 - 1.3322R^5 + 1.7232R^4 - 0.827R^3 + 0.7287R^2 + 0.1469R \tag{6.16}$$

Or, as presented by Tiab et al. (2006) and given in equation (3.30) of this work,

$$\omega = 10^{-0.8684(1-R)} \tag{6.17}$$

CHAPTER 7

NUMERICAL EXAMPLES, DISCUSSION AND CONCLUSION

7.1 Section A – When Flow Behaviour Index, n is Approximately 1.0

The pressure injectivity and fall-off test data presented by Lund and Ikoku (1981) will be used for the validation of this work's pressure behavior of Non-Newtonian/Newtonian fluid flow. We begin by analyzing this data using type curve matching technique. Assumed reservoir, well and fluid data are provided. Subsequently, the TDS technique presented in this work is applied to estimate wellbore storage coefficient, fluid rheology, permeability-effective viscosity ratio, skin, and radius of investigation. Results from both methods are then compared.

7.1.1 Example 1

Given the injectivity test data in Lund and Ikoku (1981) and the formation and fluid properties below, estimate mobility ratio, skin factor, wellbore storage, and radius of investigation.

$h = 5\ m\ (16.4\ ft)$ $\quad\quad$ $q = 0.00055204\ m^3/s (300\ b/d)$

$r_w = 0.1\ m (0.33\ ft)$ $\quad\quad$ $\mu_N = 0.003\ Pa (3.0\ cp)$

$radius\ of\ non-Newtonian\ fluid\ bank,\ r_{ai} = 40\ m (131.2\ ft)$

$k = 100\ mD$ $\quad\quad$ $Production\ time, t_p = 9.98\ days$

$\varphi = 0.2$ $\quad\quad$ $Consistency, H = 0.02\ \text{Pa}.s^n$

$n = 0.9$ $\quad\quad$ $c_t = 1 * 10^{-9}\ /Pa\ (6.89 * 10^{-6}\ /psi)$

Solution

Pressure data is converted from bar to Pascal and Figure 7.1 presents the pressure and pressure derivative log-log plot against time.

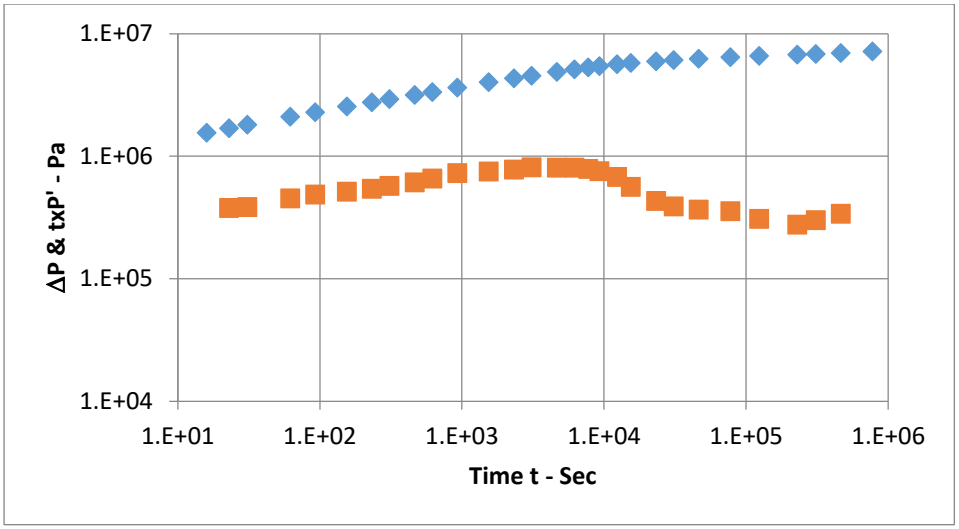

Figure 7.1: Pressure and Pressure derivative plot for Examples A1 and B3

Type Curve Matching Technique.

Several type curves were generated until a matching curve was obtained. The type curve that matches the given data in Figure 7.1 is generated at constant pressure boundary with n =0.9, R_D=60, α=0.001, ω=1, θ=0.1, R_{eD}=8000, and S=0. The match is shown in Figure 7.2 and the match points selected are:

$$(P_{DM},\ \Delta P_M) = (6, 6200000)$$

$$(t_{DM},\ \Delta t_M) = (20000, 77600)$$

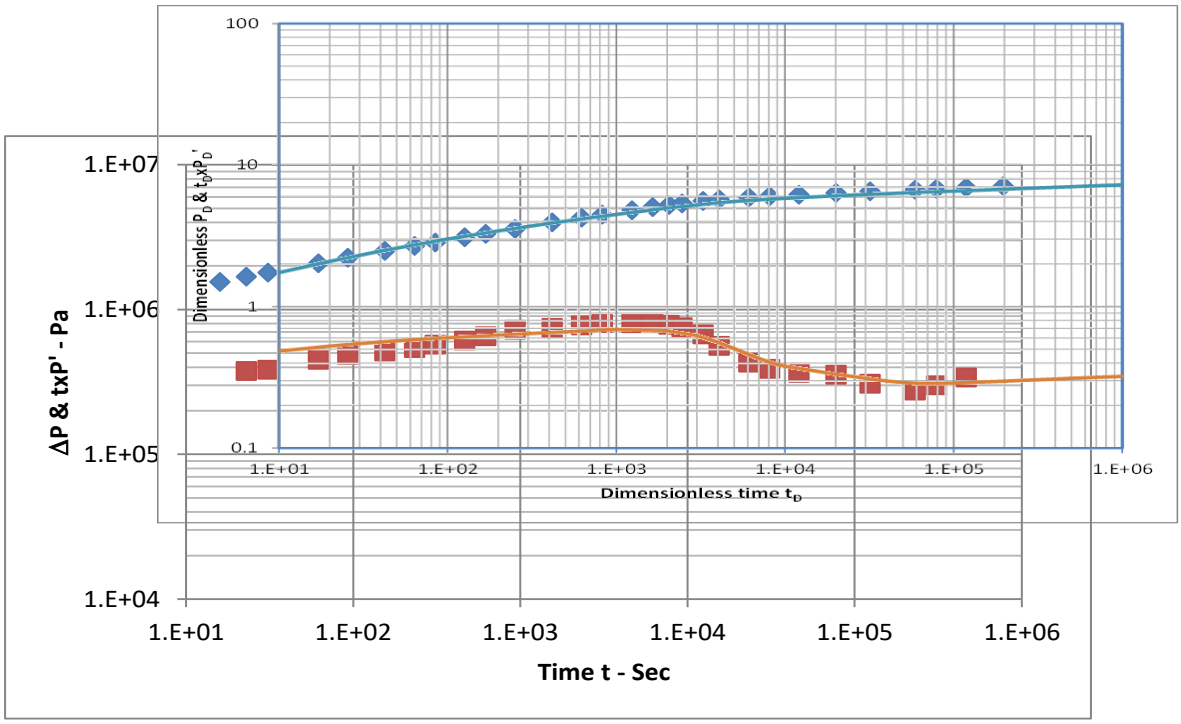

Figure 7.2: Type curve matching for Example A1

To calculate effective viscosity, μ_{eff}:

$$\mu_{eff} = \frac{H}{12}\left(9 + \frac{3}{n}\right)^{n} (150k\varphi)^{\frac{1-n}{2}}$$

$$\mu_{eff} = \frac{0.02}{12}\left(9 + \frac{3}{0.9}\right)^{0.9} \left(150 * \frac{100md * 9.869233 * (10)^{-16}m^2}{1md} * 0.2\right)^{\frac{1-0.9}{2}}$$

$$\mu_{eff} = \frac{0.02}{12} * 9.593397118 * (2.96077 * (10)^{-12})^{0.05}$$

$$\mu_{eff} = 4.24 * (10)^{-3} Pa.s$$

From equation (5.12), fluid mobility is given as:

$$\frac{k}{\mu_{eff}} = \left(\frac{P_D}{\Delta P_w}\right)_{match} \left(\frac{q}{2\pi h}\right)^{n} r_w^{1-n}$$

$$\frac{k}{\mu_{eff}} = \left(\frac{6}{6200000}\right)_{match} * 4.17146 * (10)^{-5}$$

Effective mobility of the polymer solution,

$$\lambda_{eff} = \frac{k}{\mu_{eff}} = 4.0369 * (10)^{-11} * m^{1.9}/Pa.s^{0.9}$$

$$k = 4.0369 * (10)^{-11} * 4.24 * (10)^{-3}$$

$$k = 1.7117 * (10)^{-13} m^2$$

$$k = 1.7117 * (10)^{-13} m^2 * \frac{1mD}{9.869233 * (10)^{-16} m^2} = 173.44\ mD$$

To calculate storativity,

$$\varphi c_t = \frac{k}{\mu_{eff}} * \left(\frac{t}{t_D}\right) match * \frac{1}{n\left(\frac{2\pi h}{q}\right)^{1-n} r_w^{3-n}}$$

$$\varphi c_t = \frac{k}{\mu_{eff}} \frac{77600}{20000 * 0.9 * \left(\frac{2 * 3.142 * 5}{0.00055204}\right)^{1-0.9} * 0.1^{(3-0.9)}}$$

$$\varphi c_t = \frac{k * 181.579}{\mu_{eff}}$$

$$\varphi c_t = 181.579 * 4.0369 * (10)^{-11}$$

$$\varphi c_t = 7.33 * (10)^{-9}\ /Pa$$

Calculating Radius of investigation

From Lund and Ikoku (1981), a semilog plot of dimensionless pressure vs. logarithm of dimensionless time will only give a straight line for Newtonian fluid. And a plot of dimensionless pressure vs. t^v will give a straight line for the non-Newtonian fluid. Combining the straight line plots, Figure 7.3 is obtained and a point of intersection is shown at R_D, where Newtonian pressure is equal to non-Newtonian pressure.

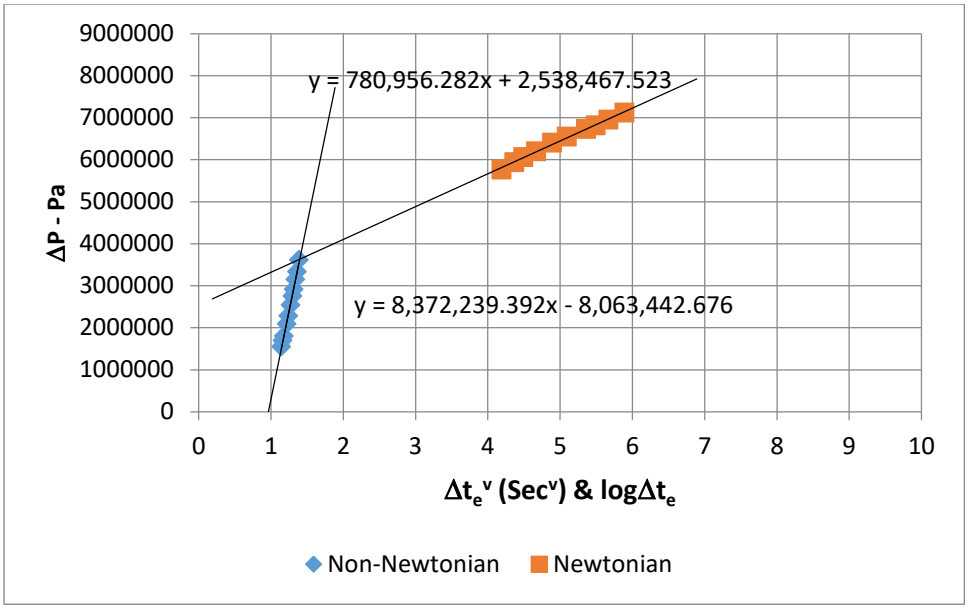

Figure 7.3: Intersection plot for Newtonian and Non-Newtonian fluid flow in Example A1

At point of intersection,

$$780956.282x + 2538467.523 = 8372239.392x - 8063442.676$$

$$8372239.392x - 780956.282x = 2538467.523 + 8063442.676$$

$$7591283.11x = 10601910.2$$

$$x = 1.39659$$

For non-Newtonian fluid,

$$t_e = x^{\frac{1}{v}}\, sec, where\ v = \left(\frac{1-n}{3-n}\right)$$

$$t_e = 1.39659^{\frac{1}{0.047619}} = 1112.878\ sec$$

Radius of investigation is important to know the radius of the non-Newtonian fluid bank at the time the well is shut-in during investigation of the falloff tests within the injected fluid bank. Radius of investigation for non-Newtonian flow in porous media is given by Ikoku and Ramey (1979) as:

$$r_{inv} = \left(\Gamma\left(\frac{2}{3-n}\right)\right)^{\frac{1}{n-1}}\left[\frac{(3-n)^2 t}{G}\right]^{\frac{1}{3-n}}$$

Where

$$G = \frac{n\varphi c_t \mu_{eff}}{k_r}\left(\frac{2\pi h}{q}\right)^{1-n} = \frac{0.9*0.2*1*10^{-9}}{4.0369*(10)^{-11}} * \left(\frac{2*3.142*5}{0.00055204}\right)^{1-0.9} = 13.3275$$

$$r_{inv} = (1.029833)^{\frac{1}{0.9-1}} * \left[\frac{(3-0.9)^2*1113}{13.3275}\right]^{\frac{1}{3-0.9}} = 12.4252\ m$$

$$r_{inv}(meter) = \left(\frac{t_e}{G}\right)^{\frac{1}{3-n}} = \left(\frac{1113}{13.3275}\right)^{\frac{1}{3-0.9}} = 8.224\ m$$

TDS method

Figure 7.1 represents Step 1 and 2

Step 3: $C = qB(\frac{t}{\Delta P_{ws}})$

But there is no early-time unit-slope, therefore $C = 0$

Step 4: $v = \frac{1-n}{3-n} = \frac{1-0.9}{3-0.9} = 0.0476$

Step 5. From Figure 7.1, at $t = 931\ sec$, $(\Delta P_{ws}) = 3610000\ Pa$, and $(t * \Delta P'_w) = 724063\ Pa$

Step 6: Using equation (6.1) which was derived from analytical solution, mobility is estimated as:

$$\frac{k}{\mu_{eff}} = \left(\frac{0.5\left(\frac{q}{2\pi h}\right)^{\frac{1+n}{3-n}} t_{IARF}^{\frac{1-n}{3-n}}}{(tx\Delta P'_w)_{IARF}(n\varphi c_t)^{\frac{1-n}{3-n}}}\right)^{\frac{3-n}{2}}$$

$$\frac{k}{\mu_{eff}} = \left(\frac{0.5*\left(\frac{0.00055204}{2*3.142*5}\right)^{\frac{1+0.9}{3-0.9}}*(931)^{\frac{1-0.9}{3-0.9}}}{724063*(0.9*0.2*1*(10)^{-9})^{\frac{1-0.9}{3-0.9}}}\right)^{\frac{3-0.9}{2}}$$

$$\frac{k}{\mu_{eff}} = \left(\frac{0.5*\left(1.75697*(10)^{-5}\right)^{0.9048}*(931)^{0.0476}}{724063*(1.8*(10)^{-10})^{0.0476}}\right)^{1.05}$$

$$\frac{k}{\mu_{eff}} = \left(\frac{3.449*(10)^{-5}}{248844.09}\right)^{1.05}$$

$$\frac{k}{\mu_{eff}} = 4.46 * (10)^{-11} * m^{1.9}/Pa.s^{0.9}$$

From fluid and reservoir parameters,

$$\mu_{eff} = 4.24 * (10)^{-3} Pa.s^{0.9}/m^{1.9}$$

Therefore, permeability:

$$k = \frac{3.909*(10)^{-11}*4.24*(10)^{-3}}{9.869233*(10)^{-16}} = 191.63\ mD$$

Step 7: Calculate the skin factor, S.

Using equation 6.3,

$$S = 4.46 * (10)^{-11} * \left(\frac{2 * 3.142 * 5}{0.00055204}\right)^{0.9} * 0.1^{1-0.9} * \left[3610000 - (724063 * \frac{3-0.9}{1-0.9})\right] + \frac{1}{1-0.9}$$

$$S = 2.18$$

Step 8: Calculate radius of investigation

$$t_e = 1.39659^{\frac{1}{0.047619}} = 1112.878 sec$$

$$G = \frac{n\varphi c_t \mu_{eff}}{k_r}\left(\frac{2\pi h}{q}\right)^{1-n} = \frac{0.9*0.2*1*10^{-9}}{7.3256*(10)^{-11}} * \left(\frac{2*3.142*5}{0.00055204}\right)^{1-0.9} = 12.10$$

$$r_{inv} = \left(\Gamma\left(\frac{2}{3-n}\right)\right)^{\frac{1}{n-1}}\left[\frac{(3-n)^2 t}{G}\right]^{\frac{1}{3-n}}$$

$$r_{inv} = (1.029833)^{\frac{1}{0.9-1}} * \left[\frac{(3-0.9)^2*1113}{13.70}\right]^{\frac{1}{3-0.9}} = 13.03\ m$$

$$r_{inv}(meter) = \left(\frac{t_e}{G}\right)^{\frac{1}{3-n}} = \left(\frac{1113}{13.70}\right)^{\frac{1}{3-0.9}} = 8.62\ m$$

7.1.2 Example 2

The pressure fall-off test data also presented by Lund and Ikoku (1981) will be used for the validation of this work's pressure behavior of Non-Newtonian/Newtonian fluid flow.

The wellbore and reservoir parameters are same as from the previous example and the pressure test data plot is shown in Figure 6.4.

Solution

Agarwal time used for fall-off tests

t_p = flow period

Δt = shut-in period of fall-off period

Δt_L = final shut-in period of fall-off period

If $\Delta t_L > t_p$, then use Agarwal time for the pressure derivatives and plot

Where Agarwal time,

$$\Delta t_e = \frac{t_p \Delta t}{t_p + \Delta t}$$

$$tp = 9.98 * 24 * 3600 = 862272sec$$

From Pressure data, final shut-in period of fall-off period, $\Delta t_L = 3100000\text{sec} = 35.87963\text{days}$ is

Since $\Delta t_L > t_p$, then we use Agarwal time for the pressure derivatives and plot. Pressure data is converted from bar to Pascal.

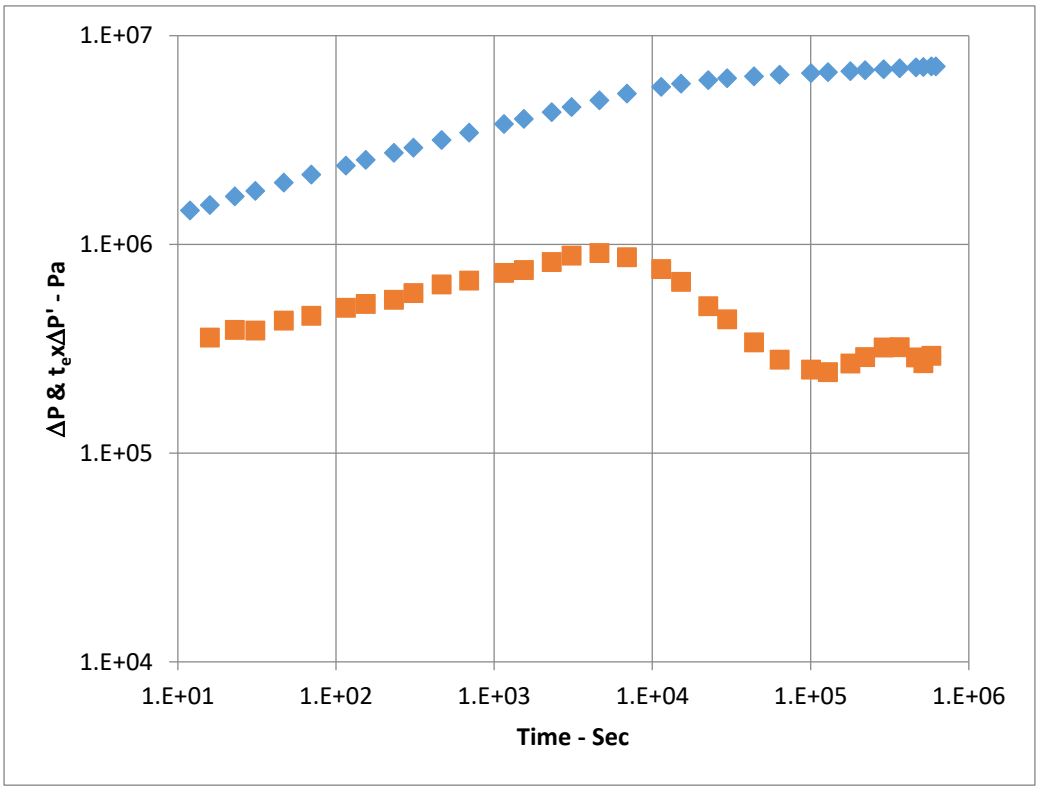

Figure 7.4: Pressure and Pressure derivative plot for Example A2 and B4

Type Curve Matching Technique.

Several type curves were generated until a matching curve is obtained. The type curve that matches the given data in Figure 6.4 is generated with n =0.9, S=-1.0, CD=0, ω=1, α=0.001, θ=0.3, R_{eD}=8000, and r_D=150. A match is shown in Figure 6.5 and the match points are:

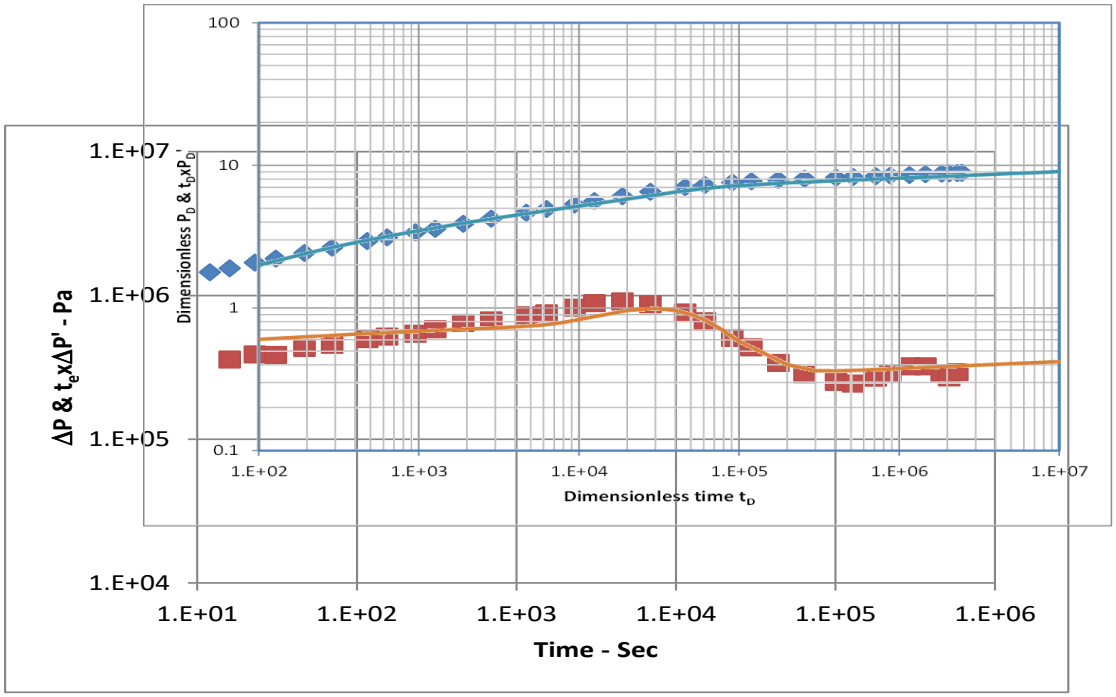

Figure 7.5: Type curve matching for Example A2

$$P_{DM} = 7$$

$$\Delta P_{wsM} = 6090000\ Pa$$

$$t_{DM} = 60000$$

$$\Delta t_{eM} = 15196\ sec$$

To calculate effective viscosity, μ_{eff}. From previous example,

$$\mu_{eff} = 4.24 * (10)^{-3} Pa.s$$

Fluid mobility is given as:

$$\frac{k}{\mu_{eff}} = \left(\frac{7}{6090000}\right)_{match} * \left(\frac{0.00055204}{2*3.142*5}\right)^{0.9} * 0.1^{(1-0.9)}$$

Effective mobility of the polymer solution,

$$\lambda_{eff} = \frac{k}{\mu_{eff}} = 4.795 * (10)^{-11} * m^{1.9}/Pa.s^{0.9}$$

$$k = 3.2976 * (10)^{-11} * 4.24 * (10)^{-3} = 2.033 * (10)^{-13} m^2$$

$$k = 2.033 * (10)^{-13} m^2 * \frac{1mD}{9.869233 * (10)^{-16} m^2} = 206mD$$

To calculate storativity,

$$\varphi c_t = \frac{k}{\mu_{eff}} * \frac{t}{t_D} * \frac{1}{n\left(\frac{2\pi h}{q}\right)^{1-n} r_w^{3-n}}$$

$$\varphi c_t = \frac{k}{\mu_{eff}} \frac{15196}{60000 * 0.9 * \left(\frac{2 * 3.142 * 5}{0.00055204}\right)^{1-0.9} * 0.1^{(3-0.9)}}$$

$$\varphi c_t = \frac{k * 15196}{\mu_{eff} * 1282.09}$$

$$\varphi c_t = 11.8525 * 4.795 * (10)^{-11} = 5.683 * (10)^{-10}$$

Wellbore storage,

Since C_D=0, $C = 2\pi hn\varphi c_t r_w^2 C_D = 0$

Calculate radius of investigation

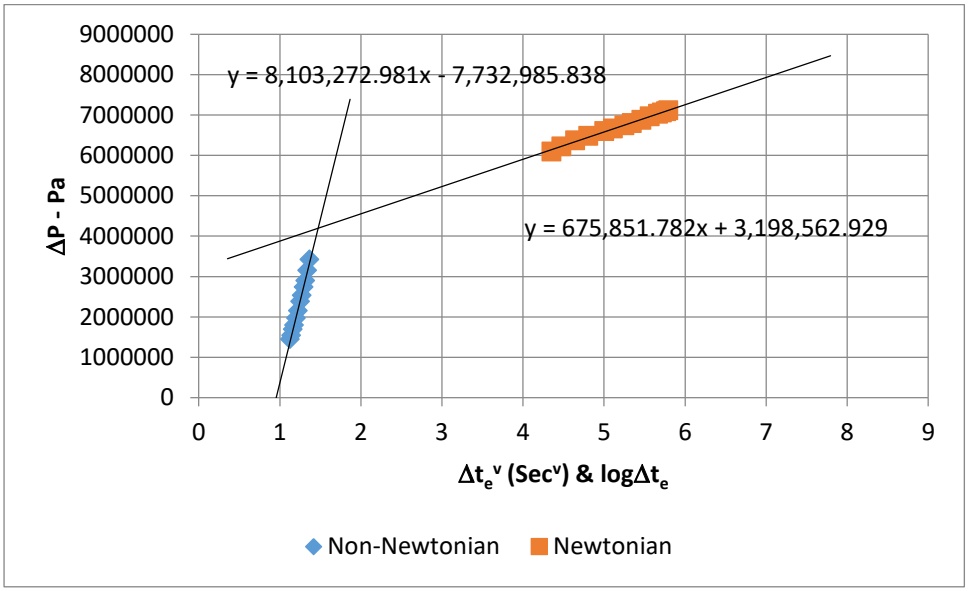

Figure 7.6: Intersection for non-Newtonian and Newtonian fluid flow in Example A2

At point of intersection,

$$675851.782x + 3198562.929 = 8103272.981x - 7732985.838$$

$$8103272.981x - 675851.782x = 3198562.929 + 7732985.838$$

$$7427421x = 10931549$$

$$x = 1.47178$$

For non-Newtonian fluid,

$$t_e = x^{\frac{1}{v}} sec = 1.47178^{\left(\frac{1}{0.047619}\right)} = 3347.469 sec$$

$$G = \frac{0.9*0.2*1*10^{-9}}{4.79478*(10)^{-11}} * \left(\frac{2*3.142*5}{0.00055204}\right)^{1-0.9} = 11.22089$$

$$r_{inv} = \left(\Gamma\left(\frac{2}{3-n}\right)\right)^{\frac{1}{n-1}} \left[\frac{(3-n)^2 t}{G}\right]^{\frac{1}{3-n}} = 0.745305 * \left[\frac{(3-0.9)^2*3347}{11.22089}\right]^{\frac{1}{3-0.9}} = 22.783m$$

$$r_{inv}(meter) = \left(\frac{t_e}{G}\right)^{\frac{1}{3-n}} = \left(\frac{3347}{11.22089}\right)^{\frac{1}{3-0.9}} = 15.08m$$

TDS Method

Step 1 and 2: Shown in Figure 7.4

Step 3. $C = qB(\frac{t}{\Delta P_{ws}})$

Since there is no early-time unit slope,

$$C = 0 \; and \; so, C_D = 0$$

Step 4: $v = \frac{1-n}{3-n} = \frac{1-0.9}{3-0.9} = 0.0476$

Step 5. At $(\Delta t_e) = 697.373 \; sec$, $(\Delta P_{ws}) = 3420000 \; Pa$ and the pressure derivative, $(t * \Delta P'_w) = 669367 \; Pa.$

Using equation (6.1) which was derived from analytical solution, mobility is estimated as:

$$\frac{k}{\mu_{eff}} = \left(\frac{0.5*\left(1.75697*(10)^{-5}\right)^{0.9048}*(697.373)^{0.0476}}{669367*(1.8*(10)^{-10})^{0.0476}}\right)^{1.05}$$

$$\frac{k}{\mu_{eff}} = \left(\frac{3.402*(10)^{-5}}{230046.3087}\right)^{1.05} = 4.77 * (10)^{-11} * m^{1.9}/Pa.s^{0.9}$$

But,

$$\mu_{eff} = 4.24 * (10)^{-3} Pa.s^{0.9}/m^{1.9}$$

Therefore, permeability:

$$k = \frac{4.77*(10)^{-11}*4.24*(10)^{-3}}{9.869233*(10)^{-16}} = 205.12 \; mD$$

Step 6: Calculate the skin factor, S.

Using equation 6.3,

$$S = \frac{k}{\mu_{eff}}\left(\frac{2\pi h}{q}\right)^{n} r_w^{1-n}\left[(\Delta P_w)_{IARF} - \frac{3-n}{1-n}(tx\Delta P'_w)_{IARF}\right] + \frac{1}{1-n}$$

$$S = 4.77 * (10)^{-11} * \left(\frac{2 * 3.142 * 5}{0.00055204}\right)^{0.9} * 0.1^{1-0.9} * \left[3420000 - (669367 * \frac{3-0.9}{1-0.9})\right] + \frac{1}{1-0.9}$$

$$S = 2.31$$

Step 7: Calculate radius of investigation

For non-Newtonian fluid,

$$t_e = x^{\frac{1}{v}} sec = 1.47178^{\left(\frac{1}{0.047619}\right)} = 3347.469 sec$$

$$G = \frac{0.9*0.2*1*10^{-9}}{7.29*(10)^{-11}} * \left(\frac{2*3.142*5}{0.00055204}\right)^{1-0.9} = 11.3$$

$$r_{inv} = \left(\Gamma\left(\frac{2}{3-n}\right)\right)^{\frac{1}{n-1}}\left[\frac{(3-n)^2 t}{G}\right]^{\frac{1}{3-n}} = 0.745305 * \left[\frac{(3-0.9)^2 * 3347}{9.26}\right]^{\frac{1}{3-0.9}} = 22.74\, m$$

$$r_{inv}(meter) = \left(\frac{t_e}{G}\right)^{\frac{1}{3-n}} = \left(\frac{3347}{9.26}\right)^{\frac{1}{3-0.9}} = 15.05\, m$$

7.2 Section B – General Solution (For Any Values of n)

7.2.1 Example 3

Same question as Example 1. But,

$$n = 0.6$$

Solution

Pressure data is converted from bar to Pascal and Figure 7.1 presents the pressure and pressure derivative log-log plot against time.

Type Curve Matching Technique.

Several type curves were generated until a matching curve is obtained. The type curve that matches the given data in Figure 7.1 is generated at constant pressure boundary with n =0.6, R_D=80, α=0.001, ω=1, θ=0.1, R_{eD}=8000, and S=0.5. The match is shown in Figure 7.7 and the match points are:

$$(P_{DM}, \Delta P_M) = (8, 3610000)$$

$$(t_{DM}, \Delta t_M) = (70, 62)$$

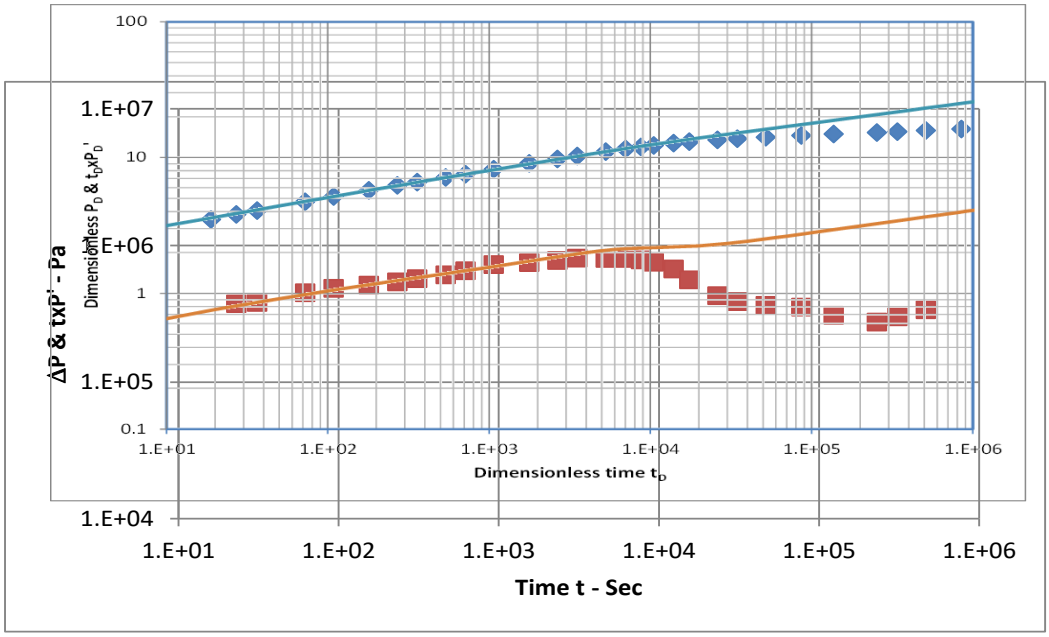

Figure 7.7: Type curve matching for Example B3

To calculate effective viscosity, μ_{eff}:

$$\mu_{eff} = \frac{0.02}{12}\left(9 + \frac{3}{0.6}\right)^{0.6}\left(150 * \frac{100md * 9.869233 * (10)^{-16}m^2}{1md} * 0.2\right)^{\frac{1-0.6}{2}}$$

$$\mu_{eff} = \frac{0.02}{12} * 4.87166 * 4.963 * (10)^{-3} = 4.016 * (10)^{-5} Pa.s$$

From equation (5.12), fluid mobility is given as:

$$\lambda_{eff} = \frac{k}{\mu_{eff}} = \left(\frac{8}{3610000}\right)_{match}\left(\frac{0.00055204}{2 * 3.142 * 5}\right)^{0.6} 0.1^{1-0.6} = 1.2372 * (10)^{-9} * m^{1.9}/Pa.s^{0.9}$$

$$k = 1.2372 * (10)^{-9} * 4.016 * (10)^{-5} = 4.968 * (10)^{-14} m^2$$

$$k = 4.9855 * (10)^{-14} m^2 * \frac{1mD}{9.869233 * (10)^{-16} m^2} = 50.35mD$$

To calculate storativity,

$$\varphi c_t = \frac{k_r}{\mu_{eff}} \frac{62}{70*0.6*\left(\frac{2*3.142*5}{0.00055204}\right)^{1-0.6} *0.1^{(3-0.6)}}$$

$$\varphi c_t = \frac{k_r*4.64567}{\mu_{eff}} = 4.64567 * 1.2372 * (10)^{-9} = 5.75 * (10)^{-9}/Pa$$

Calculate radius of investigation

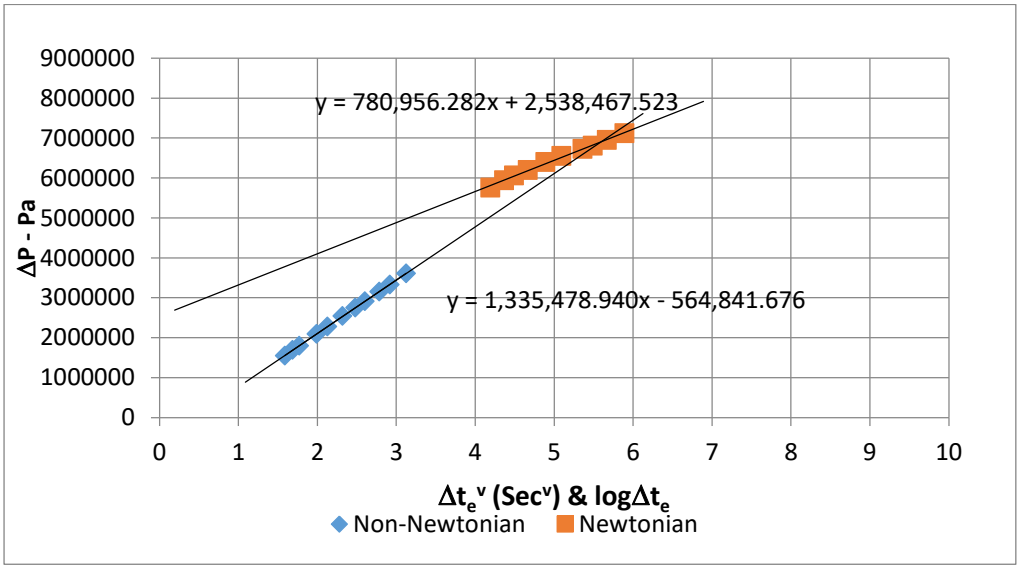

Figure 7.8: Intersection for Newtonian and Non-Newtonian fluid flow in Example 3

From Figure 7.8, at point of intersection between Newtonian and non-Newtonian fluid:

$$1335478.94x - 564841.676 = 780956.282x + 2538467.523$$

$$1335478.94x - 780956.282x = 564841.676 + 2538467.523$$

$$554522.7x = 3319424$$

$$x = 5.986$$

For non-Newtonian fluid,

$$v = \frac{1-n}{3-n} = \frac{1-0.6}{3-0.6} = 0.1667$$

$$t_e = x^{\frac{1}{v}} sec = 5.986^{\frac{1}{0.1667}} = 46006.6sec$$

Radius of investigation for non-Newtonian flow in porous media is given by Ikoku and Ramey (1979) as:

$$r_{inv} = \left(\Gamma\left(\frac{2}{3-n}\right)\right)^{\frac{1}{n-1}}\left[\frac{(3-n)^2 t}{G}\right]^{\frac{1}{3-n}}$$

Where

$$G = \frac{n\varphi c_t \mu_{eff}}{k_r}\left(\frac{2\pi h}{q}\right)^{1-n} = \frac{0.6*0.2*1*10^{-9}}{1.2372*(10)^{-9}} * \left(\frac{2*3.142*5}{0.00055204}\right)^{1-0.6} = 7.74166$$

$$r_{inv} = (1.128787)^{\frac{1}{0.6-1}} * \left[\frac{(3-0.6)^2*48010.87}{7.74166}\right]^{\frac{1}{3-0.6}} = 23.08m$$

$$r_{inv}(meter) = \left(\frac{t_e}{G}\right)^{\frac{1}{3-n}} = \left(\frac{48010.87}{7.74166}\right)^{\frac{1}{3-0.6}} = 37.37m$$

TDS method

Figure 7.1 represents Step 1 and 2

Step 3. $C = qB(\frac{t}{\Delta P_{ws}})$

But there is no early-time unit-slope, therefore $C = 0$

Step 4: $v = \frac{1-n}{3-n} = \frac{1-0.6}{3-0.6} = 0.1667$

Step 5. At $t = 931sec$, $(\Delta P_{ws}) = 3610000Pa$, and $(t * \Delta P'_w) = 724063Pa$.

Step 6: Mobility is estimated as:

$$\frac{k}{\mu_{eff}} = \left(\frac{0.5*\left(1.75697*(10)^{-5}\right)^{0.6667}*(931)^{0.1667}}{724063*(1.2*(10)^{-10})^{0.1667}}\right)^{1.2}$$

$$\frac{k}{\mu_{eff}} = \left(\frac{1.056*(10)^{-3}}{16068.52}\right)^{1.2} = 2.41 * (10)^{-9} * m^{1.9}/Pa.s^{0.9}$$

From fluid and reservoir parameters,

$$\mu_{eff} = 4.016 * (10)^{-5} Pa.s^{0.9}/m^{1.9}$$

Therefore, permeability:

$$k = \frac{2.41*(10)^{-9}*4.016*(10)^{-5}}{9.869233*(10)^{-16}} = 97.8\, mD$$

Step 7: Calculate the skin factor, S.

Using equation 6.3,

$$S = \frac{k}{\mu_{eff}}\left(\frac{2\pi h}{q}\right)^{n} r_w^{1-n}\left[(\Delta P_w) - \frac{3-n}{1-n}(tx\Delta P'_w)\right] + \frac{1}{1-n}$$

$$S = 2.403 * (10)^{-9} * \left(\frac{2 * 3.142 * 5}{0.00055204}\right)^{0.6} * 0.1^{1-0.6} * \left[3610000 - (724063 * \frac{3-0.6}{1-0.6})\right] + \frac{1}{1-0.6}$$

$$S = 1.999$$

Step 8: Calculate radius of investigation

For non-Newtonian fluid,

$$v = \frac{1-n}{3-n} = \frac{1-0.6}{3-0.6} = 0.1667$$

$$t_e = 46006.6sec$$

Radius of investigation for non-Newtonian flow in porous media is given by Ikoku and Ramey (1979) as:

$$G = \frac{n\varphi c_t \mu_{eff}}{k_r}\left(\frac{2\pi h}{q}\right)^{1-n} = \frac{0.6*0.2*1*10^{-9}}{1.953*(10)^{-9}} * \left(\frac{2*3.142*5}{0.00055204}\right)^{1-0.6} = 3.99$$

$$r_{inv} = (1.128787)^{\frac{1}{0.6-1}} * \left[\frac{(3-0.6)^2*48010.87}{4.90}\right]^{\frac{1}{3-0.6}} = 75.50\, m$$

$$r_{inv}(meter) = \left(\frac{t_e}{G}\right)^{\frac{1}{3-n}} = \left(\frac{48010.87}{4.90}\right)^{\frac{1}{3-0.6}} = 49.28\, m$$

7.2.2 Example 4

Question is same as in example 2. The pressure test data plot is shown in Figure 7.4.

Solution

From Pressure data, final shut-in period of fall-off period, $\Delta t_L = 3100000\text{sec} = 35.87963\text{days}$

Type Curve Matching Technique.

Several type curves were generated until a matching curve is obtained. The type curve that matches the given data in Figure 6.4 is generated with n =0.6, S=0.65, CD=0, ω=1, α=0.001, θ=0.1, R_{eD}=8000, and R_D=150. A match is shown in Figure 7.9 and the match points are:

$$P_{DM} = 4$$

$$\Delta P_{wsM} = 1450000\ Pa$$

$$t_{DM} = 60$$

$$\Delta t_{eM} = 12\ sec$$

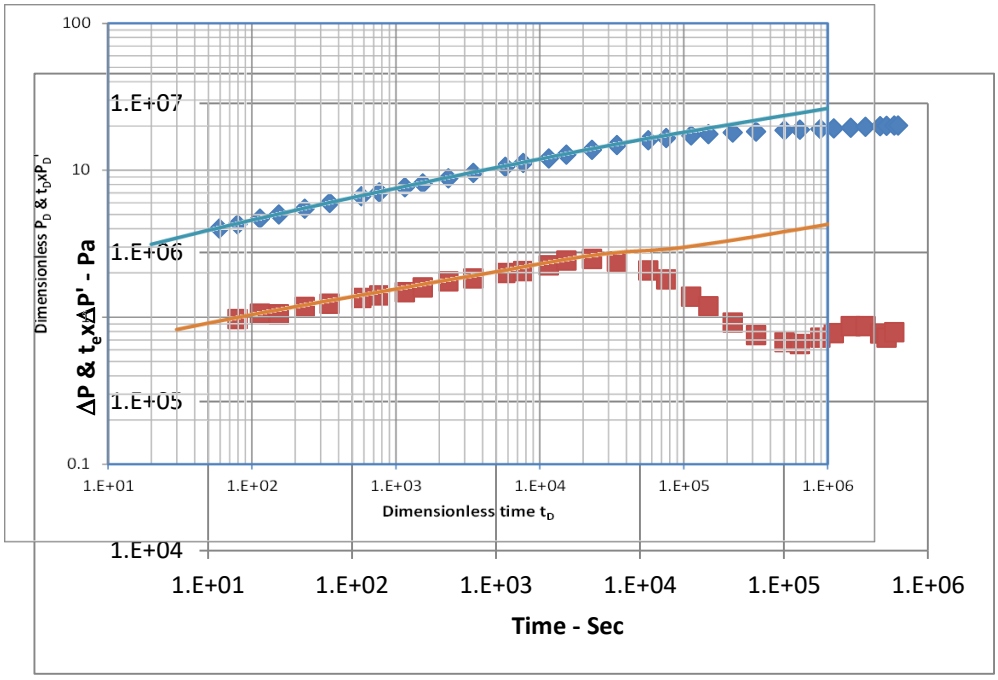

Figure 7.9: Type curve matching for Example B4

To calculate effective viscosity, μ_{eff}:

$$\mu_{eff} = 4.016 * (10)^{-5} Pa.s$$

From equation (5.12), fluid mobility is given as:

$$\lambda_{eff} = \frac{k_r}{\mu_{eff}} = \left(\frac{4}{1450000}\right)_{match} \left(\frac{0.00055204}{2*3.142*5}\right)^{0.6} 0.1^{1-0.6} = 1.54 * (10)^{-9} * m^{1.9}/Pa.s^{0.9}$$

$$(k_r) = 1.54 * (10)^{-9} * 4.0297 * (10)^{-5} = 6.185 * (10)^{-14} m^2$$

$$(k_r) = 6.185 * (10)^{-14} m^2 * \frac{1mD}{9.869233*(10)^{-16} m^2} = 62.67mD$$

To calculate storativity,

$$\varphi c_t = \frac{k_r}{\mu_{eff}} \frac{12}{60*0.6*\left(\frac{2*3.142*5}{0.00055204}\right)^{1-0.6} * 0.1^{(3-0.6)}}$$

$$\varphi c_t = \frac{k_r * 1.049022}{\mu_{eff}} = 1.049022 * 1.54 * (10)^{-9}$$

$$\varphi c_t = 1.62 * (10)^{-9}/Pa$$

Wellbore storage,

Since C_D=0, $C = 2\pi hn\varphi c_t r_w^2 C_D = 0$

Radius of investigation:

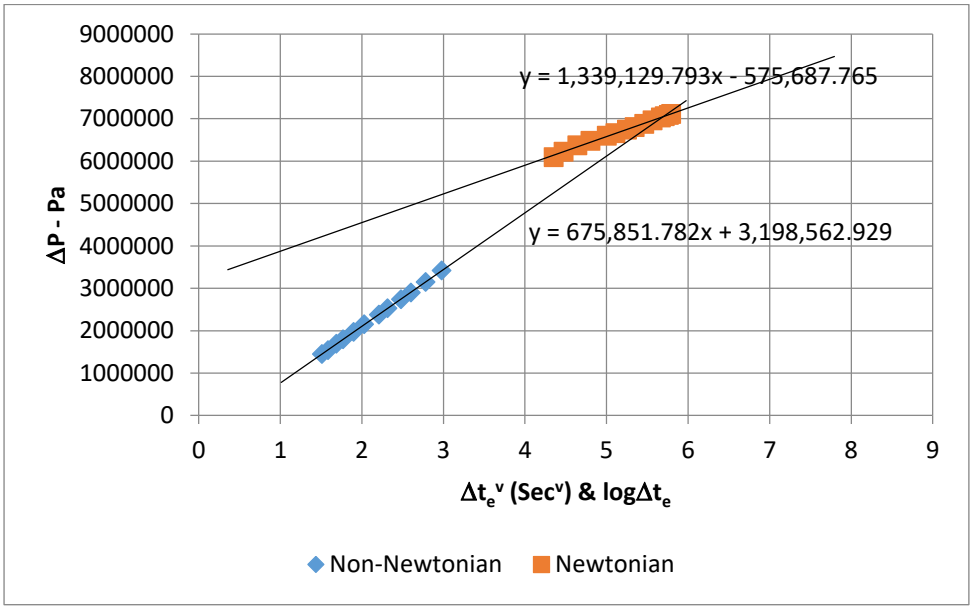

Figure 7.10: Intersection for non-Newtonian and Newtonian fluid flow for Example B4

At point of intersection,

$$675851.782x + 3198562.929 = 1339129.793x - 575687.765$$

$$1339129.793x - 675851.782x = 3198562.929 + 575687.765$$

$$663278.011x = 3774250.694$$

$$x = 5.69$$

For non-Newtonian fluid,

$$t_e = x^{\frac{1}{v}} sec = 5.69^{\frac{1}{0.1667}} = 33937sec$$

Radius of investigation for non-Newtonian flow in porous media is given by Ikoku and Ramey (1979) as:

$$r_{inv} = \left(\Gamma\left(\frac{2}{3-n}\right)\right)^{\frac{1}{n-1}} \left[\frac{(3-n)^2 t}{G}\right]^{\frac{1}{3-n}}$$

Where

$$G = \frac{n\varphi c_t \mu_{eff}}{k_r}\left(\frac{2\pi h}{q}\right)^{1-n} = \frac{0.6*0.2*1*10^{-9}}{1.54*(10)^{-9}} * \left(\frac{2*3.142*5}{0.00055204}\right)^{1-0.6} = 6.219$$

$$r_{inv} = (1.128787)^{\frac{1}{0.6-1}} * \left[\frac{(3-0.6)^2*33866.29}{6.219}\right]^{\frac{1}{3-0.6}} = 22.27m$$

Or

$$r_{inv}(meter) = \left(\frac{t_e}{G}\right)^{\frac{1}{3-n}} = \left(\frac{33866.29}{6.219}\right)^{\frac{1}{3-0.6}} = 36.03m$$

TDS Method

Step 1 and 2: Figure 6.4

Step 3. $C = qB(\frac{t}{\Delta P_{ws}})$

Since there is no early-time unit slope,

$C = 0\ and\ so, C_D = 0$

Step 4: $v = \frac{1-n}{3-n} = 0.1667$

Step 5. At $(\Delta t_e) = 154.969\ sec$, $(\Delta P_{ws}) = 2530000\ Pa$ and the pressure derivative, $(t * \Delta P'_w) = 516668\ Pa.$

Step 6. Using equation (6.1) which was derived from analytical solution, mobility is estimated as:

$$\frac{k}{\mu_{eff}} = \left(\frac{0.5*\left(1.75697*(10)^{-5}\right)^{0.6667}*(154.969)^{0.1667}}{516668*(1.2*(10)^{-10})^{0.1667}}\right)^{1.2}$$

$$\frac{k}{\mu_{eff}} = \left(\frac{1.006*(10)^{-3}}{14854.697}\right)^{1.2} = 2.49 * (10)^{-9} * m^{1.2}/Pa.s^{0.6}$$

Therefore, permeability:

$$k = \frac{2.52*(10)^{-9}*4.0297*(10)^{-5}Pa.s}{9.869233*(10)^{-16}} = 101.5\ mD$$

Step 7: Calculate the skin factor, S.

Using equation 6.3,

$$S = 2.49 * (10)^{-9} * \left(\frac{2*3.142*5}{0.00055204}\right)^{0.6} * 0.1^{1-0.6} * \left[3420000 - (669367 * \frac{3-0.6}{1-0.6})\right] + \frac{1}{1-0.6}$$

$S = 2.08$

Step 8: Calculate radius of investigation

For non-Newtonian fluid,

$t_e = 5.69^{\frac{1}{0.1667}} = 33937sec$

$G = \frac{n\varphi c_t \mu_{eff}}{k_r}\left(\frac{2\pi h}{q}\right)^{1-n} = \frac{0.6*0.2*1*10^{-9}}{2.595*(10)^{-9}} * \left(\frac{2*3.142*5}{0.00055204}\right)^{1-0.6} = 3.84$

$r_{inv} = \left(\Gamma\left(\frac{2}{3-n}\right)\right)^{\frac{1}{n-1}}\left[\frac{(3-n)^2 t}{G}\right]^{\frac{1}{3-n}}$

$r_{inv} = (1.128787)^{\frac{1}{0.6-1}} * \left[\frac{(3-0.6)^2*33866.29}{3.80}\right]^{\frac{1}{3-0.6}} = 27.22\ m$

$r_{inv}(meter) = \left(\frac{t_e}{G}\right)^{\frac{1}{3-n}} = \left(\frac{33866.29}{3.80}\right)^{\frac{1}{3-0.6}} = 44.07\ m$

7.3 Discussion of Results

Tables 7.1 and 7.2 summarize the results obtained in the above examples. As indicated, formation and fluid properties from Lund and Ikoku (1981) were used to run simulations and generate type curves for the examples. Both injection and fall-off responses were considered. It is important to point out that getting the right type curve match points can be quite tasking when working with field data. However, the type curve method of estimating reservoir properties is dependable with a good match point.

In all the type curves generated, the non-Newtonian fluid flow generated lower pressure increases compared to the Newtonian fluids been attributed to its dependence on the flow index behavior which is determined by the viscosity and therefore the pressure. Wellbore storage effect and NFR parameters are not considered in any of the examples, but a method for estimating them is provided in the work. Thus, this work presents a general analytical approach to transient pressure derivative responses for a well in a two-region composite reservoir.

Table 7.1: Summary of Injectivity Test Estimated Properties

Example	**Lund and**	**Section A1**		**Section B3**	
	Ikoku (1981)	**Type curve**	**TDS**	**Type curve**	**TDS**
Flow index, n	0.6	0.9		0.6	
Effective viscosity, μ_{eff} (Pa.s)		$4.24 * (10)^{-3}$		$4.016 * (10)^{-5}$	
Effective mobility, k/μ_{eff} ($m^{1.9}/Pa.s^{0.9}$)		$4.0369 * (10)^{-11}$	$4.46 * (10)^{-11}$	$1.2372 * (10)^{-9}$	$2.40 * (10)^{-9}$
Permeability, mD	100	173.44	191.63	50.35	97.8
Storativity, (Pa^{-1})	$2 * (10)^{-10}$	$7.33 * (10)^{-9}$		$5.75 * (10)^{-9}$	
Skin factor, S		0.0	2.18	0.5	1.999
Radius polymer bank	40 m	$8.224\ m$	$8.62\ m$	38.0374 m	$49.28\ m$

Table 7.2: Summary of Fall-off Test Estimated Reservoir and Wellbore Properties

Example	**Lund and**	**Section A2**		**Section B4**	
	Ikoku (1981)	**Type curve**	**TDS**	**Type curve**	**TDS**
Flow index, n	0.6	0.9		0.6	
Effective viscosity, μ_{eff} (Pa.s)		$4.24 * (10)^{-3}$		$4.016 * (10)^{-5}$	
Effective mobility, k/μ_{eff} ($m^{1.9}/Pa.s^{0.9}$)		$4.795 * (10)^{-11}$	$4.774 * (10)^{-11}$	$1.54 * (10)^{-9}$	$2.49 * (10)^{-9}$
Permeability, mD	100	206.0	205.12	62.67	101.5
Storativity, (Pa^{-1})		$5.683 * (10)^{-10}$		$1.615 * (10)^{-9}$	
Skin factor, S		-1.0	2.31	0.65	2.07
Radius of inv.	40 m	$15.08\ m$	$15.05\ m$	$36.03\ m$	$44.07\ m$

CHAPTER 8

CONCLUSIONS AND RECOMMENDATIONS

8.1 Conclusions

1. Analytical solutions were derived for estimating reservoir and wellbore parameters in the radial flow of non-Newtonian, power law fluids through composite homogeneous or naturally fractured reservoir systems. The solutions are obtained for three scenarios.
    - When the flow behavior index of injected non-Newtonian fluid comes in contact with same type of fluid.
    - When the flow behavior index of the injected non-Newtonian fluid comes in contact with another non-Newtonian fluid of different flow index (example is heavy crude oil) in the reservoir.
    - When the non-Newtonian fluid comes in contact with a Newtonian fluid (crude oil) in the reservoir
2. New type curves for interpretation of non – Newtonian pressure data in homogeneous and naturally fractured reservoirs with wells located near infinite, no-flow and constant pressure boundaries were developed. The derivatives curves showed the characteristics fingerprints needed for identifying the parameters.
3. Parameters considered for the pressure transient analyses in the composite reservoir include skin (S), wellbore storage (C), mobility ratio (θ), alpha, storativity ratio (ω), interporosity capacity (λ), distance between polymer front (R_D).
4. From the long time analytical solution and from literature, a procedure of well test interpretation using Tiab Direct Synthesis (TDS) technique is proposed.
5. The pressure transient analysis procedure was applied to two cases were one is when the non-Newtonian fluid is approximately Newtonian and another is for a general case. Two example problems of polymer injection (an injectivity and a falloff test) from Lund and Ikoku (1981) were used to demonstrate the applicability of the procedure and a slightly approximate match was obtained. The examples were studied using type curve matching and TDS.

8.2 Recommendations

1. Since the examples are simulated, further studies are necessary to conclude on the validity of the procedures demonstrated.
2. Further studies could also investigate the effects of skin and wellbore storage on the mathematical model developed.
3. Studies should be made to investigate effects of a non-pivotlike mobility displacement (viscous fingering) as well as gravity on the test data.
4. This paper considered injection of power law (pseudo-plastics) non-Newtonian fluids; other research could address other polymer fluids, chemicals and even go beyond that to gas and steam injection.

NOMENCLATURE

α	geometry parameter
B	formation volume factor, RB/STB
β	order of Bessel function
C_D	dimensionless wellbore storage
c_t	total compressibility
δ	partial derivative
G	group defined by equation (3.4)
h	formation thickness, ft
H	consistency index (power-law parameter)
$I_i(z, sfs)$	modified Bessel function of the first kind of order, i
k	formation permeability, md
$K_i(z, sfs)$	modified Bessel function of the second kind of order, i
m, n	flow behavior index (power-law parameter), dimensionless
P_D'	dimensionless wellbore pressure derivative
P_D	dimensionless wellbore pressure drop
Pi	initial pressure, psi
P_{wD}	dimensionless wellbore flowing pressure, psi
$\bar{P}_D$	dimensionless pressure drop in Laplace space
q	volumetric flow rate
r	radial distance, ft
r_D	dimensionless radial distance at any point, (r/r_w)
R_{eD}	dimensionless radial distance at boundary conditions (external)
r_w	wellbore radius, ft
S	skin factor, dimensionless
t	test time, hr
$t*\Delta P'$	pressure derivative, psi
$t_D*\Delta P_D'$	dimensionless pressure derivative, psi
t_D	dimensionless time based on wellbore radius
$\Gamma(x)$	gamma (factorial) function
ΔP	pressure drop
φ	porosity, fraction of bulk volume

λ	interporosity flow parameter, dimensionless
Δ	change, drop
μ	viscosity, cp
θ	effective mobility ratio for a two-region composite reservoir
ω	storage capacity ratio, dimensionless
π	3.142

Subscripts

1	referring to region 1, inner region
2	referring to region 2, outer region for two-region composite reservoir
D	dimensionless quantity
eff	effective
inv	investigation
R	infinite acting radial flow
w	wellbore

REFERENCES

Abbaszadeh, M & Kamal, M. (1989). Pressure Transient Testing of Water-Injection Wells, *SPE Res. Engineering*, 4, 115-124, https://doi.org/10.2118/116744-PA.

Alzaabi, M. A. et al. (2020). Polymer Injectivity Test Design Using Numerical Simulation. *Polymers* 2020, 12, 801(1-23), https://doi.org/10.3390/polym12040801.

Ahmad Ali Manzoor (2020). Modeling and Simulation of Polymer Flooding with Time-Varying Injection Pressure. *ACS Omega 2020*, 5, 5258-5269, https://dx.doi.org/10.1021/acsomega.9b04319.

Ambastha, A. K (1988). Pressure Transient Analysis for Composite Systems, *Stanford Geothermal Program Interdisciplinary Research in Engineering and Earth Sciences*, Stanford University, Stanford, California.

Ertekin, T., Adewumi, M. A., & Daud, M. E. (1987). Pressure Transient Behaviour of Non-Newtonian/Newtonian Fluid Composite Systems in Porous Media with a Finite Conductivity Vertical Fracture, SPE 17053, *Soc. Pet. Eng. J.*, https://doi.org/10.2118/17053-PA.

Escobar, F. H., Martinez, J. & Montealegre-Madero, M. (2010). Pressure and Pressure Derivative Analysis for a Well in a Radial Composite Reservoir with a Non-Newtonian/Newtonian Interface, *CT&F – Ciencia, Technologia y Futura*, 4(2), 33-42.

Gencer, C. S. & Ikoku, C. U. (1984). Well Test Analysis for Two-Phase Flow of Non-Newtonian Power-Law and Newtonian Fluids, *ASME Journal of Energy Resources Technology*, 106(295 - 305).

Gogarty, W. B. (1967). Rheological Properties of Pseudoplastic Fluids in Porous Media, SPE 1566, *Soc. Pet. Eng. J.*, 149-160, https://doi.org/2118/1566-PA.

Huh, C. & Snow, T. M. (1985). Well Testing with a Non-Newtonian Fluid in the Reservoir, SPE 14453, *Soc. Pet.Eng. J.*, https://doi.org/10.2118/14453-MS.

Igbokoyi, A. O. & Tiab, D. (2007). New Type Curves for the Analysis of Pressure Transient Data. Dominated by Skin and Wellbore Storage – Non-Newtonian Fluid, SPE 106997, *Soc. Pet. Eng. J.*, https://doi.org/10.2118/106997-MS.

Ikoku, C. U. & Ramey, H. J. (1979). Transient Flow of Non-Newtonian Power-Law Fluids in Porous Media, SPE 7139, *Soc. Pet. Eng. J.*, 19(3):164-174, https://doi.org/10.2118/7139-PA.

Jia, Z., Li. D. & Lu, D. (2015). Development of a Numerical Well Test Simulator for Polymer Surfactant Flooding and the Pressure Transient Response Study, *International Conference on Advances in Energy and Environmental Science (ICAEES)*, 1448-1451.

Jia, Z., Li, D., Yang, J., Xue, Z. and Lu, D. (2015). Numerical Well Test Analysis for Polymer Flooding considering the Non-Newtonian Behavior, *Journal of Chemistry*, http://dx.doi/10.1155/2015/107625

Katime-Meindl, I. & Tiab, D. (2001). Analysis of Pressure Transient Test of Non-Newtonian Fluids in Infinite Reservoir and in the Presence of a Single Linear Boundary by the Direct Synthesis Technique, SPE 71587, *Soc. Pet. Eng. J.*, https://doi.org/10.2118/71587-MS.

Lund, O. & Ikoku, C. U. (1981). Pressure Transient Behaviour of Non-Newtonian/Newtonian Fluid Composite Reservoirs, SPE 9401, *Soc. Pet. Eng. J.*, 271-280, https://doi.org/10.2118/9401PA.

Manrique, E., Ahmadi, M. & Samani, S. (2017). Historical and Recent Observations in Polymer Floods: An Update Review, *CT&F – Ciencia, Technologia y Futura*, 6(5), 17-48.

McDonald, A. E. (1979). Approximate Solutions for Flow of Non-Newtonian Power Law Fluids through Porous Media, SPE 7690. *American Institute of Mining, Metallurgical, and Petroleum Engineers, Inc.*, 175-182, https://doi.org/10.2118/7690-MS.

Murtha, J. A. & Ertekin, T. (1983) Numerical Simulation of Power-Law Fluid Flow in a Vertically Fractured Reservoir, *SPE-AIME*, https://doi.org/10.2118/12011-MS

Odeh, A. S. & Yang, H. T. (1979). Flow of Non-Newtonian Power Law Fluids through Porous Media, SPE 7150, *Soc. Pet. Eng. J.*, 155-163, https://doi.org/10.2118/7150-PA.

Olarewaju, J. S. & Lee, W. J. (1987). An Analytical Model for Composite Reservoirs Produced at Either Constant Bottom-hole Pressure or Constant Rate, SPE 16763, *Soc. Pet. Eng. J.*, 217 https://doi.org/10.2118/16763-MS.

Olarewaju, J. S. & Lee, W. J. (1989). A Comprehensive Application of a Composite Reservoir Model to Pressure Transient Analysis, SPE 16345, *SPE Reservoir Engineering.*, 325-331, https://doi.org/10.2118/16345-PA.

Omosebi, O. & Igbokoyi, A. (2015). Analysis of pressure falloff tests of non-Newtonian power-law fluids in naturally-fractured bounded reservoirs, *KeAi*, Petroleum 1 (2015) 318-341 http://dx.doi.org/10.1016/j.petlm.2015.10.006.

Raghavan, R. & Chen, C. (2018) Fractured-Injection-Well Performance under Non-Newtonian, Power Law Fluids, SPE 187955, *SPE Reservoir Eval. & Eng.*, https://doi.org/10.2118/187955-PA.

Rajput, R. K. (2011) A Textbook of Fluid Mechanics and Hydraulic Machines, International (5^{th}) Edition, pp 4-8.

Savins, J. G. (1969) Non-Newtonian Flow through Porous Media, *Ind. And Eng. Chem*, 61(10)18-47., https://doi.org/10.1021/ie50718a005

Stehfest, H. (1970) Algorithm 368: Numerical Inversion of Laplace Transforms [D5], *Communications of the ACM*., https://doi.org/10.1145/361953.361969.

Tariq Fariss Al-Fariss. (1984). Non-Newtonian Oil Flow through Porous Media, *PhD Dissertation*, University of British Columbia.

Tiab, D., Restrepo, D. P., & Igbokoyi, A. (2006). Fracture Porosity of Naturally Fractured Reservoirs, SPE 104056, *Soc. Pet. Eng. J.*, https://doi.org/10.2118/104056-MS.

Van Poollen, H. K. & Jargon, J. R. (1969). Steady-State and Unsteady-State Flow of Non-Newtonian Fluids through Porous Media, SPE 1567, *Soc. Pet. Eng. J.*, https://doi.org/10.2118/1567-PA.

Vogel, P & Pusch, G. (1981) Some Aspects of the Injectivity of Non-Newtonian Fluids in Porous Media, Enhanced Oil Recovery, F. J Fayers, *ed. Elsevier Sci*, 177-195.

Warren, J. E. & Root, P. J. (1963). The Behaviour of Naturally Fractured Reservoirs, SPE 426, *Soc. Pet. Eng. J.*, 3(03), 245-255, https://doi.org/10.2118/426-PA.